

# **INCREASING DISSOLVED OXYGEN CONCENTRATIONS USING AERATING DRAFT TUBES**

Aaron Manzali

Department of Civil Engineering and Applied Mechanics

McGill University  
Montreal, Quebec, Canada  
April 2018

A thesis submitted to McGill University in partial fulfillment of the requirements of the degree  
of Master of Engineering

© Aaron Manzali, 2018

## **ABSTRACT**

The storage of water in large, deep reservoirs upstream of hydropower dams raise several environmental concerns, one of which is the deoxygenation of water due to thermal stratification in warmer climates. In the summer, the surface waters are heated and form a less-dense relatively thin layer called the epilimnion, below which lies the hypolimnion with colder and hence more dense water. This stratification inhibits mixing between the epilimnion and hypolimnion and results in low dissolved oxygen levels in the hypolimnion due to biological activity requiring dissolved oxygen that cannot be replenished. Turbines extracting water at depth lead to the tailwaters containing the anoxic water of the hypolimnion leading to a range of environmental and ecological effects that can persist for many kilometers downstream. The focus of this study is draft tube aeration for the purpose of increasing dissolved oxygen concentrations. A scale model study of a deflector in a simplified horizontal flow was implemented. It was used to study the influence of the geometric configuration of the deflector on the oxygen transfer rate, the differential pressure between the air inlet and a position just upstream of the deflector, and to qualitatively describe the injected bubble swarm. The injected bubble swarm was found to coalesce in the lee of the deflector at velocities close to those found in prototype draft tubes leading to an inability to set the size distribution of the injected bubbles. The pressure gradient between the ambient atmosphere and the air inlet downstream of the deflector was found to exhibit a scale effect with respect to the deflector size and air inlet position. A regression of the non-dimensional oxygenation coefficients found no dependence on the size of the deflector, but this was thought to be the result of problems with obtaining the experimental data. A qualitative description of the behavior and physics of the aeration is given. A regression for the non-dimensional aeration coefficient and a discussion of the loss coefficient of the deflectors, for use in the initial design stage of draft tube deflector aeration systems, were provided.

## RÉSUMÉ

Le stockage de l'eau dans de grands et profonds réservoirs en amont des barrages hydroélectriques, soulève plusieurs préoccupations environnementales, dont notamment la désoxygénation de l'eau due à la stratification thermique dans les climats chauds. En été, les eaux de surface, appelée épilimnion, sont chauffées et forment une couche relativement mince et peu dense. En dessous de celle-ci, se trouve la couche hypolimnion composée d'eau plus froide et donc plus dense. La stratification empêche le mélange entre l'épilimnion et l'hypolimnion, ce qui entraîne à de faibles niveaux d'oxygène dissous dans l'hypolimnion car l'activité biologique nécessitant de l'oxygène dissous ne peut être reconstituée. Les turbines extrayant en profondeur l'eau anoxique de l'hypolimnion, la reconduisent au niveau aval, ce qui peut engendrer une chaîne d'effets environnementaux et écologiques sur plusieurs kilomètres du courant d'eau. L'objectif de cette étude est l'aération par tube d'aspiration, dans le but d'augmenter les concentrations d'oxygène dissous. L'étude d'un prototype de déflecteur dans un écoulement horizontal simplifié a été mise en œuvre utilisant l'implantation d'un modèle réduit du déflecteur. Le prototype a été utilisé pour étudier (1) l'influence de la configuration géométrique du déflecteur sur le taux de transfert d'oxygène, (2) la pression différentielle entre l'entrée d'air et une position juste en amont du déflecteur et (3) pour décrire qualitativement l'essaim de bulles injectées. Il a pu être constaté que l'essaim de bulles injectées se coalescent à l'abri du déflecteur, aux mêmes vitesses que les bulles trouvées dans le prototype de tubes d'aspiration nous empêchant d'établir la taille de distribution des bulles injectées. Les variations de pression entre l'atmosphère ambiante et l'entrée d'air en aval du déflecteur s'est révélé d'avoir un effet d'échelle, prenant en compte la taille du déflecteur et la position de l'entrée d'air. Une régression des coefficients d'oxygénation non dimensionnelle n'a révélé avoir aucune dépendance sur la taille du déflecteur, mais ceci pourrait être dû à la façon dont les données expérimentales ont été obtenues. Voici une description qualitative du comportement

et de la physique de l'aération. Les informations sur la régression du coefficient d'aération non dimensionnelle ainsi qu'une discussion sur le coefficient de perte des déflecteurs pour l'utilisation durant l'étape de conception initiale des systèmes d'aération des déflecteurs à tubes d'aspiration ont été fournies.

## ACKNOWLEDGEMENTS

I would like to thank Professor Susan J. Gaskin for her extensive support and trust in me throughout these two years. Her continued effort has helped me become an independent researcher ready for a multitude of industry projects.

I would also like to Suk Yi Lo, Hydraulic Engineer at Andritz Hydro Canada, for her technical oversight throughout the length of this project. Her support was a crucial aspect of this research.

I greatly appreciate the work that John Bartczak, the lab supervisor, put into this project. His help in designing the test rig and various practical aspects of this study were a key reason of its success.

I'd like to thank Sam Minter, and the rest of the Mechanical Engineering Machine Shop team for their help in providing the machining services for this project.

To my lab colleagues and summer interns: Claudio Consuegra Martinez, Max Milanovic, Stephen Camozzi, Michel Samson, Labib Kallas, Andrea Mellado, their attitude kept the mood light and helped the productivity of this project.

A special thanks to Mohammed Ayman Shalaby who put in a great many hours towards the end of the project running additional experiments and assisting in the analysis of a huge dataset. Thanks to him for reviewing parts of this thesis.

I'd like to thank Dr. Jose Pedro Matos and Dr. Netercia Mendes of Lausanne, CH for housing me during my travels to the Vevey test rig and for their input during a fast-paced time of this study.

I appreciate the work of Alexandre Genevey and Stephen Stojanovic-Roth in setting up the Vevey test rig and acting as my test engineers during my experiments.

I'd like to express gratitude to my girlfriend, Dahlia Snaiderman, who read and reviewed this thesis countless times, all while supporting and guiding me.

I appreciate the support of my parents without whom it would've been difficult to keep a level head during this project.

Montreal Friends, thanks for countless memories.

This project would not have been possible without the funds provided by the NSERC ENGAGE and MITACS Accelerate programs.

# Table of Contents

<b>LIST OF FIGURES .....</b>	<b>VIII</b>
<b>LIST OF TABLES .....</b>	<b>X</b>
<b>LIST OF SYMBOLS AND ABBREVIATIONS .....</b>	<b>XI</b>
<b>CHAPTER 1: INTRODUCTION.....</b>	<b>1</b>
1.1 Novelty of the Study .....	2
1.2 Research Objectives.....	3
<b>CHAPTER 2: LITERATURE REVIEW .....</b>	<b>5</b>
2.1 Dissolved Oxygen Monitoring and Regulations .....	5
2.2 Governing equations.....	7
2.2.1 Air admission in hydro turbines .....	7
2.2.2 The Oxygen Mass Transfer Equation .....	10
2.2.3 The Liquid Film Coefficient; <i>KL</i> .....	13
2.2.4 The specific interstitial contact area; $a = A/V$ .....	15
2.3 Aeration in Hydraulic Structures for increasing DO concentrations .....	17
2.3.1 Model and Full-scale studies.....	21
2.3.2 Laboratory studies.....	26
<b>CHAPTER 3: METHODOLOGY .....</b>	<b>31</b>
3.1 McGill Experimental Apparatus.....	31
3.2 Vevey Experimental Apparatus .....	48
3.3 Test Parameters .....	52
3.4 Signal Acquisition and Data Analysis .....	55
<b>CHAPTER 4: RESULTS AND DISCUSSION .....</b>	<b>59</b>
4.1 Pre-Tests.....	59
4.1.1 Comparison between Inflow and Sample Pot DO measurements .....	61
4.1.2 Repeatability .....	64
4.2 Qualitative Observations of the Bubble Swarm created by the deflectors .....	65
4.2.1 Defining parameters of the bubble size.....	66
4.2.2 Effect of a mesh at the air inlet .....	69
4.2.3 Air Recirculation in the lee of the deflector.....	70

<b>4.3 Air Entrainment Results .....</b>	<b>71</b>
4.3.1 Pressure difference between injection point and upstream flow without aeration, high velocity .....	72
4.3.2 Effect of aeration on pressure difference between injection point and upstream water pressure .....	75
<b>4.4 Oxygenation Results .....</b>	<b>79</b>
4.4.1 Oxygenation coefficients .....	80
<b>4.5 Sources of Error.....</b>	<b>88</b>
<b>CHAPTER 5: SUMMARY AND CONCLUSIONS .....</b>	<b>89</b>
<b>5.1 Recommendations for future work .....</b>	<b>91</b>
<b>REFERENCES.....</b>	<b>93</b>
<b>APPENDIX A: DISCUSSION OF MEASUREMENT ERRORS.....</b>	<b>96</b>

## List of Figures

Figure 1-1: Deflectors placed around periphery of draft tube leading to air entrainment and oxygen exchange .....	2
Figure 2-1: Example thermal profile in a stratified lake (Jacobs, 2014) .....	6
Figure 2-2: Air void ratio in draft tube (Hopping <i>et al.</i> , 2009).....	10
Figure 2-3: Air inlets placed at negative pressures within a Francis turbine; runner cone (blue), hollow turbine blades (green), vacuum breaker system (red), discharge ring (yellow) (March, 2011).....	19
Figure 2-4: Bubble characteristics for two aeration systems at three turbine operating conditions (Papillon <i>et al.</i> , 2002).....	23
Figure 2-5: Air pockets formed downstream of air inlet in a coflow (Jun & Jain, 1993).....	27
Figure 3-1: McGill Test Rig Layout .....	31
Figure 3-2: McGill Test Chamber with test block visible .....	32
Figure 3-3: Brass test block with and without deflector configuration attached .....	33
Figure 3-4: Cross-sectional view of test block .....	33
Figure 3-5: McGill air supply system .....	34
Figure 3-6: Reservoir with air relief valve.....	35
Figure 3-7: Bubble extraction system through Venturi air pump .....	36
Figure 3-8: Pump and water flowmeter (Midwest Instrumentation and Controls).....	37
Figure 3-9: Modification from commercially available standard pipe elbow to deflector .....	38
Figure 3-10: Final deflector design with orienting pegs.....	38
Figure 3-11: Deflector (H = 10 mm) before being attached to PVC strip (L/H = 0).....	39
Figure 3-12: Deflector attached to PVC Strip (H = 16.5mm, L/H = 1).....	39
Figure 3-13: McGill test rig measurement locations .....	40
Figure 3-14: Test chamber with pressure measurement manifolds .....	41
Figure 3-15: Sketch of DO measurement apparatus .....	42
Figure 3-16: Downstream DO measurement apparatus.....	43
Figure 3-17: Point evolution of DO concentration .....	46
Figure 3-18: Vevey test rig layout .....	48
Figure 3-19: Vevey test chamber.....	49
Figure 3-20: MONOVAR regulation valve .....	50
Figure 3-21: Vevey experimental measurement locations.....	51
Figure 3-22: Deflector and Experimental parameters.....	53
Figure 3-23: Mesh Deflector Configuration with reference sample (H = 16.5, L/H = 1, D/H = 1) .....	54
Figure 3-24: Electronic Control Box Schematic.....	56
Figure 4-1: Validation Tests Results.....	61
Figure 4-2: Raw DO data comparison at low and high water velocities, $Q_a/Q_w = 10\%$ for both	63
Figure 4-3: Inflow vs Sample Pot Readings comparison.....	64
Figure 4-4: Oxygen transfer efficiency by water velocity and air flow ratio; repeatability experiments; H = 13.5; L/H = 1; U = [0.38, 0.88, 1.38, 2.00] m/s; $Q_a/Q_w = [3, 5, 7, 10] \%$ ; no mesh .....	65
Figure 4-5: Schematic diagram of flow past a deflector with two locations of bubble formation shown with white arrows. White dashed line indicates approximate extents of stable air bubble at high velocities. (a) No aeration; (b) aeration at L/H = 0; (c) aeration at L/H = 1; aeration at L/H = 2.....	67

Figure 4-6: Bubble injection in deflector $H = 10\text{mm}$ , $L/H = 0$ . Top – $U = 0.38\text{ m/s}$ , Middle – $U = 1.38\text{ m/s}$ , Bottom – $U = 7\text{ m/s}$ . $Q_a/Q_w = 3\%$ .....	69
Figure 4-7: Effect of the mesh presence on the injected bubble swarm .....	70
Figure 4-8: Start-up freeze-frame showing air flow recirculation; $V_w = 0.38\text{ m/s}$ , $Q_a/Q_w = 3\%$ .	71
Figure 4-9: P1-P2 vs water velocity for high water velocities without aeration .....	73
Figure 4-10: Bernoulli Loss Coefficient, No Aeration; $U = [7, 10, 15]\text{ m/s}$ .....	74
Figure 4-11: Dimensionless parameter dependence; $L/H = 1$ , No Aeration .....	75
Figure 4-12: P1-P2 vs $U$ at high water velocities with aeration; $H = 10\text{mm}$ .....	76
Figure 4-13: P1-P2 vs $U$ at high water velocities with aeration; $H = 13.5\text{mm}$ .....	77
Figure 4-14: P1-P2 vs $U$ at high water velocities with aeration; $H = 16.5\text{mm}$ .....	77
Figure 4-15: P1-P2 vs $U$ at low water velocities with aeration; $H = 10\text{mm}$ .....	78
Figure 4-16: P1-P2 vs $U$ at low water velocities with aeration; $H = 13.5\text{mm}$ .....	79
Figure 4-17: P1-P2 vs $U$ at low water velocities with aeration; $H = 16.5\text{mm}$ .....	79
Figure 4-18: Oxygen Transfer Efficiency vs. Air Void Ratio at specific water velocities.....	81
Figure 4-19: Oxygen Transfer Efficiency vs. Water Velocity at specific air/water flow ratios...	81
Figure 4-20: Effect of deflector presence. Oxygen Transfer Efficiency vs. Air Void Ratio at specific water velocities.....	82
Figure 4-21: Effect of mesh presence. Oxygen Transfer Efficiency vs. Air Void Ratio at specific water velocities .....	83
Figure 4-22: Total Aeration Constant vs Air Void Ratio at specific water velocities .....	84
Figure 4-23: $K_L a$ vs Water Velocity; $H = 13.5\text{ mm}$ , $L/H = 2$ .....	85
Figure 4-24: Measured vs Modelled Total Aeration Coefficient.....	87

## List of Tables

Table 2-1: Threshold daily mean DO concentrations taken from ( <i>Canadian Water Quality Guidelines for the Protection of Aquatic Life - DISSOLVED OXYGEN (freshwater)</i> , 1999) and (USEPA, 1988) .....	7
Table 3-1: Instruments list for McGill Experimental Apparatus .....	47
Table 3-2: Instruments list for Vevey Experimental Apparatus .....	52
Table 3-3: McGill Test Parameter Ranges.....	54
Table 3-4: Vevey Test Parameter Ranges.....	54
Table 3-5: Geometric configurations of deflector samples.....	55
Table 4-1: Validation Tests, Results and Parameters .....	60

## List of Symbols and Abbreviations

$^{\circ}\text{C}$	<i>degrees Celsius</i>
<b>1D</b>	<i>one-dimensional</i>
<b>3D</b>	<i>three-dimensional</i>
<b>A</b>	<i>interstitial contact area between water and air bubbles</i>
<b>a</b>	<i>specific interstitial contact area between water and air bubbles</i>
<b>A<sub>b</sub></b>	<i>surface area of bubble</i>
<b>α</b>	<i>channel slope</i>
<b>AVT</b>	<i>auto venting turbine</i>
<b>β</b>	<i>free exponent</i>
<b>C</b>	<i>oxygen concentration</i>
<b>C<sub>1</sub></b>	<i>upstream oxygen concentration</i>
<b>C<sub>2</sub></b>	<i>downstream oxygen concentration</i>
<b>C<sub>a</sub></b>	<i>oxygen concentration in air</i>
<b>CFD</b>	<i>computational fluid dynamics</i>
<b>C<sub>s</sub></b>	<i>oxygen saturation concentration</i>
<b>C<sub>T</sub></b>	<i>proportionality constant</i>
<b>C<sub>w</sub></b>	<i>oxygen concentration in water</i>
<b>D</b>	<i>molecular diffusivity of oxygen in water</i>
<b>D</b>	<i>diameter of air inlet</i>
<b>DAQ</b>	<i>data acquisition system</i>
<b>dC</b>	
$\frac{dC}{dt}$	<i>Lagrangian rate of change of oxygen concentration in water</i>
$\frac{dm}{dt}$	<i>oxygen mass flux into water</i>
<b>DO</b>	<i>dissolved oxygen</i>
<b>e</b>	<i>exponential</i>
<b>E</b>	<i>oxygen transfer efficiency</i>
<b>ε</b>	<i>dissipation rate of turbulent kinetic energy</i>
<b>g</b>	<i>acceleration due to gravity</i>
<b>γ</b>	<i>ratio of specific heats at constant volume and constant pressure</i>
<b>H</b>	<i>Henry's Law constant</i>
<b>H</b>	<i>characteristic size of the deflector</i>
<b>K</b>	<i>transfer coefficient</i>
<b>K</b>	<i>degrees Kelvin</i>
<b>K</b>	<i>proportionality constant</i>
<b>K<sub>l</sub></b>	<i>liquid film coefficient</i>
<b>K<sub>l</sub>a</b>	<i>total aeration coefficient</i>
<b>K<sub>s</sub></b>	<i>equivalent sand roughness height</i>
<b>L</b>	<i>bubble travel distance between measurement points</i>
<b>L</b>	<i>channel length</i>
<b>L/H</b>	<i>relative position of air inlet</i>

$\mathcal{L}$	<i>integral length scale of turbulent eddies</i>
<b>Mach</b>	<i>Mach number</i>
<b>NPS</b>	<i>National Pipe Size</i>
<b>NPSH</b>	<i>Net Positive Suction Head</i>
<b>NPT</b>	<i>National Pipe Thread</i>
<b>NPTF</b>	<i>National Pipe Thread Female</i>
$\nu_l$	<i>kinematic viscosity of water</i>
$P_1$	<i>upstream water pressure</i>
$P_2$	<i>air inlet pressure</i>
$P_{air\ inlet}$	<i>pressure at air inlet</i>
$P_{atm}$	<i>atmospheric pressure</i>
$Pe_b$	<i>bubble Péclet number</i>
$\phi$	<i>air void ratio</i>
$\pi$	<i><math>\rho_i</math></i>
<b>PVC</b>	<i>poly vinyl chloride</i>
$P_w$	<i>water pressure</i>
$q_w$	<i>water discharge per unit width</i>
$Q_w$	<i>water flow rate</i>
$(q_w)_c$	<i>characteristic water discharge per unit width</i>
$R_b$	<i>mean bubble radius</i>
$Re_b$	<i>bubble Reynolds number</i>
$\rho_a$	<i>gas density</i>
$\rho_l$	<i>density of liquid</i>
<b>Sc</b>	<i>Schmidt number</i>
$\sigma$	<i>surface tension between gas and liquid</i>
$T$	<i>temperature</i>
$t$	<i>time</i>
$T$	<i>residence time of bubbles between measurement points</i>
$T_0$	<i>reference temperature</i>
$\tau_w$	<i>residence time of water in recirculating flow</i>
<b>TDSS</b>	<i>Total Dissolved Suspended Solids</i>
$U$	<i>mean water velocity</i>
$U_a$	<i>gas velocity</i>
$V$	<i>volume of air/water flow mixture</i>
$V_b$	<i>volume of spherical bubble</i>
<b>VOF</b>	<i>volume of water</i>
$\zeta$	<i>scale effect parameter</i>

## Chapter 1: Introduction

For centuries, humanity has harnessed the power of water for energy production. From water wheel mills in the Eastern Han dynasty to modern pump-turbines, it is difficult to find a waterway close to settlements that has not been manipulated by humans. Hydropower dams are a fundamental part of our modern energy supply. However, large impoundments of water behind hydropower dams are vulnerable to several environmental concerns, one of which is the deoxygenation of water due to thermal stratification in the reservoirs.

During the summer months, the reservoirs' surface waters are heated by the sun, forming a less-dense (higher-buoyancy), relatively thin layer called the epilimnion. The water under this layer, in the hypolimnion, does not get warmed due to inhibition of mixing across the thermocline due to the stratification, resulting in a colder, denser, and less-buoyant layer of water. This stratification occurs and is not disrupted in reservoirs located in warm climates (Wilhelms *et al.*, 1987) In northern climates there is overturning of the water column due to surface cooling as the point of maximum density for water of 4°C is attained in the spring and fall months.

Thermal stratification of reservoirs can lead to discrete layers of dissolved oxygen (DO) concentration, which mirrors the thermal stratification. Biological activity and the decomposition of organic sediments require oxygen, which, in the hypolimnion, cannot be replenished from the atmosphere. The surface waters remain oxygenated due to contact with the atmosphere; wind and waves result in the dissolution and mixing of oxygen throughout the epilimnion. Turbines extracting water at depth release the low dissolved oxygen (DO) water of the hypolimnion downstream, resulting in adverse environmental impacts. Many new hydropower licenses have provisions to require proper control of DO concentration to protect the ecosystem (Black *et al.*, 2002; EPRI, 2002).

Several methods exist for aerating deoxygenated flows in hydropower installations. The focus of this study is draft tube aeration using elbow deflectors. The elbow deflector directs the flow away from the wall of the draft tube causing flow separation and creating a low-pressure wake in which an air inlet will naturally aspirate air, as shown in Figure 1-1. This project seeks to quantify the performance of these elbow deflectors in terms of their aerating capacity and their resulting oxygen transfer efficiency. It should be noted that the presence of deflectors in draft tubes creates efficiency losses in turbine operation. The prediction and measurement of these losses are beyond the scope of this study. However, a review of these impacts is given in Sections 2.2.1 & 2.3.1

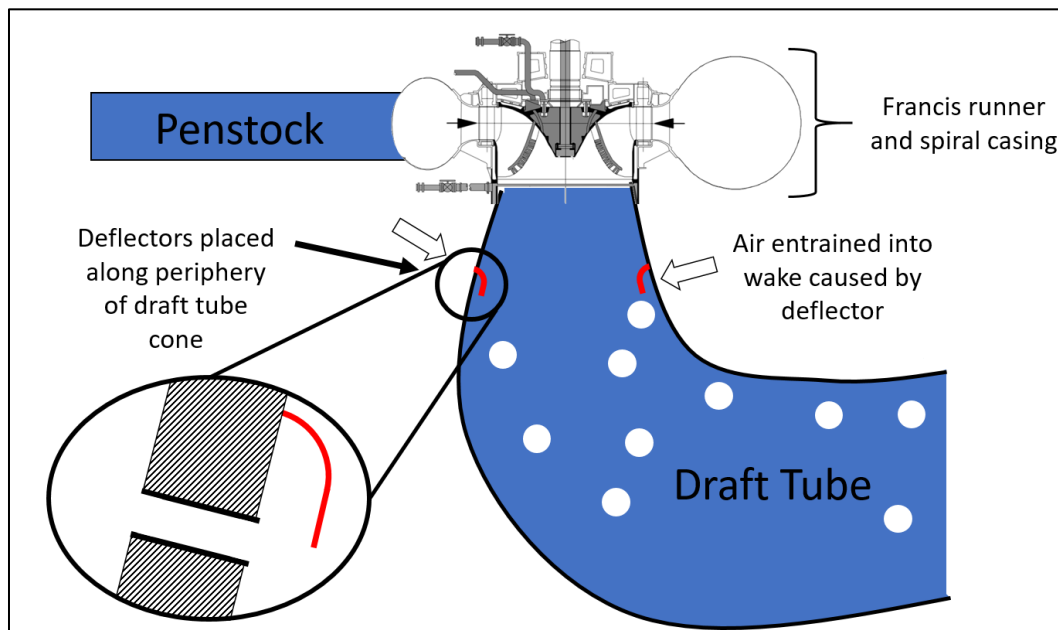


**Figure 1-1: Deflectors placed around periphery of draft tube leading to air entrainment and oxygen exchange**

### 1.1 Novelty of the Study

The mechanisms of two-phase flow in closed conduits are complex and researchers have taken various approaches to increase understanding the physics of these flows. Generally, two techniques are possible: (1) computational models and (2) physical models. Physical models can

be further broken down into (1) full-scale studies with prototype turbines and (2) simplified, laboratory-scale models. In the case of physical models, the many degrees of freedom and the incomplete understanding of the mechanisms of gas exchange mean that a simplified model should first be thoroughly understood before tackling the full-scale problem. A simplified model gathers data, which can then be used to validate a computational fluid dynamics (CFD) model. The validated and calibrated CFD model (i.e. multiphase modelling, gas dynamic behavior, and turbulence model) can then be used for design at the full scale. This study has reduced the many degrees of freedom within deflector-induced draft tube aeration to the key gas, geometric, and hydraulic parameters. With this reduction, the importance of each parameter can be analyzed, and the underlying physics of the gas exchange process can be elucidated. This study collected data for a range of operating conditions to provide the information needed to develop the framework for a more complete experimental investigation of the process in the future.

## **1.2 Research Objectives**

A scale model investigation of draft tube aeration was performed to study the effect of the geometric configuration of the deflector on the entrainment rate of air, the oxygen mass transfer rate into the flow and the resulting bubble swarm characteristics. The lower water velocity data (0.38-2 m/s) will also be used to validate computational fluid dynamics modelling of oxygen mass transfer in draft tubes. Simplified upstream boundary conditions are modelled due to space and budget limitations, and thus, instead of the deflectors being placed in the draft tube downstream of a turbine runner, which would impose swirl on the flow, the deflectors will be studied in a horizontal pipe with no swirl. The low velocity tests quantified the relative oxygenation possible with different geometric configurations of the deflector setup, namely – the size and placement of the air intake port relative to the deflector, through analysis of DO levels measured at two locations downstream of the deflector and from qualitative images of the bubble swarm produced. High-

velocity tests ranked the different geometric configurations for aeration efficiencies (i.e. which deflector setup can more effectively draw in air flow for a given water velocity). The experimental results from the low-velocity tests permitted the development of a theoretical description of the mass transfer in horizontal bubbly flows and were used to calibrate a relation predicting oxygen uptake rates for a range of water velocities and gas void ratios. The high velocity test data was used to elucidate the scale effects in the measured pressure wake between different sizes of deflectors and for a range of high water velocities. The ultimate aim of the project is the prediction of oxygen uptake rates in draft tubes using elbow deflectors. To summarize, in collaboration with Andritz Hydro Canada, the specific objectives of this research are:

1. To quantify the oxygen mass transfer rate for three sizes of deflector, having three air entrainment inlet port locations for a range of flow velocities (0.38 – 2 m/s) and air/water discharge ratios (0 – 10%)
2. To determine the air entrainment rates of the different geometric configurations of the deflectors, based on the pressure difference between the upstream water and the injection point
3. To elucidate the scale effects from comparison of the results for the three deflector sizes to inform the design of deflectors at the prototype scale
4. To collect data to calibrate and validate a computational model that is being developed as a parallel project at Andritz Hydro Canada

## **Chapter 2: Literature Review**

This chapter will present the literature on oxygen mass transfer in turbine aeration. The regulatory environment requiring oxygenation downstream from turbines is presented first as it provides the motivation for the study. A theoretical description of the oxygen mass exchange process in draft tubes follows. Finally, the previous laboratory, model, and prototype aeration studies are reviewed.

### **2.1 Dissolved Oxygen Monitoring and Regulations**

Reservoir stratification occurs in warm climates, and both its hydraulics and biology have been extensively studied. The stratification arises from the thermal gradient produced by heating from the sun. A relatively thin layer of warm, buoyant water called the epilimnion forms above the colder, denser depths of the reservoir, called the hypolimnion. This stratification inhibits vertical mixing across the metalimnion (lying between the epilimnion and the hypolimnion). Biological activity requires DO throughout the water column, which cannot be replenished in the hypolimnion due to the lack of contact with the atmosphere and lack of mixing with the epilimnion. The lack of vertical mixing, present mainly in large, deep reservoirs where velocities are low, leads to very low DO concentrations in the hypolimnion. When turbines, extracting water at depth, release this water downstream, DO concentrations can remain low in the river for several kilometers and aquatic life effectively suffocates (EPRI, 1990; Grenier *et al.*, 2010; March, 2011). An example of a thermal profile in a stratified lake is shown in Figure 2-1.

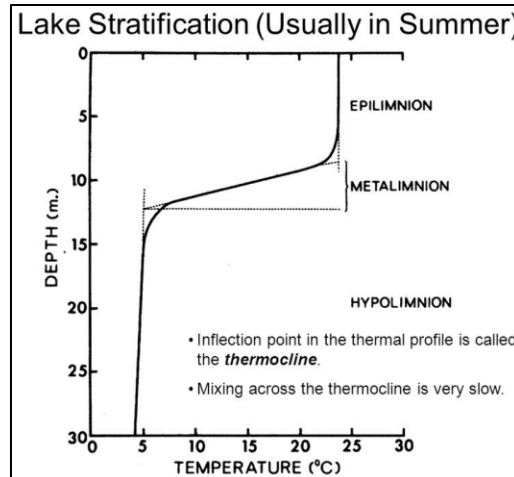


**Figure 2-1: Example thermal profile in a stratified lake (Jacobs, 2014)**

The absence of DO in the reservoir water also impacts the complex physiochemical balance present in water. DO impacts the presence of hydrogen sulfide, heavy metals, sulfates, and phosphates in addition to other parameters (Pastorok *et al.*, 1982; USEPA, 1988; Wilhelms *et al.*, 1987). The aeration of turbines may also affect these other parameters but are outside the scope of this study.

In the US, the 1972 Clean Water Act prevents the release of pollutants into waterways without a National Pollutant Discharge Elimination System permit issued by the Environmental Protection Agency (USEPA). The release of anoxic water by turbine operators is regulated by the 1986 Electric Consumers Protection Act (Peterson *et al.*, 2003) as anoxic conditions can remain for many kilometers downstream of turbines, impacting aquatic life. A 1988 report from the USEPA standardized DO concentration limits in waterways as a function of whether they were warm or cold-water sources. Several major reports have been published on the general methods of aerating an anoxic hypolimnion and on the effect of low DO on various forms of aquatic life (EPRI, 1990, 2002; Pastorok *et al.*, 1982).

As reservoir stratification usually occurs in warm climates (Southern US latitudes), Canada lacks the legislation that the US federal and state governments have. In the US, a 2002 report showed that 40.2% of hydropower plants relicensing procedures had specific language regarding the mitigation and/or monitoring of low DO concentrations in hydropower plant tailwaters (Black et al., 2002). The approach from Canada has been to develop DO concentration limits using the USEPA guidelines as a reference. Table 2-1 shows these limits in the US and Canada. The difference in DO requirement between the cold and warm-water species is because of the higher DO solubility in cold-water, increasing the levels of DO cold-water aquatic life is accustomed to.

**Table 2-1: Threshold daily mean DO concentrations taken from (*Canadian Water Quality Guidelines for the Protection of Aquatic Life - DISSOLVED OXYGEN (freshwater), 1999*) and (USEPA, 1988)**

Country	Ecosystem	Early life stages	Other life stages
Canada	warm-water	6 mg/L	5.5 mg/L
Canada	cold-water	9.5 mg/L	6.5 mg/L
United States	warm-water	5.0 mg/L	3.0 mg/L
United States	cold-water	8.0 mg/L	4.0 mg/L

## 2.2 Governing equations

### 2.2.1 Air admission in hydro turbines

The admission of air into turbines is driven by the pressure difference between the ambient atmosphere and the lower pressure at the air inlet within the turbine. Natural aspiration may be possible if the pressure at the air inlet is negative when compared to the ambient, but this depends on the submergence of the runner. If natural aspiration is not possible, forced aeration may be necessary. Low pressure zones are present naturally at several locations within a Francis turbine.

These are:

1. Along the trailing edge of the turbine runner blade
2. At the runner cone
3. Along the discharge ring

The quality and characteristics of the aeration occurring through each of these three locations is described in Section 2.3.1

Air admission through turbines is a promising method to introduce air into the deoxygenated water flowing through the hydropower plant. However, many times, the high capital cost prevents the development of an aerating turbine, or site-specific restrictions prevent the implementation of aerating schemes within the turbine itself. In these situations, the draft tube of the hydropower plant is an excellent place to introduce air into a turbine and may outperform turbine aeration schemes. The velocity of water in the draft tube does not generally differ from that in the turbine, but the pressure is lower due to the energy extracted from the flow in the turbine and the incompressibility of water. It is possible to create a large negative pressure zone at the wall of the draft tube by inducing flow separation in this moderate-velocity but low-pressure flow. As described in previous sections, deflectors placed along the periphery of the draft tube create a low-pressure zone, which, if connected to the ambient atmosphere via an air supply system, results in the entrainment of air into the water flowing through the draft tube.

The sharp gradients of pressure and velocity within the aeration system and at the air inlet location within the draft tube require the use of a complex form of the Bernoulli equation to calculate the air flow rate through the air supply system, regardless of the aeration scheme used (Cantwell, 2005). At the air inlet within the draft tube, the sharp gradient in pressure is moderated by slight changes in density. To accurately quantify the air flow rate, the air pressure at the air inlet must be measured. In practice this is difficult and therefore the air pressure and flow rate are generally measured at a location far upstream within the air supply system. To calculate the air pressure at the air inlet the isentropic, steady, sub-sonic 1D compressible flow equation is used to

determine the flow rate through the air supply system using measurements far upstream (Cantwell, 2005):

$$\frac{P_{atm}}{P_{air\ inlet}} = \left(1 + \frac{\gamma - 1}{2} * Mach_{air\ inlet}^2\right)^{\frac{\gamma}{\gamma-1}} \quad [1]$$

where  $\gamma$  = the ratio of the specific heat at constant pressure and at constant volume of the flowing gas. The air flow rate can be modified in several ways and is also dependent on the turbine operating point. It can be adjusted by changing the pressure at the air inlet in the draft tube wall by placing deflectors or baffles just upstream of the air inlet in the turbine which lowers  $P_{air\ inlet}$ , or a compressor or blower can be attached to the upstream end of the air supply system to increase  $P_{atm}$  to greater than atmospheric pressure. The turbine operating point (i.e. the level to which the turbine wicket gates are opened) can change the water pressure within the draft tube near the air inlet, also affecting the air flow rate. The operating conditions of the turbine and the aeration system, which set the flow rates of water and air respectively, set the void ratio of air in the water (Figure 2-2). The DO increase between the headwaters and the tailwaters of the turbine are a function of the void ratio of the air, the characteristics of the voids such as the bubble size distribution, and the turbulent characteristics of the air/water flow mixture. The increase in DO comes at the cost of the mean turbine efficiency due to losses, due to form drag on the deflectors and due to the aeration of the flow.

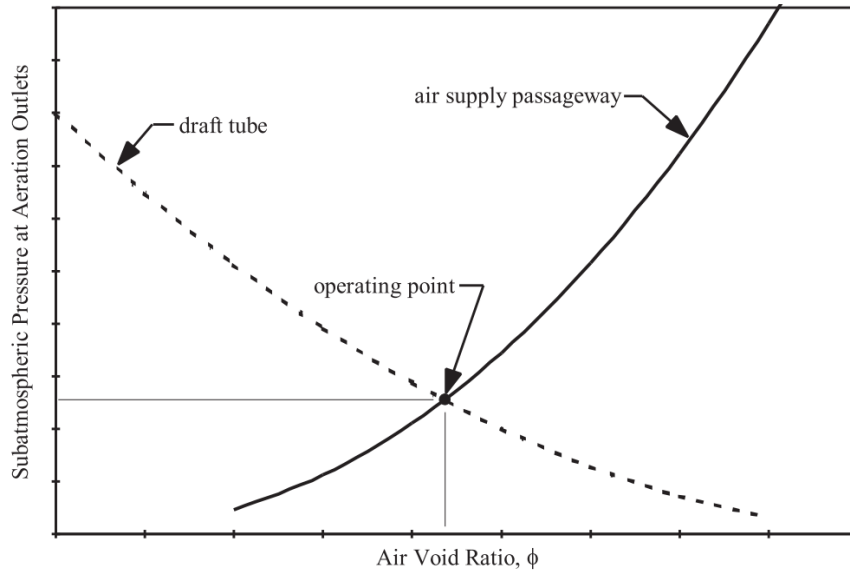


**Figure 2-2: Air void ratio in draft tube (Hopping *et al.*, 2009)**

The entrainment of air into the draft tube results in turbine efficiency losses. Equations for the efficiency losses due to air entrainment are semi-empirical and have been developed for specific aeration systems (see Section 2.3.1 ). Almquist *et al.* (1991) developed theoretical relations to estimate turbine efficiency loss due to the presence of air downstream of the turbine and compared them with losses measured in a prototype study. The equations predicted the trend in efficiency losses but were not accurate enough for prototype design indicating that model studies are required for improved estimations.

### 2.2.2 The Oxygen Mass Transfer Equation

The development of an equation predicting oxygen exchange between injected bubbles and anoxic water flowing through a draft tube is based on mass conservation. The simplest form of the equation, as stated by Gulliver *et al.* (1990) is:

$$\frac{dm}{dt} = KA \left( \frac{C_a}{H} - C_w \right) \quad [2]$$

where  $dm/dt$  = oxygen mass flux into the water;  $K$  = transfer coefficient;  $A$  = interstitial surface area between the bubbles and the water;  $C_a$  = concentration of oxygen within the air bubble (9.01

mg/L);  $C_w$  = concentration of oxygen in the water; and  $H$  = Henry's Law constant. In the case of oxygen, the constants can be combined, and the equation takes the form:

$$\frac{dC}{dt} = K_l a (C - C_s) \quad [3]$$

Where  $C$  = oxygen concentration in water,  $K_l$  = liquid film coefficient (a parameter governing the exchange of oxygen across the liquid-gas interface),  $a$  = specific contact area of the air-water flow mixture [ $A/V$ ],  $A$  = as defined above,  $V$  = control volume of the air-water flow mixture, and  $C_s = C_a/H$  = saturation concentration of oxygen in water. The Henry's Law constant has a dependence on temperature described by the Van't Hoff equation (Atkins & De Paula, 2006):

$$H(T) = H(T_0) e^{\left[-C_T \left(\frac{1}{T} - \frac{1}{T_0}\right)\right]} \quad [4]$$

Where  $H(T)$  = the temperature dependent Henry's Law constant;  $H(T_0)$  = reference Henry's Law constant at  $T_0$  (usually 293.15 K);  $C_T$  = proportionality constant of 1700;  $T$  = temperature in K.

The term  $K_l a$  is referred to as the total aeration coefficient. When integrated, a non-dimensional, oxygen transfer efficiency ( $E$ ) can be derived, as stated by Thompson and Gulliver (1997):

$$-\ln(1 - E) = K_l a t \quad [5]$$

where:

$$E = \frac{C_2 - C_1}{C_s - C_1} \quad [6]$$

The oxygen transfer efficiency can be calculated either by measuring the difference in DO between two points along the travel path of the bubbly mixture or by measuring the evolution with time of the DO concentration at a single point in a recirculating flow. In the first case,  $C_2 =$

downstream oxygen concentration (such as in the tailwaters of a dam);  $C_1$  = upstream oxygen concentration (such as in the headwaters of a dam); and  $t$  = residence time of the bubbles between the two measurement points. The calculation of  $t$  commonly takes the form of:

$$t = \frac{L}{U(1 + \phi)} \quad [7]$$

where  $L$  = bubble travel distance;  $U$  = mean water velocity; and  $\phi$  = gas void ratio [ $Q_a/(Q_a + Q_w)$ ] (Jun, 1991). In the case of a recirculating flow with only one oxygen measurement point,  $C_2$  and  $C_1$  are any two oxygen concentration measurements; and  $t$  is the time interval between these two measurements.

Gulliver et al. (1990) developed an equation to convert the measured gas transfer efficiency at specific gas temperatures, surface tensions, and viscosities to other conditions. They developed two equations, with one being a simplified quadratic approximation of the other expression. A standard approach is to use their equation to standardize the oxygen exchange measured to a standard temperature of 20°C so that results of other studies can be compared to a baseline (Ruane & McGinnis, 2007; Unsal *et al.*, 2008).

The total aeration coefficient describes the average bulk efficiency; however, it does not describe the local aeration mechanisms. The total aeration coefficient is not constant throughout the bubbly flow (due to changes in the bubble size and turbulent intensity) and must be separated into its constituent parts for implementation in CFD (Chanson, 2002). The following sections describe different techniques for separately modelling the liquid film coefficient and the specific interstitial contact area.

### 2.2.3 The Liquid Film Coefficient; $K_l$

Jun (1991) measured the evolving dissolved oxygen concentration at a single point in a recirculating flow with air injection occurring. He calculated the total aeration coefficient and modelled the contribution of the interstitial contact area by measuring the mean bubble size in the aeration region through an imaging technique. His relation was:

$$K_l = k \frac{U^{1.36} \mathcal{L}^{0.36}}{\nu_l^{0.36} \phi^{0.225}} \quad [8]$$

Where  $U$  = mean water velocity;  $\mathcal{L}$  = integral length scale of turbulent eddies;  $\nu_l$  = kinematic viscosity of water;  $\phi$  = gas void ratio. The equation fit the study data well, however, the strong dependence on gas void ratio,  $\phi$ , has not been observed in other experimental aeration studies (Thompson & Gulliver, 1997).

Chanson (1996) wrote a comprehensive textbook on air-water flows and gave several semi-empirical correlations and analytical formulations for the gas transfer process. He reviewed both work he was directly involved with and the work of others. Approaches in calculating the gas transfer coefficients varied, with some quantifying the liquid film coefficient through empirical constants and traditional hydraulic non-dimensional numbers and others modeling the oxygen transfer efficiency using the traditional gas transfer equation. The full description is found within the reference. As an example, Chanson (1996) presented his own equation for modeling the non-dimensional gas transfer efficiency as:

$$E = \left(1 - \frac{q_w}{(q_w)_c}\right)^{(15.38 - 0.035 * T) * (\sin \alpha)^{-\frac{1}{3.13}}}; (q_w)_c = 0.0805 * L^{1.403} * (\sin \alpha)^{0.388} * k_s^{0.0975} \quad [9]$$

Where  $q_w$  = water discharge per unit width  $\left(\frac{m^2}{s}\right)$ ,  $(q_w)_c$  = characteristic water discharge per unit width  $\left(\frac{m^2}{s}\right)$ ,  $\alpha$  = channel slope ( $^\circ$ ),  $T$  = water temperature (K),  $L$  = channel length (m), and  $k_s$  = equivalent sand roughness height (m), (the other variables as defined above).

Thompson and Gulliver (1997) developed an equation relating  $K_l$  to the water velocity, turbulence characteristics and gas coefficients. They combined the work of Levich (1962) and Azbel (1981), who respectively studied the velocities of different sized bubbles, and the gas dissolution process in which the dissolution process is modeled as driven by the turbulence caused by rising bubbles in a stagnant fluid. As the dissolution process in draft tubes is not driven by similar turbulence characteristics, the equation of Thompson *et al.* (1997) was modified, by adding a free variable,  $\beta$ , which allows the equation to be calibrated for different aeration systems (aerating turbines, aerating weirs, hydraulic jumps, etc.).

$$K_l = k \left( \frac{DU^\beta}{L^{2-\beta} \nu_l^{\beta-1}} \right)^{\frac{1}{2}} \quad [10]$$

Where  $D$  = molecular diffusivity of oxygen gas in water, (the other variables are as defined above). As they were interested in a similarity relation for the oxygen transfer efficiency, the constant of proportionality was not calculated.

Politano *et al.* (2010) studied the total dissolved gas dynamics in the tailrace of a dam spillway. A 3D volume of fluid (VOF) model was developed and the total dissolved gas concentration was analyzed as it evolved within the spillway tailrace. The liquid film coefficient was taken as the maximum value between that for bubbles rising in a quiescent fluid and that for bubbles in a turbulent flow:

$$K_l = \max \left[ \frac{DP_b^{0.5}}{\sqrt{\pi} Re_b} \left( 1 - \left( \frac{2}{3 \left( 1 + 0.09 Re_b^{\frac{2}{3}} \right)^{0.75}} \right) \right), 0.4 Sc^{-\frac{1}{2}} (\nu_l \epsilon)^{\frac{1}{4}} \right] \quad [11]$$

where  $P_b$  = bubble Péclet number;  $Sc$  = Schmidt number;  $Re_b$  = bubble Reynolds number; and  $\epsilon$  = dissipation rate of turbulent kinetic energy per unit mass. This is because, depending on the turbulent characteristics within each individual cell, different dissolution mechanisms govern, and the model was developed to accurately switch between the two mechanisms.

#### 2.2.4 The specific interstitial contact area; $a = A/V$

The surface area and volume of a spherical bubble area are given by,

$$A_b = 4 \pi R_b^2 \quad [12]$$

$$V_b = \frac{4}{3} \pi R_b^3 \quad [13]$$

Where  $R_b$  = mean bubble radius;  $A_b$  = surface area of bubble; and  $V_b$  = volume of a spherical bubble. The volume of the air/water mixture in a bubbly flow is approximated by  $V = V_b/\phi$ .

Completing the necessary substitutions, the specific interstitial contact area is:

$$a = \frac{3\phi}{R_b} \quad [14]$$

Azbel (1981) studied the bubble size distribution for a variety of gas void ratios in bubbly flows. He verified the above simple relation for  $\phi = [0, 20]$  % and developed a more complex equation valid at higher gas void ratios. Calculation of the interstitial contact area requires a precise measurement of the mean bubble size.

Hinze (1955) studied the mean bubble size between two rotating cylinders and suggested that the mean diameter was dependent on the ratio between the surface tension and shear forces within the fluid.

$$R_b = k \left( \frac{\sigma}{\rho_l} \right)^{\frac{3}{5}} \epsilon^{-\frac{2}{5}} \quad [15]$$

Where  $\sigma$  = surface tension between the gas and liquid; and  $\rho_l$  = the density of the liquid, the other variables are as defined above. Other studies validated the above equation, changing only the proportionality constant for different aeration configurations (Thompson & Gulliver, 1997).

Jun (1991) performed experiments to observe the bubble size distribution in a vertical pipe downstream of an air inlet in a recirculating flow using an imaging technique. Assuming an oblate spheroid shape for the bubbles, the major and minor axis of the bubble diameter is taken for each bubble in the image. The interstitial contact area was calculated using the total surface area of all visible bubbles.

Wilkinson *et al.* (1994) injected air into a stagnant column of water deoxygenated with sodium sulfite under high pressure. Using an imaging technique, they developed an equation for the mean bubble size valid over a broad range of air void ratios, pressures, and air velocities.

$$R_b = \frac{3}{2} g^{-0.44} \sigma^{0.34} \nu_l^{0.22} \rho_l^{-0.45} \rho_a^{-0.11} U_a^{-0.02} \quad [16]$$

Where  $g$  = acceleration due to gravity;  $\rho_a$  = density of gas;  $U_a$  = the gas velocity. This empirical relation, while relatively simple, has shown good agreement in other laboratory settings, although it does not consider the effect of bubble breakup and coalescence (Yin *et al.*, 2012).

Xu and Xu (2002) used a force balance on an air bubble detaching from a circular hole in a liquid co-flow to develop a theoretical equation of the bubble size as a function of the air inlet diameter and the flow velocity.

$$1.95 * 10^8 R_b^{10} + 2.08 U^2 R_b^6 = D^8 U_a^4 \quad [17]$$

Where  $D$  = diameter of the air inlet. The bubble sizes predicted for a range of fluid velocities and hole diameters were verified with an imaging technique and with data from other literature. The calculated bubble sizes fell completely within the experimental range of bubble sizes of the compared literature.

Chanson (2002) studied the interstitial contact area in flows over with a range of air void ratios and developed a probe capable of measuring the mean bubble size and velocity. Exploiting the difference in electrical resistivity between air and water, a conductive probe with two electrodes arranged in an annular configuration can capture when the probe tip is within an air pocket in the flow. With a large enough sampling time, the bubble size distribution was quantified, and the interstitial contact area calculated.

### **2.3 Aeration in Hydraulic Structures for increasing DO concentrations**

Aeration is an important feature of hydraulic structures. Aeration can be beneficial or detrimental. Aeration on spillways is used to mitigate cavitation on concrete spillway faces. Francis runners can be aerated to attenuate pressure fluctuations in the draft tube. Bottom outlets need aeration to prevent cavitation at the downstream lip of the control gate (Chanson, 1996; Smith & Saskatchewan, 1995). These schemes contribute to increasing DO of flows passing through a hydropower plant. Turbine aeration is an attractive choice for increasing DO concentrations as it minimally impacts hydropower plant operation. Alternatives such as spilling, sluicing, or siphoning the water to aerate the flow would reduce the flow through the turbines, impacting the

revenue stream. Turbine aeration allows the thermal stratification in the reservoir to be maintained, thus supporting cold water fisheries in hydropower plant tailwaters (Hopping et al., 2009).

Francis turbine aeration has long been used to stabilize pressure pulsation for critical part-load operations. Environmental use of aeration began in the 1950's, when a Wisconsin hydropower plant used an existing vacuum breaker system to treat waste from the pulp and paper industry passing through its turbine (Thompson & Gulliver, 1997). In the 1950's in Europe, researchers began the development of aerating turbines specifically to increase DO concentrations in water passing through low-head dams. By 1961, 18 hydropower plants in the United States had vacuum breaker aeration systems which stabilized turbine operations and, as a by-product, increased DO concentrations, but with high efficiency losses to the turbine operation. Typically, these systems have the lowest cost as they are already in place and, for the purpose of increasing DO concentrations, only need to be modified to operate for longer periods of time (*Best Practice Catalog - Francis Turbine Aeration*, 2012).

During the 1970's and 80's, the Tennessee Valley Authority developed aerating turbines, which injected air at locations where negative pressures naturally existed. They used streamlined baffles and deflectors placed on the turbine runner cone, head cover, or along the discharge ring to minimize turbine efficiency losses. These locations are shown in Figure 2-3. At the Tennessee Valley Authority's Norris project, runner cone aeration showed uptakes of 2-3 mg/L of oxygen with additional turbine losses of 1-2% when the turbine was aerating. The Tennessee Valley Authority partnered with Voith Hydro during the 1980's to optimize aerating turbine designs. They developed hollow turbine blades through which air could be injected at the runner exit. These systems were by far the most efficient at the time but were very costly. Since DO is generally a seasonal problem, aerating schemes with reduced turbine efficiencies create a constant loss to

hydropower plant operators that are undesirable especially when the initial turbine is so expensive  
(*Best Practice Catalog - Francis Turbine Aeration*, 2012).

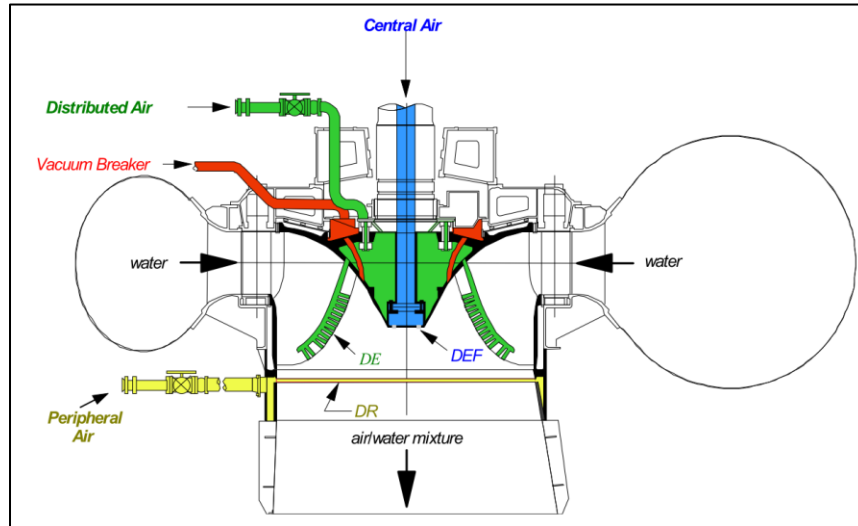


**Figure 2-3: Air inlets placed at negative pressures within a Francis turbine; runner cone (blue), hollow turbine blades (green), vacuum breaker system (red), discharge ring (yellow) (March, 2011)**

As an alternative to modifying the turbine design, adding deflectors around the periphery of the draft tube wall provides a cheap method by which air can be admitted into the turbine discharge as needed without significantly impacting turbine efficiencies during periods of non-aeration. If site-specific access exists, deflectors or baffles can be placed just upstream of air inlets in the draft tube to lower the local pressure, which are vented to the ambient atmosphere. Substantial volumes of air can be entrained without the need for compressors or blowers. During seasons where low DO is not a concern, these baffles or deflectors could be designed to be easily removed and normal turbine efficiency is maintained.

The state-of-the-art in increasing DO concentrations in water passing through turbines has experienced substantial improvement in the last few decades. The EPRI has published a series of five reports on the topic of reaerating turbine outlets for the purpose of increasing DO

concentrations in tailwaters. EPRI (1990) provided a step-by-step guide in selecting an aerating solution based on site-specific characteristics. As the first report in the series, it extensively covered the biological impacts of low DO and the range of aeration solutions available. Turbine venting is cited as a low-cost solution, when compared to reservoir de-stratifiers or oxygenators, but having high efficiency losses and unpredictable behavior. The need for greater research and accessible industry guidelines was expressed. The report stated that a mixed aeration approach is often the most cost-effective with turbine aeration coupled with reservoir destratification or pure oxygen injection in the forebay. EPRI (1997) provided a design guide-book for aerating weir design. At sites where the increased capital cost can be justified, aerating weirs provide a constant source of aeration, without impacting the sometimes-beneficial thermal stratification in the reservoir that supports downstream fisheries. EPRI (2002) was an update to the 1990 report which was written when specific hydropower plant licensing stipulations regarding DO levels were still new. The state-of-the-art in turbine venting technologies was discussed in addition to case studies of several hydropower plants. DO uptakes of between [2, 4] mg/L showed the ongoing optimization of systems from the 1990 report, when similar uptakes were generally only possible when turbine venting was used in conjunction with other aeration solutions. EPRI (2009) & EPRI (2013) gave additional case studies and focused primarily on turbine venting solutions. Given the low cost and the large room for improvement, turbine aeration has been selected as the most attractive solution to increasing DO levels. However, the lack of a central database of aeration studies precludes the continued optimization of aeration solutions. A unified approach must be developed to allow all hydropower plant operators to meet threshold DO levels.

Retrofit aeration implementations, in addition to aerating turbines were the subject of extensive testing between 1990 and 2010. Prototype implementations at numerous hydropower

plants have allowed for evaluation of a range of aerating solutions. An overview of these studies is given in the next section. A subsequent section details the laboratory tests studying oxygen exchange rate under simplified conditions. A key difference between the model/full-scale and laboratory studies is that the aeration in the model/full-scale studies occurs due to natural aspiration driven by negative pressure at the injection point, which is difficult to replicate in a small-scale laboratory setup.

### **2.3.1 Model and Full-scale studies**

A 1994 study at the Deer Creek powerplant showed that turbine aeration was an attractive solution in increasing DO concentrations by aeration from the central runner cone. The safety of the system was a key as aeration was previously thought to potentially induce dangerous stresses in and produce vibrations of the runner. Measurements reported that the vibrations were within the safety margins. Oxygen transfer efficiencies of between [10, 50] % were correlated with turbine efficiency losses of [-3, 6] %. The gain in turbine efficiency, given as a negative turbine efficiency loss, is due to the destruction of the stable cavitation vortex usually occurring at part load. The injection of air fills the space where the vortex would be created and thus improves the efficiency. However, the efficiency losses were substantial at normal and peak loads, showing the limitations of a central runner cone aeration scheme (Wahl *et al.*, 1994).

Thompson and Gulliver (1997) partnered with the Norris Tennessee Valley Authority project to study the oxygen exchange process in vacuum breaker turbine aeration over a range of flow conditions. From their parametric study a similitude relation for the oxygen transfer rate based on the theoretical work of Azbel (1981) and Hinze (1955) was developed. This equation contains a free exponent which can be used to calibrate the similitude relation for different aerating schemes (see Section 2.2.32.2.2 ).

Papillon *et al.* (2002) observed the quantity and quality of aeration through a Francis turbine with air being injected at locations where negative pressures naturally develop. Aeration through the runner cone, a modified runner cone with baffles, a modified runner cone with a step in the middle and a band around the draft tube were all studied for their ability to entrain air and create an optimized bubble swarm capable of distributing the bubbles evenly throughout the flow. The effects of each aerating scheme, with and without activation of the aeration, on the turbine efficiency was also measured. At part loads, aeration through the runner cone at small air void ratios, with and without modifications, always served to increase the efficiency of the turbine. The water flow downstream of the turbine runner was more streamlined and cavitation was not observed. However, at peak and full loads, any volume of air flow entrained by the different schemes served to reduce the turbine efficiency as described by an equation developed by Almquist *et al.* (1991). Air flow through a draft tube ring without deflectors produced reduced aeration comparable to the other schemes; however, it created a more evenly distributed bubble swarm which is optimal for oxygen mass transfer. High speed photographs, shown in Figure 2-4, demonstrate the preferred spacing of the bubbles under discharge ring aeration.

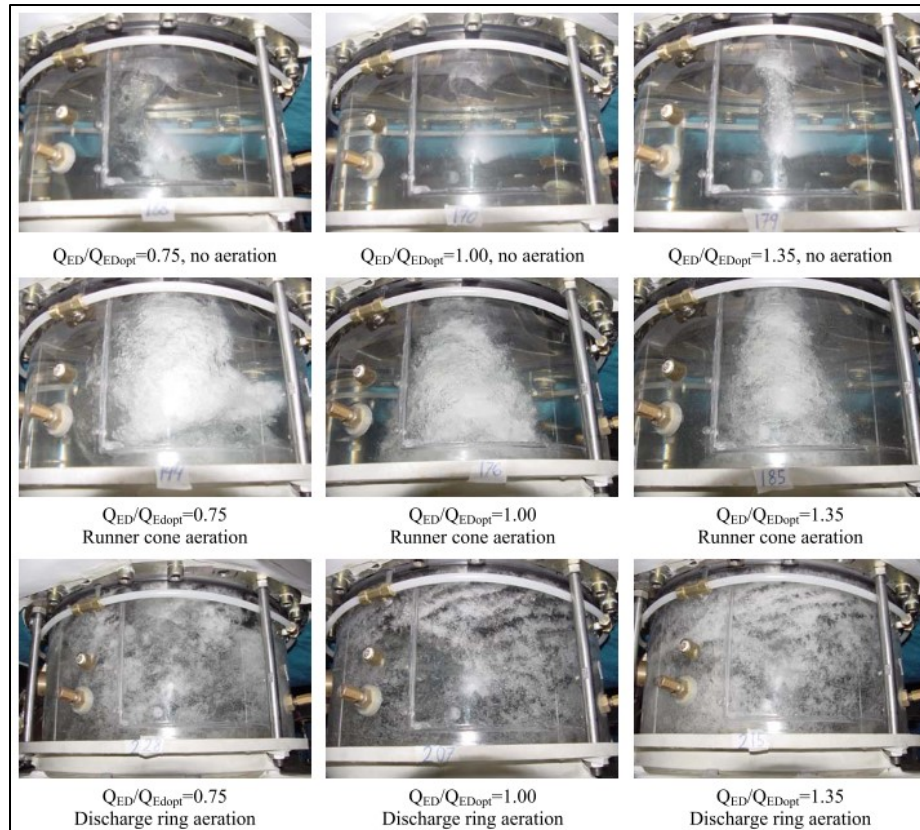


**Figure 2-4: Bubble characteristics for two aeration systems at three turbine operating conditions (Papillon et al., 2002)**

Desy *et al.* (2004) were tasked with solving anoxic conditions at the Canyon Ferry hydropower plant in Montana. Interestingly, as a reservoir located in a relatively cold climate, where the highest annual water temperature is 13°C, the occurrence of reservoir stratification goes against the commonly-held belief that an anoxic hypolimnion can only occur in warm climate reservoirs. The site-specific conditions of the hydropower plant suggested that natural aspiration of air into the draft tube without any modifications would be difficult. Deflectors were placed around the periphery of the draft tube to locally drop the wall pressure where an air inlet was placed. An elbow-type deflector was selected due to its decreased turbine efficiency loss coupled with an increased air flow rate at a given turbine operating point. As the flow in the turbine was

increased, the air void ratio and DO uptake was observed to decrease. This was due to an increase in backpressure which prevented air entrainment and a reduction in the bubble residence time.

Fraser *et al.* (2005) subjected two Francis turbines to aeration tests measuring the DO uptake and efficiency losses through the three different non-retrofit turbine centered aeration schemes: runner cone aeration, hollow blade aeration, and discharge ring aeration. The similarity equation developed by Thompson and Gulliver (1997) was validated for the two different turbine models. Interestingly, the DO uptake measurements did not show significant differences between the aerating scheme used, and efficiency impacts for the aeration schemes were comparable to other studies. Runner cone aeration stabilized operation at part load conditions but hollow blade aeration had the least impact over the range of turbine operations.

Several studies at the Osage hydropower plant at the Bagnell Dam were undertaken to optimize an aeration system tasked with solving a seasonal low DO condition in the tailwaters. After the implementation of runner cone aeration systems on several units in 2002 and 2004, DO levels in the tailwaters were still below the Missouri state threshold of 5 mg/L. AmerenUE conducted a cost-benefit analysis for a variety of aeration techniques for plant implementation. An aerating turbine was selected as having the largest potential for DO increase with low efficiency losses. In 2008, Voith Hydro was contracted to supply and install two hollow blade turbines. The DO uptake was measured for a variety of air flow rates. Air flow always increased with increasing turbine output. However, since the void ratio is the important parameter for DO uptake, it was shown that the increase in air flow was not mirrored by a proportional increase in the void fraction above certain water discharges. Above discharges of [3900-4100] cfs the void ratio decreased, correlating with a plateau in the DO uptake measured between the penstock and the tailwaters. The void ratio that the aerating turbine could supply ranged from [3, 7] % corresponding to uptakes of

oxygen between [3.4, 5.1] mg/L. The DO uptake was not strongly correlated with the discharge passing through the turbine. However, the efficiency cost per mg/L DO uptake increased with increasing DO uptake. This signals the need to optimize the designed system with respect to turbine efficiency losses (J. M. Foust *et al.*, 2009; Ware & Sullivan, 2006).

Grenier *et al.* (2010) were tasked with solving anoxic conditions at the John H. Kerr hydropower plant. The objectives of the project were that air had to be drawn in naturally and a minimum DO uptake of 3 mg/L met. A site-specific manifold within the draft tube was exploited to distribute air to air inlets placed in the lee of deflectors. A model study showed that, as for the Canyon Ferry study, an elbow type deflector geometry showed the best compromise between decreased turbine efficiency losses and increased air flow rates. The air void ratio and DO uptake were negatively correlated with the turbine discharge, changing from [5, 2] % and [4.9, 3.1] mg/L respectively as the discharge was increased from [4723, 6692.5] cfs. However, the threshold DO uptake was met at every operating point. DO uptake prediction solely with CFD proved difficult and the success was possible due to extensive model and prototype testing supporting the CFD.

In a 2011 presentation, Voith presented a comprehensive review of their aerating turbine design. Through a combination of CFD and model studies, it was shown that the bubble swarm created by hollow blade injection distributed the bubbles more evenly throughout the draft tube. This applies especially to draft tubes that bifurcate before releasing water into the tailrace. An unknown but sizable proportion of oxygen exchange occurs in the tailrace, which is increased when the bubbles are more evenly distributed. Their work resulted in a discretized oxygen exchange equation to be used in CFD studies at the prototype scale for DO uptake predictions (J. Foust & Coulson, 2011).

### **2.3.2 Laboratory studies**

Developing models for DO uptake valid across a range of aerating schemes is difficult due to the many degrees of freedom involved. Researchers have simplified the problem to correlate void ratios of injected air with observed DO uptakes without the presence of the turbine runner providing the required negative pressure to naturally aspirate air.

Jun and Jain (1993) modelled a vertical draft tube in a recirculating flow and injected air at an inlet, changing the void ratio, water flow rate, and air inlet diameter. By measuring the DO concentration at one location as the DO concentration steadily increased with air injection, they quantified the total aeration coefficient. The specific aeration coefficient was calculated by measuring the bubble size distribution downstream of the injection point. The equation developed for the specific aeration coefficient allows for CFD studies to predict DO uptakes regardless of the aeration method used.

Jun and Jain (1993) also studied the influence of a mesh at the air inlet used to set the initial bubble size. However, the reduced inertia of the air injected into a co-flow led to air pockets being formed downstream of the injection from which the bubbles were then sheared off, see Figure 2-5. The presence and size of the mesh holes did not break up the bubbles and the bubble diameter was dependent on the turbulent intensity and distance downstream from the injection point.

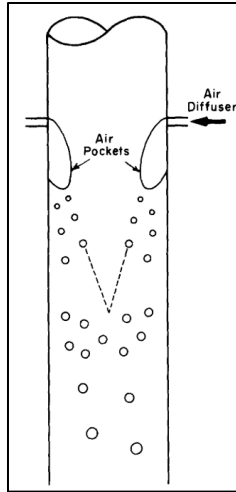


**Figure 2-5: Air pockets formed downstream of air inlet in a coflow (Jun & Jain, 1993)**

Since a turbine imparts a swirl on the downstream flow, Jun and Jain (1993) also measured the bubble size distribution and aeration coefficients after imparting swirling flow to their experiment. Their results showed no significant differences in DO uptake at swirl ratios close to those found in actual turbines. Their results showed that a simplified boundary condition in an experiment (i.e. no swirl) was sufficient for studying the DO uptake in pipes.

Yin et al. (2012) set up a horizontal recirculating flow with air injection for a range of void ratios and hydraulic conditions. In contrast to Jun and Jain (1993), the DO concentration was measured at two points downstream of the injection and the aeration coefficient was calculated using the residence time of the bubbles and DO concentration difference between the two measurement points. The experimental results showed good agreement with a CFD model developed using the work of Politano et al. (2010). The model used a constant bubble size not considering break-up or coalescence, based on the work of Wilkinson et al. (1994), which has shown good agreement in other laboratory settings but goes contrary to theoretical considerations. The bubble size distribution changes constantly due to a complex balance of bubble breakup and coalescence processes. Their conclusions allow for a commercial software such as ANSYS

FLUENT to be used in predicting DO uptakes at prototype scales but, it requires more experimental work to validate quantitative results.

Unsal *et al.* (2008) studied aeration in a high-head horizontal pipe controlled by a sluice gate. The air flow rate and DO uptake were measured for a range of gate openings and water velocities. The DO measurements occurred in the supply and exit reservoirs. The length of the horizontal pipe was varied from [2, 4, 6] m and, interestingly, was found to not affect the DO uptake. This was thought to be due to the high level of turbulence in the presence of the free surface occurring in the pipe. The injected air formed a foam-like mixture with the water at the high velocities studied. At many operating points, the largest DO uptake measured was for the shortest distance between the oxygen measurement points. However, this was also explained as likely being the result of experimental error and sensor error. The conclusions of this study were partially validated by Yin *et al.* (2012).

Bunea *et al.* (2010) injected bubbles into a stagnant column of deoxygenated water through a series of meshes and measured the evolving DO concentration within the column. The power required to inject a certain void ratio was used to select an optimal mesh size to increase DO concentrations while minimizing head losses within the air supply system. The mesh pattern could break up the injected bubbles without coalescence immediately occurring. The size of the individual mesh holes was negatively correlated with the measured DO uptake, showing the importance of the bubble size in the oxygen transfer process. However, the breakup of the bubbles observed was only possible because the air was injected at the bottom of a quiescent column of water. The results of other aeration studies show that any magnitude of water velocity will serve to coalesce the bubbles immediately after injection.

Kuhlert and Ware (2004) developed a CFD model to study the oxygenation and bubble formation process of air injected through the head cover of a Francis turbine. They developed a framework for studying the aeration process within several sub-regions of the aerating turbine. As the void ratio, saturation concentration, air flow rate, and oxygen content have sharp gradients at several points in the turbine/draft tube system, the use of sub-regions allows for incremental data checks that ensure more meaningful results. The rate of oxygen uptake was reduced due to the large losses in the air supply system, but the analysis identified potential areas where losses could occur which could be solved on-site for a prototype.

Ruane and McGinnis (2007) studied the oxygenation process in an aerating turbine injecting air downstream of baffles placed on the runner hub and through hollow blades at the Saluda hydropower plant. They sought to develop a prediction method to inform turbine operators of the necessary turbine operating conditions for increasing DO levels. A FORTRAN Discrete Bubble Model (DBM) was developed with inputs of:

1. 15-minute flow data downstream of the dam
2. Temperature and DO level of water upstream of the turbine
3. 15-minute tailwater elevation data

Regulations stipulated various DO limits in the form of instantaneous minimums, 7-day minimums and averages, daily averages and 30-day averages. Measured DO concentrations in the tailrace from the United States Geological Survey (USGS) showed sharp temporal gradients in DO concentrations as a function of the turbine discharge. The multiple time-scales proved difficult to model accurately. However, aeration solutions already implemented at the project were accurately modelled at steady operating conditions. Site conditions showed that runners placed at higher elevations above the tailwater could aspire larger amounts of air and thus led to higher DO uptakes for a given turbine discharge. The model noted that a turbine operating policy optimized for DO

uptake was necessary to provide adequate levels of DO. The effect of aerating schemes should be paired with standardized unit operations and a decision-making chart stating the aeration operating conditions based on required turbine discharges and DO levels. They noted that deviations from this strict approach explained the observed differences between their models and measured DO levels in the tailwaters.

## Chapter 3: Methodology

This chapter will present the methodology of the two experimental test rigs used in this research. The experimental test rigs were used to quantify the oxygenation and aspiration capacity of the deflectors in a simplified flow. The experimental test rigs are also the test-cases for the parallel CFD model development at Andritz Hydro.

### 3.1 McGill Experimental Apparatus

An experimental test rig housing a deflector in a simplified flow has been constructed in the Hydraulics Laboratory, Civil Engineering at McGill University. The test chamber, a machined PVC block with a viewing window, housed the deflector geometry and was placed in a straight horizontal pipe section of a recirculating flow system connected to a reservoir. The building's air supply was connected to the test chamber, injecting air in the lee of the elbow deflector. Oxygen transfer occurs in the length of pipe extending from downstream of the test chamber to the reservoir. The water discharge was controlled by a valve upstream of the reservoir. Figure 3-1 shows an overview of rig layout.

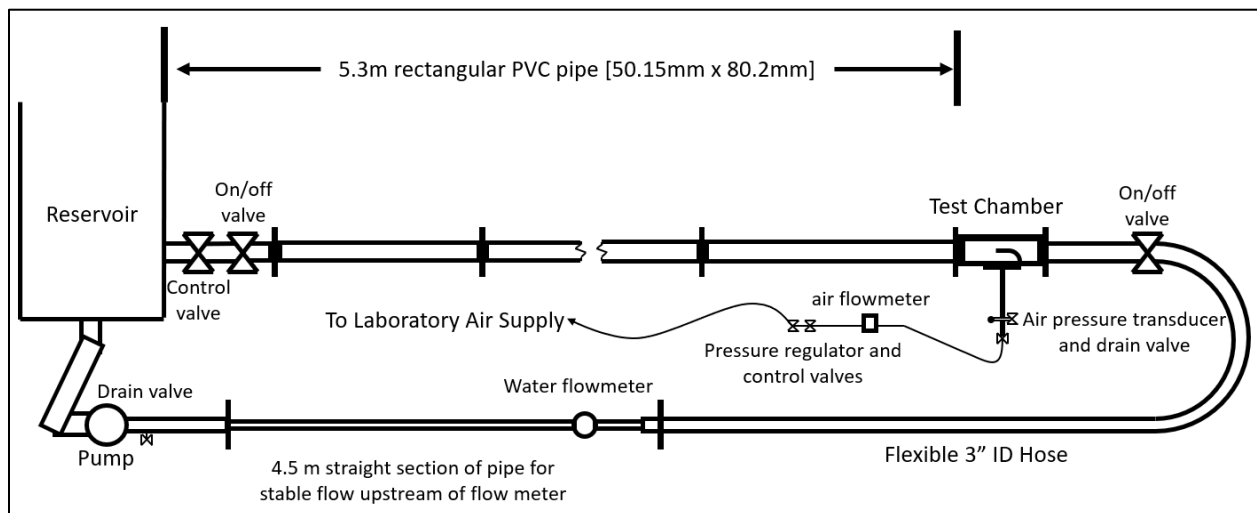


**Figure 3-1: McGill Test Rig Layout**

The McGill test chamber was machined specifically for this experiment. It contains a rectangular cross-sectional channel (50.15 x 80.2 mm), two viewing windows, and a rectangular

slot at the bottom (160 x 50.15 mm) that accepts the test block to which the different deflector geometry configurations can be attached (Figure 3-2).

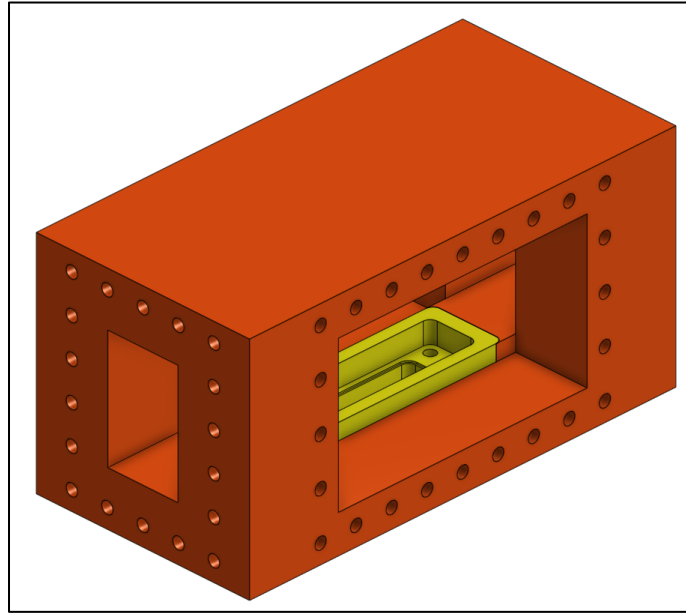


**Figure 3-2: McGill Test Chamber with test block visible**

In the test chamber, the performance of different geometries of the elbow deflector was studied by varying the size of the deflector and the configuration of the air inlet. The base of the test chamber was a removable brass block to which PVC strips holding the various deflector configurations were attached and placed flush with the flow. Figure 3-3 shows the test block before and after a deflector configuration is attached. The deflector configurations consisted of a PVC strip (34 x 100 x 12.7 mm) to which 3D-printed ABS deflectors were cemented. The PVC strips were machined to accept the range of deflector sizes as well as the different air inlet positions and sizes. A hole (3/4" NPTF) in the base of the brass block accepted the air injection system, detailed in the next paragraph. An inner chamber in the brass block distributed air to the different air inlet positions (Figure 3-4).

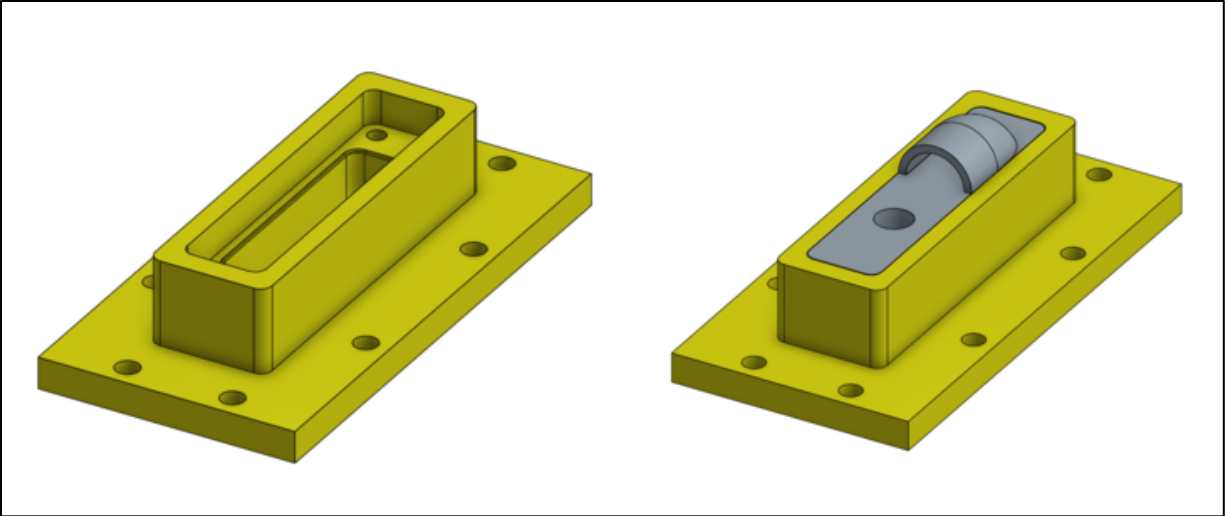


**Figure 3-3: Brass test block with and without deflector configuration attached**

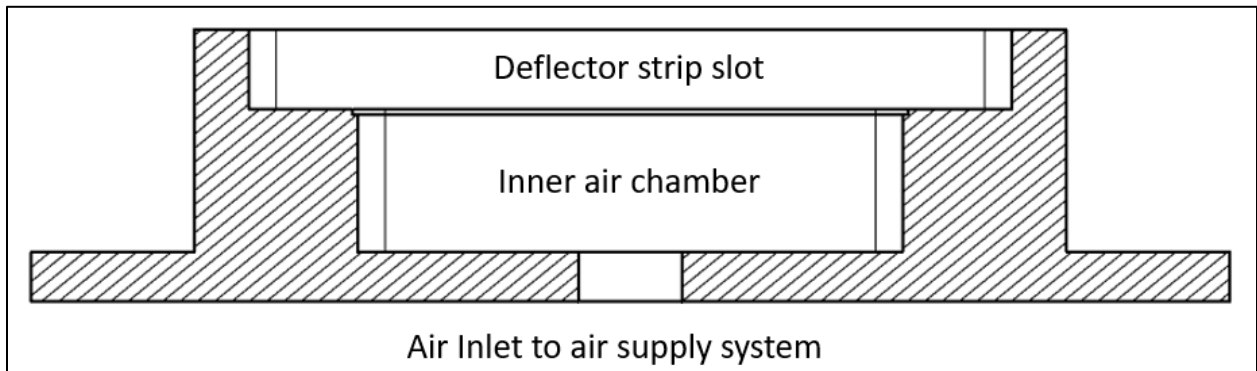


**Figure 3-4: Cross-sectional view of test block**

To quantify the oxygenation possible of different deflector geometries and hydraulic operating points, air was injected into the test chamber in the lee of the deflector. The building air supply, at 655 kPa gauge pressure, supplied the injected air. A regulator reduced the pressure to the test air pressure over the range of [34, 103] kPa gauge pressure. The regulator and a series of ball valves were used to control the flow rate of the air, which was then measured by an air flowmeter (ALICAT MS-250SLPM) rated for a mass flowrate of [0, 5] sL/s (standard liters per second, a measure of mass flow rate), standardized to 100 kPa and 20°C to provide air/water flow ratios of [0, 10] %. A flexible tube directs the air to a series of fittings and a check valve (1/4" NPT Valve, 6" copper pipe nipple, 1/2" brass check valve, 12" copper pipe nipple) where a pressure

transducer (DRUCK PDCR 4010) measured the air pressure, to the inner chamber of the brass block from where the air is injected into the lee of the deflector. Figure 3-5 shows the air injection system.

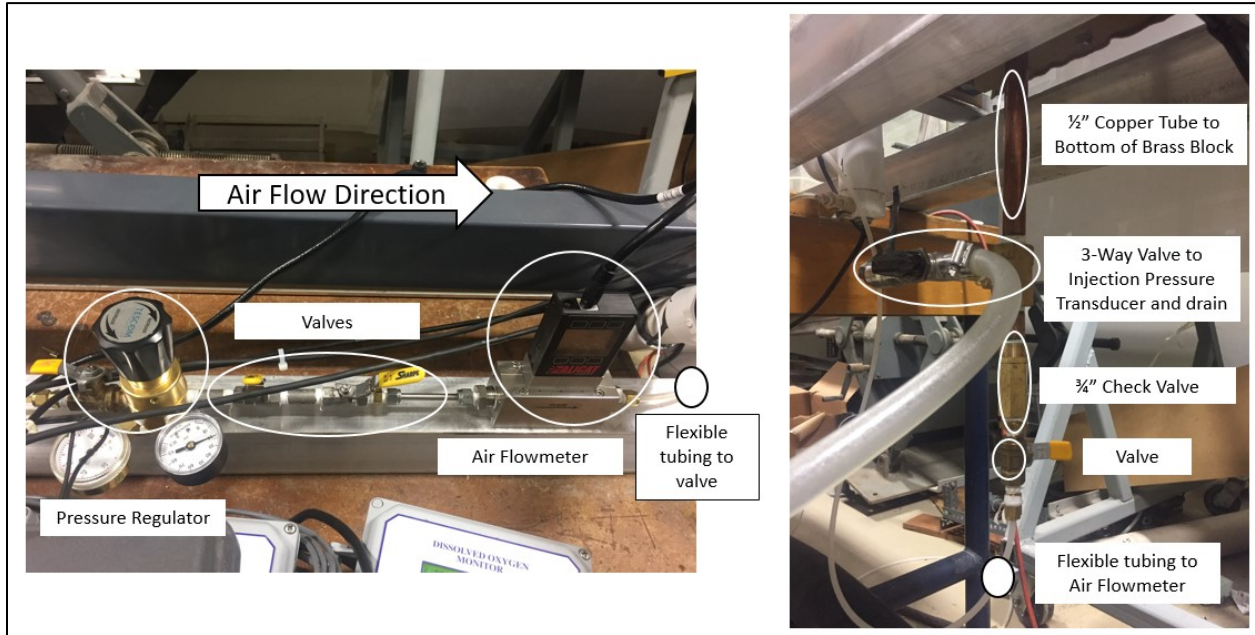


**Figure 3-5: McGill air supply system**

To measure the oxygenation coefficients as described in Equation [5], the oxygen concentration must be measured at two longitudinal positions within the recirculating flow. Downstream of the test chamber was a 5.3 m length of rectangular pipe. The dissolved oxygen concentration was measured at a distance along this pipe of 0.23 m and 4.3 m downstream of the test chamber.

The bubbles of injected air in the pipe downstream of the test chamber must be removed from the recirculating flow to ensure that any measured DO uptake is due to the newly injected air at the deflector. To facilitate the removal of the injected bubbles, an air relief valve (1/4" NPT), placed 4.3m downstream of the test chamber, on the crown of the pipe above the location of the downstream DO measurement, was kept open for the duration of the tests.

A reservoir, with a volume of 500L, was placed at the downstream end of the pipe, downstream of the test chamber (see Figure 3-6). A pump recirculated water from this reservoir ([0.91 x 0.66 x 0.66] m and made of polyethylene) around the test rig. The reservoir was open to the atmosphere to allow the injected air to escape the tank as the bubbles rose in the reservoir. However, to limit contact with the atmosphere and reduce the oxygen transfer rate with the air above the water surface, a plastic bag was stretched over the top of the reservoir. A vacuum system was installed to remove air from above the reservoir free surface and collect the incoming air bubbles from the air injection upstream. This system consisted of a perforated tube, placed around the top edge of the tank and connected to a vacuum Venturi pump driven by the laboratory air supply, as shown in Figure 3-7. When the Venturi pump was turned on, the bag sealed to the free surface of the water and evacuated the air bubbles from the reservoir via the perforated tube.

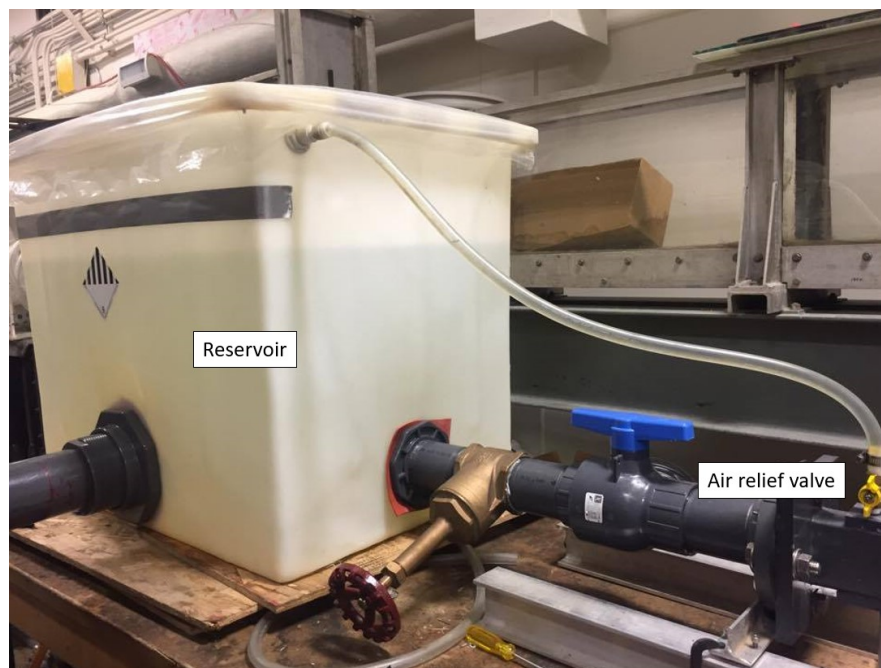


**Figure 3-6: Reservoir with air relief valve**

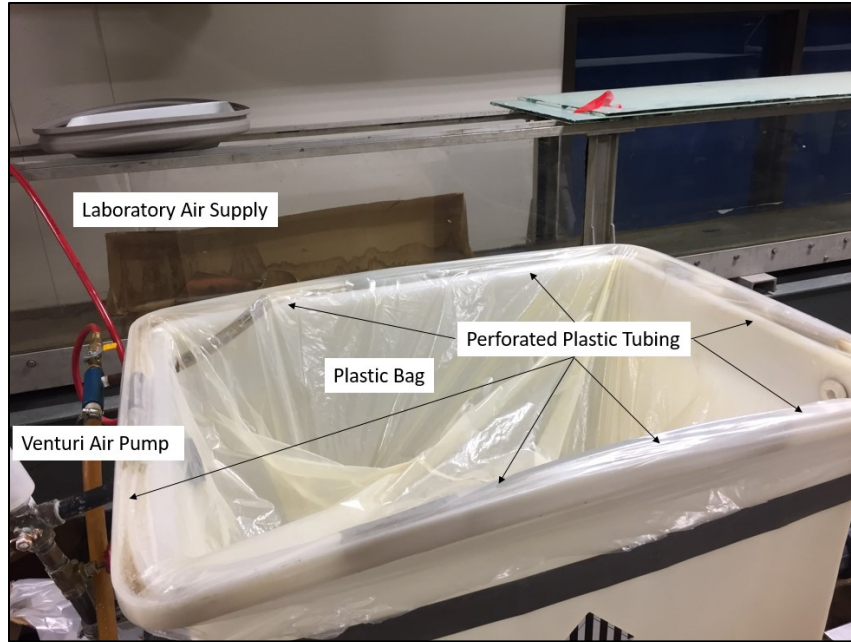


**Figure 3-7: Bubble extraction system through Venturi air pump**

The maximum increase in DO concentration can be observed at a maximum oxygen deficit (i.e. greatest potential for increase in oxygen concentration up to the point of saturation). Therefore, prior to a test the recirculating flow was to be deoxygenated to a level close to 0 mg/L. An oxidation reaction between sodium sulfite ( $\text{Na}_2\text{SO}_3$ ) and the DO ( $\text{O}_2$ ), catalyzed with cobalt chloride ( $\text{CoCl}_2$ ), was used to precipitate sodium sulfate thereby removing the DO as detailed below.



Approximately 1.2 - 2 times more sodium sulfite than the theoretical requirement of 7.9 mg/L per mg/L of DO (corresponding to an initial saturation concentration of ~8.6 mg/L of DO) was added to ensure that all the DO was removed in the chemical reaction. With each subsequent experiment, only the sodium sulfite had to be added again, as the cobalt chloride is not consumed in the reaction. To maintain the water quality, the water was periodically changed as the total dissolved and suspended solids (TDSS) concentration increased (Ghaly & Kok, 1988). The

deoxygenating chemicals were poured into the reservoir through a valve at the water surface level and the pump recirculated the flow.

The pump recirculating the water through the test rig and test chamber provided the range of hydraulic operating points for the different experiments. The pump (Goulds 3656 3x4 – 7 Option B 1750 RPM) was capable of a flow of 30 L/s with a head in the range of [4, 10] m of water. It was placed downstream of the reservoir and at a lower elevation (1 m) to provide the NPSH (required net positive suction head or submergence). The flow rate was measured at the outlet side of the pump with a pipe-mounted paddle flow meter (Midwest Instruments Flow Meter Model 9002) rated at 10 – 125 gpm ([0.63, 8.0] L/s), set into a Size 1.5 NPS PVC pipe. It has an accuracy of 1% as it was placed in a straight section of pipe with the required length of 50 diameters upstream and 5 diameters downstream (see Figure 3-8).

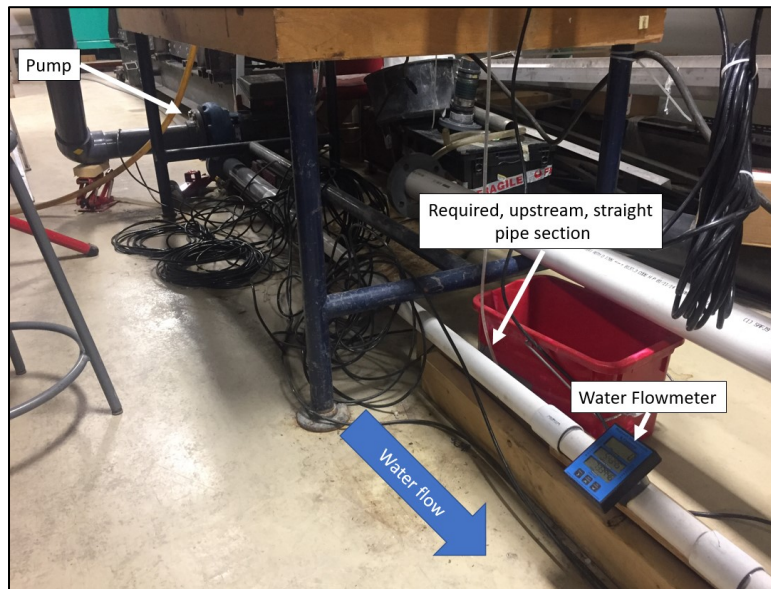


**Figure 3-8: Pump and water flowmeter (Midwest Instrumentation and Controls)**

The geometry of the deflectors is modelled after previous studies at the John H. Kerr dam and commercially available pipe elbows (Grenier et al., 2010) as shown in Figure 3-9. This shape

with the addition of two orienting pegs on its base, shown in Figure 3-10, was 3-D printed. Figure 3-11 and Figure 3-12 show the deflector before and after being attached to a PVC strip.

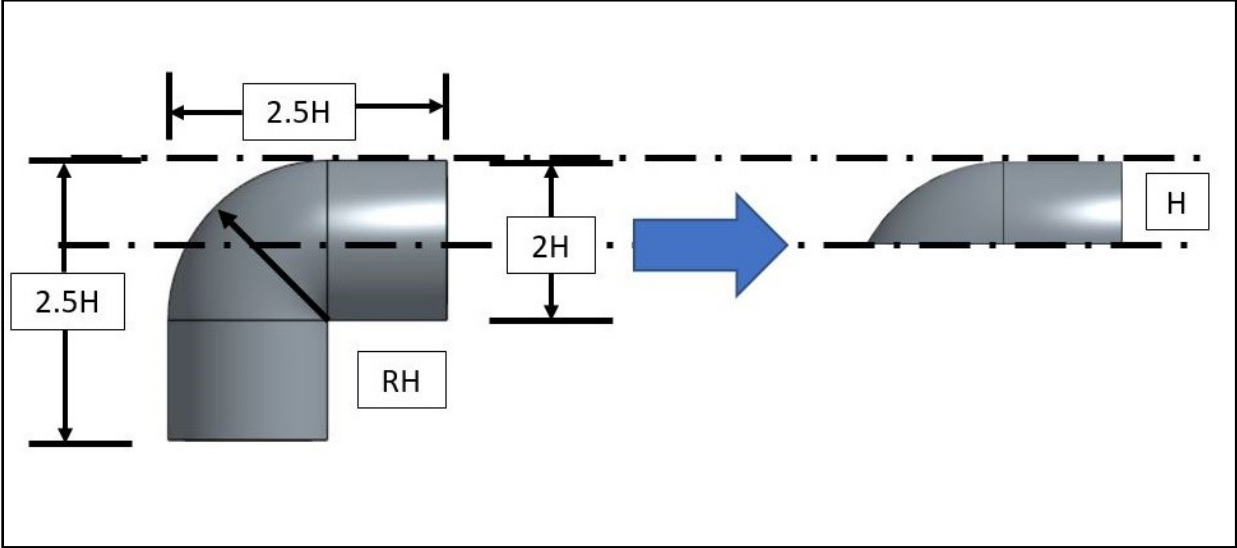


**Figure 3-9: Modification from commercially available standard pipe elbow to deflector**

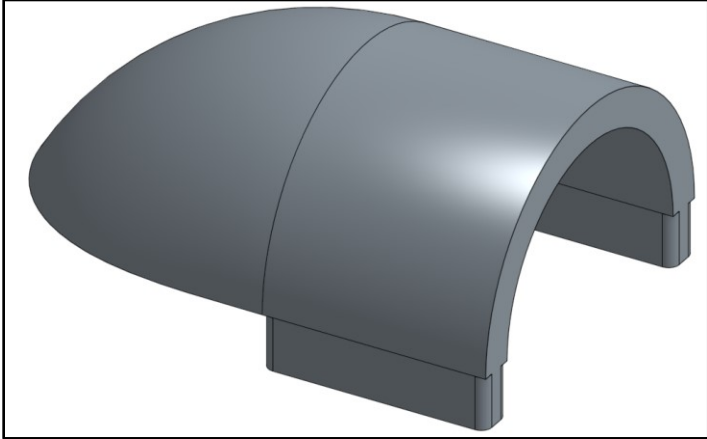


**Figure 3-10: Final deflector design with orienting pegs**

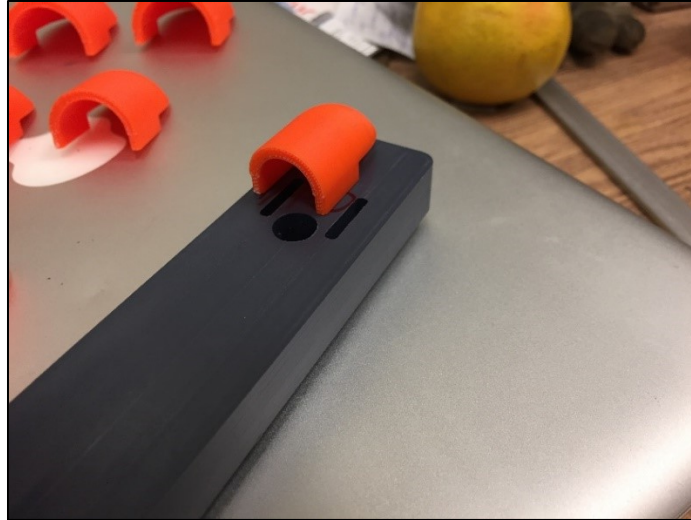


**Figure 3-11: Deflector ( $H = 10 \text{ mm}$ ) before being attached to PVC strip ( $L/H = 0$ )**

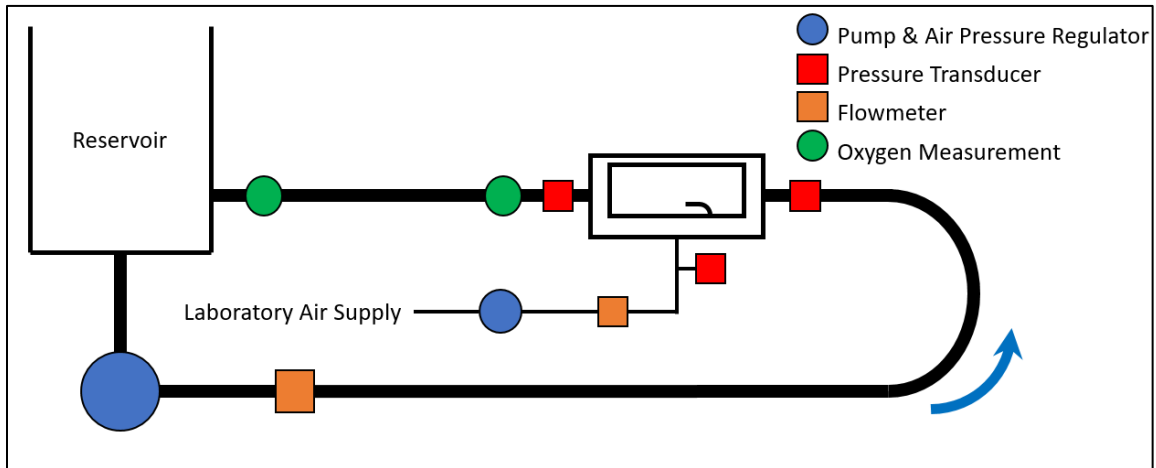


**Figure 3-12: Deflector attached to PVC Strip ( $H = 16.5\text{mm}$ ,  $L/H = 1$ )**

To quantify the oxygenation of the different deflector configurations and provide a data set for late calibration and validation of the Andritz CFD model, the following measurements were taken:

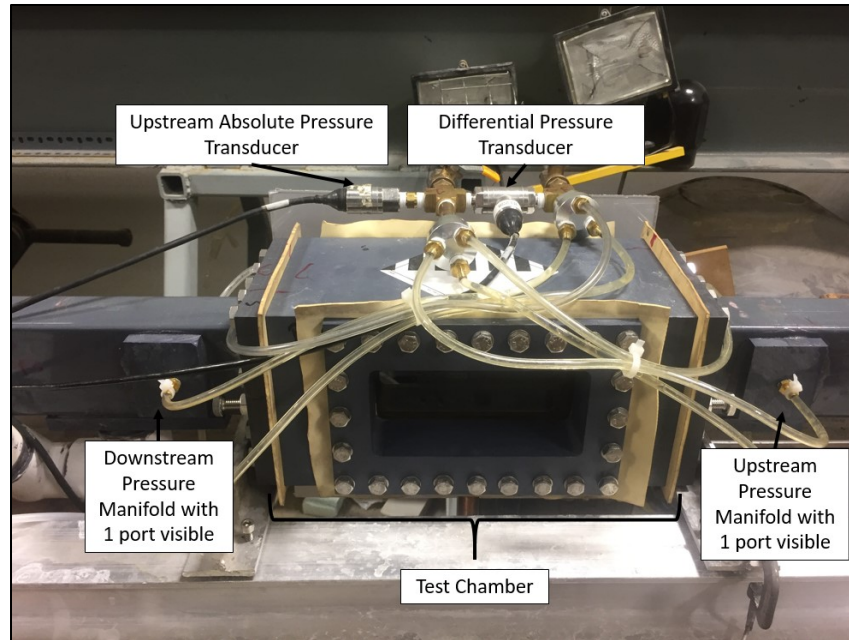
- Water pressure upstream of test chamber
- Air inlet pressure
- Differential pressure across the test chamber
- DO concentration measurements at 2 locations downstream of the deflector

Figure 3-13 shows the location of these measurements in a schematic of the test rig.



**Figure 3-13: McGill test rig measurement locations**

The oxygen saturation concentration and the boundary conditions of the Andritz CFD model require the knowledge of the upstream water pressure. The pressure difference across the test chamber was also measured as it can be used to provide an estimate of efficiency losses. To accomplish this, a manifold system was constructed at points immediately upstream and downstream of the test chamber (0.15m in each direction). A port was placed on the midline of the pipe at the sides and at the bottom (total of 3 ports) and then connected to a manifold. This served to average the pressure at the three faces. These ports were connected to the absolute and differential transducers (DRUCK PDCR 4010 & 2110). Figure 3-14 shows the test chamber with the pressure transducer manifolds visible.



**Figure 3-14: Test chamber with pressure measurement manifolds**

Flow visualization was required to characterize the injected bubble swarm and interpret the aeration rates for different deflector configurations and hydraulic operating points. A high-speed video (1/9900 Hz exposure) using an iPhone 6 was taken through the viewing window for each experiment.

The DO concentration in the flow was required during the experimental runs to determine the effectiveness of the elbow deflectors as aeration devices. The most accurate assessment of oxygenation requires the greatest change of DO concentration, i.e. where the measurement points are the furthest apart. DO concentration was measured, just downstream of the deflector and at the furthest point downstream of the deflector before the flow entered the reservoir, using PDO-1 Barben sensors. These sensors were used to continuously measure the inflow concentration. However, because they required  $\sim 300$ s to stabilize the reading and, in the recirculating flow DO concentrations were continually increasing, leading to uncertainty in the readings, DO was also measured in sample pots located at the same point as the inflow sensors (Figure 3-15 and Figure

3-16). In the sample pots, the water was extracted for the duration of the inflow DO measurements and allowed to stabilize to the final DO value at the conclusion of aeration. The sensors took readings every 100s. The inflow DO sensors were read for 200s and the sample pot DO sensors were read for 300s.

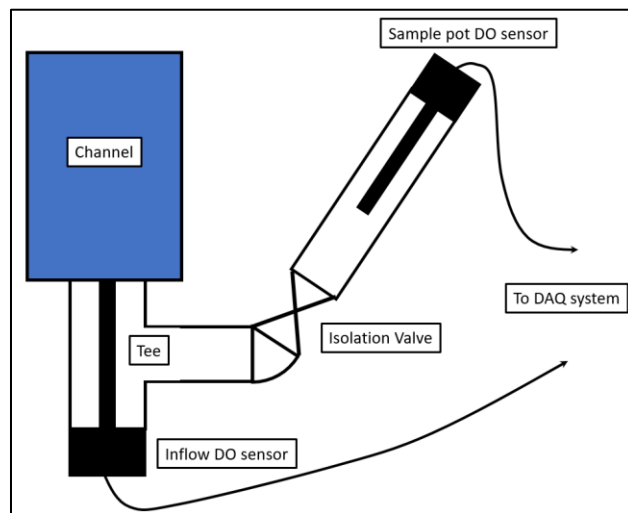


**Figure 3-15: Sketch of DO measurement apparatus**

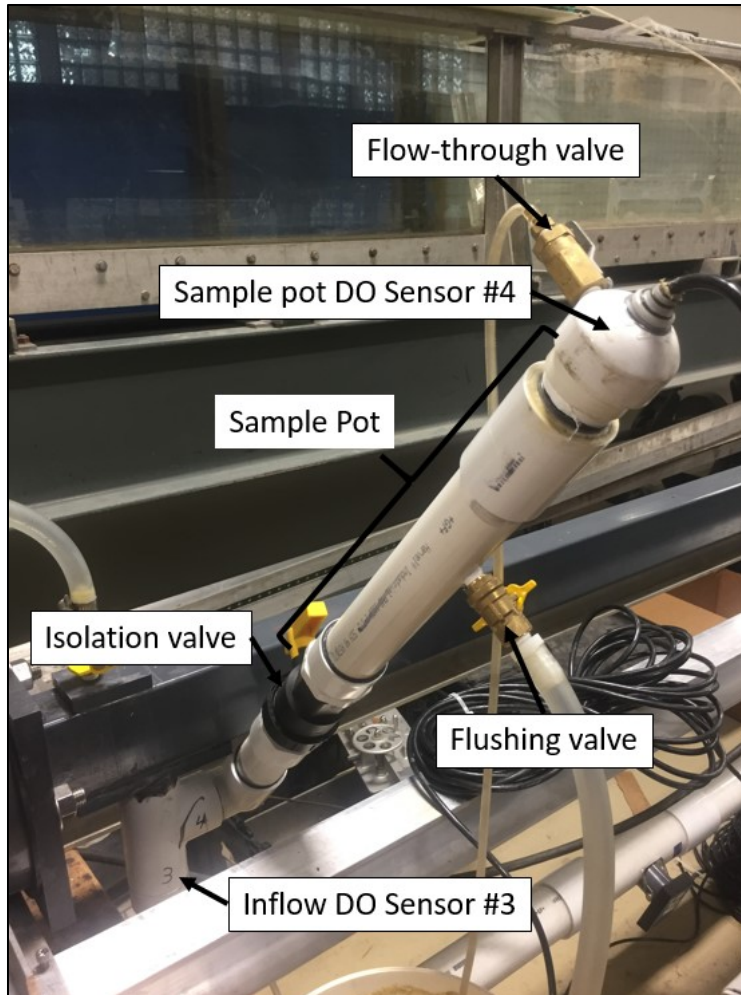


**Figure 3-16: Downstream DO measurement apparatus**

The measurement of oxygen using the inflow sensors is straight-forward and requires little consideration in the post-processing of the measured data. However, since water was being passed through the sample pots for the duration of the inflow measurements (with aeration occurring in the recirculating flow), the sample pot inflowing water had a steadily increasing concentration of DO which required some analysis to ascertain the accuracy of this methodology. The sample pots were only read at the end of the inflow measurements (after ~200s of aeration) to allow for the measurement to stabilize. Thus, a mass balance studying the Eulerian evolution of the DO concentration at the sample pot extraction points is necessary, to ensure that the final sample pot

DO concentrations are not close to saturation (thus minimizing the change in DO between the two points, potentially within the sensor error of 0.1 mg/L). Based on two previous studies, Yin *et al.* (2012) and Thompson *et al.* (1997), the oxygen transfer efficiency was conservatively taken to be about 0.1 corresponding to a bubble residence time of 1 second and a gas void ratio of 10%, the experimental operating point with the largest rate of oxygenation. Using Equations [3] & [5] the total aeration coefficient is calculated from:

$$K_l a = -\frac{\ln(1-E)}{t} = 0.105 \quad [18]$$

A mass balance of oxygen entering and leaving the reservoir, where total mixing is assumed, results in the following equation, used to characterize the Eulerian evolution of the DO concentration within the flow:

$$\frac{dC}{dt} = \frac{1}{\tau_w} * ((1 - e^{-K_l a T}) * (C_s - C)) \quad [19]$$

Where  $\frac{dC}{dt}$  = rate of DO buildup (mg/L/s);  $\tau_w$  = residence time of water within the flow;  $C$  = DO concentration within the tank;  $K_l a = 0.105 \text{ s}^{-1}$  (calculated from the example values in Yin *et al.* (2012) and Thompson *et al.* (1997)); and  $T$  = residence time of bubbles in the flow, (i.e. the quotient of the distance between the air inlet and the air valve and the water velocity within the recirculating flow (2.0 m/s, the maximum value for the study)). This separable ordinary differential equation (ODE) can be integrated to estimate the evolution of the DO concentration at a single point within the recirculating flow, assuming an initial concentration of 0 mg/L, given by:

$$C(t) = C_s \left( 1 - e^{-\frac{ft}{\tau_w}} \right) \quad [20]$$

where:  $f = 1 - e^{-K_l a T}$ . Figure 3-17 shows that over the length of the aeration period ( $\sim 200$  s, corresponding to the length of time required to read the inflow sensors) the maximum change in DO is  $\sim 2.0$  mg/L. The oxygen mass transfer equation relates the oxygen transfer efficiency to the two-phase flow parameters (turbulence characteristics, oxygen diffusivity in water and the interstitial air-water area). It is assumed that holding the hydraulic conditions constant, the oxygen transfer efficiency will stay the same throughout the experiment. An increase or decrease in the initial oxygen deficit will balance with a decrease or increase in the absolute DO uptake, holding the full term,  $(C_2 - C_1)/(C_1 - C_s)$ , constant (Yin, (2012)). It is important to note that the oxygen transfer efficiency is not the same term as the oxygen absorption term described in Yin *et al.* (2012), which is dependent on the upstream oxygen content itself and changes throughout a recirculating experiment. Assuming an oxygen transfer efficiency of 0.1, taken from the literature as the highest expected value for the experimental parameters of this research, and an upstream DO concentration of 2.0 mg/L, the DO value at the time the dissolved oxygen is measured by the sample pots, the DO uptake is 1.75 mg/L, well outside the margin of error for the sensors. The steady build-up of DO concentration flowing into each sample pot does not affect the DO concentration difference between the sample pots because the sample pots had the same flowrates through them (varied with the pressure in the test rig) and were kept open for the same length of time ( $\sim 200$ s).

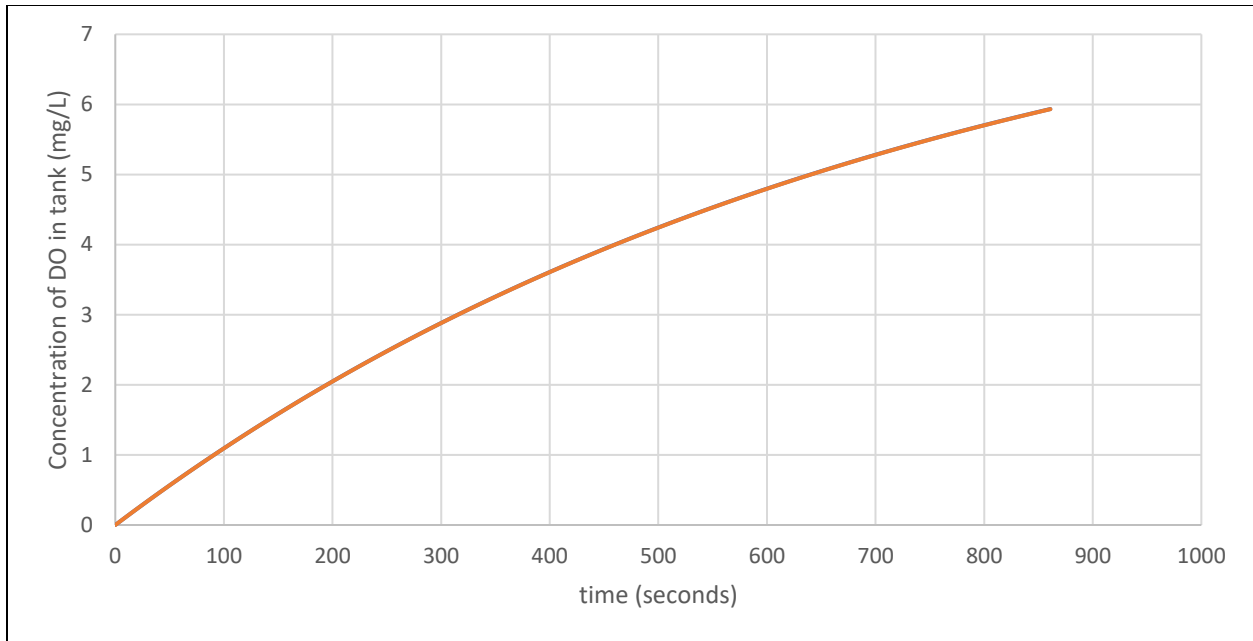


**Figure 3-17: Point evolution of DO concentration**

The following describes the steps of the experimental procedure. Table 3-1 lists the sensors used for this experimental apparatus.

The system is filled with tap water that has passed through a sand filter and water softener to improve the water quality to maintain a clear view through the test chamber viewing windows. Cobalt chloride (35 mg) was added to the reservoir as a catalyzer for the deoxygenating chemical reaction. The pump is turned on and a steady flow rate is established as required by the test operating point. Sodium sulfite (amount determined by DO concentration in reservoir) is added to the flow at the reservoir to increase the initial oxygen deficit, and thus maximizing the measured DO uptake. 203 minutes are required for the full chemical reaction to occur. At the conclusion of the chemical reaction, when the DO concentration was observed to have reached a minimum and had begun to increase again within the reservoir, air injection for the experimental operating point commences. The sample pots are opened, flushed, and then filled, and data is collected from the inflow DO sensors, upstream water and injection air pressure transducers, and the air flowmeter

for 200 seconds. When the sample pots are opened, a timer is started and the water flowing through the first sample pot is collected in a bucket, and weighed at the conclusion of the test, to correct the velocity of the air/water mixture between the two DO measurement points. The act of removing water from the first DO sensors lowers the water velocity after this point due to conservation of mass. After data acquisition ends for the inflow DO sensors and the pressure transducers measuring the upstream water and injection air pressures, the sample pots are closed, the timer is stopped, and data is collected for 300 seconds from the sample pot DO sensors. Sodium sulfite is then added to the water again and the procedure restarts for the next experiment. The water was periodically changed in the whole system to maintain the water quality and prevent rust from accumulating in the pump (sodium sulfite is slightly corrosive).

**Table 3-1: Instruments list for McGill Experimental Apparatus**

Measurement Name	Measurement Label	Instrument	Output Range	Accuracy
Upstream Inflow DO	DO 1	PDO Barben -1	[4, 20] mA	0.1 mg/L
Upstream Sample pot DO	DO 2	PDO Barben -1	[4, 20] mA	0.1 mg/L
Downstream Inflow DO	DO 3	PDO Barben -1	[4, 20] mA	0.1 mg/L
Downstream Sample pot DO	DO 4	PDO Barben -1	[4, 20] mA	0.1 mg/L
Water flow rate	$Q_w$	Midwest Instrumentation & Controls flowmeter	[0.6, 8.0] L/s	0.073 L/s
Air flow rate	$Q_a$	Alicat 250-SLPMS	[0, 5.0] SL/s	0.001 L/s
Upstream water pressure	$P_1$	DRUCK PDCR 4010	[0, 344.7] kPa	0.14 kPa
Air inlet pressure	$P_2$	DRUCK PDCR 4010	[0, 344.7] kPa	0.14 kPa
Differential pressure	$P_3$	DRUCK PDCR 2110	[0, 344.7] kPa	0.34 kPa

### 3.2 Vevey Experimental Apparatus

A high-velocity cavitation test rig at the Andritz Hydraulic Laboratory in Vevey, VD, Switzerland was used to study the performance of the deflector at high flows. The pressure difference between a point upstream of the deflector and the air inlet, for a range of deflector geometries and hydraulic operating points, was determined from measurements of the upstream water pressure, the injection air pressure, and the air/water flow ratio. A test chamber, similar to the McGill test chamber, was placed in a recirculating loop. Figure 3-18 shows a layout of the experimental test rig.

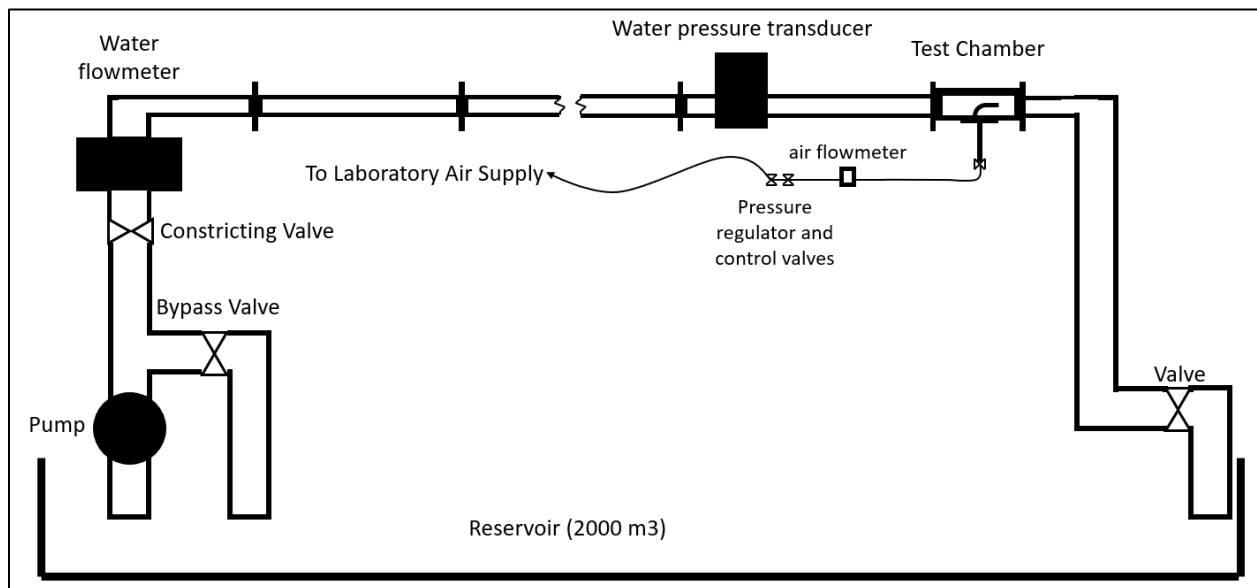


**Figure 3-18: Vevey test rig layout**

In the Vevey test chamber (Figure 3-19), the aspiration capacity of the different deflector configurations was studied for a range of high velocity, hydraulic operating points by measuring the pressure difference between a point 300mm upstream of the deflector and the air inlet position, with and without aeration. The Vevey test chamber was similar to the McGill test chamber except for different channel dimensions (54 x 74 mm at Vevey vs 51 x 80 mm at McGill), and a longer viewing area (300 mm). It contained two viewing windows, one on either side of the channel, and

a rectangular slot (54 x 160 mm) on the bottom of the chamber through which the McGill test block could be inserted flush with the chamber bed. The method of attaching the deflectors to the test block and placing them into the flow was the same as the McGill experimental setup.

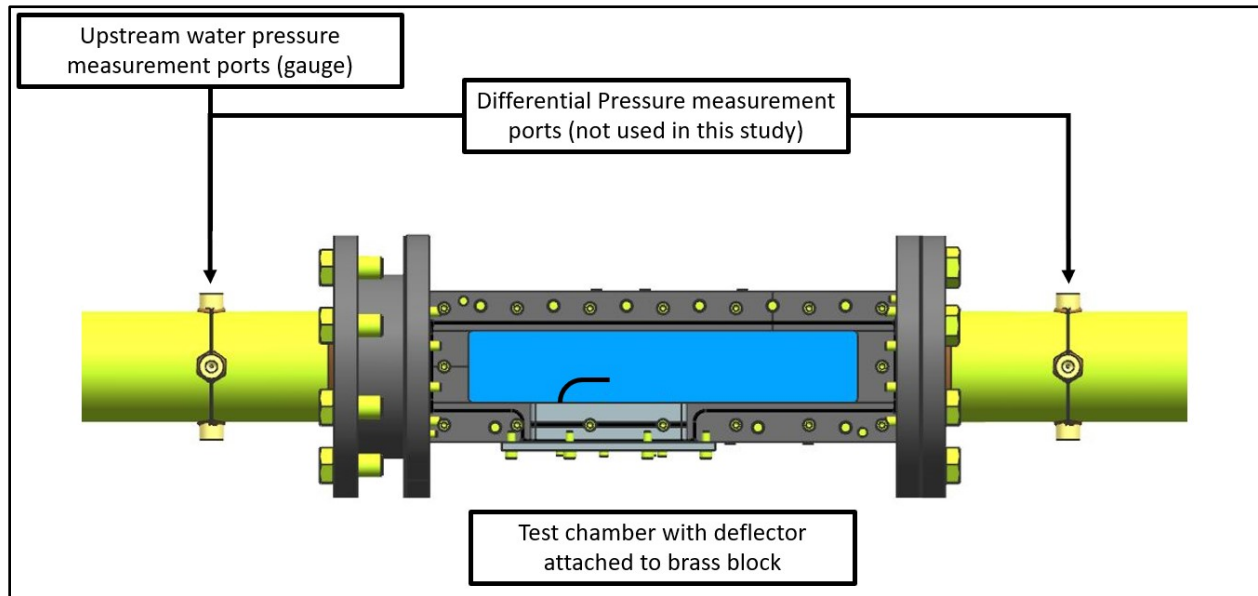


**Figure 3-19: Vevey test chamber**

To quantify the aspiration capacity of the different deflector configurations, air was injected in the lee of the deflector through a hole in the bed. The air supply system and the pressure and air flow rate measurements for the Vevey setup were equivalent to the McGill experimental setup, except that the 12” McGill pipe nipple within the air supply system was a 6” pipe nipple in Vevey. The laboratory air supply (at 700 kPa) supplied the injected air. A pressure regulator brought the pressure down to the test pressure of [37, 117] kPa. The air was then routed by a series of ball valves and flexible tubing to an air flow meter (ALICAT 250-SLPMS) and a 6” brass pipe nipple where an offline pressure transducer measured the injection air pressure.

To study the different deflector configurations at velocity scales close to those found in prototype draft tubes, a high-speed pump was used to provide the required flowrate. The pump, capable of providing a water pressure of 1000 kPa and a flow rate of 12 L/s, extracted water from

a reservoir (2000 m<sup>3</sup>) located beneath the laboratory floor, and was controlled by a series of constricting and bypass valves. The water was then measured by a flowmeter (ABB NW 80) located far upstream of the test chamber and an absolute pressure transducer (ROSEMOUNT 3051S1) (300mm upstream of the deflector) while being directed to the test chamber by a horizontal length (12 m) of rectangular stainless-steel pipe (54 x 74 mm). The water pressure within the test rig was controlled by a “Multijet” valve (Figure 3-20) placed 10 m downstream of the test chamber, just upstream of the return back to the reservoir.



**Figure 3-20: MONOVAR regulation valve**

The aspiration capacity of each deflector requires the knowledge of the pressure difference between a point just upstream of the deflector and the air inlet point. Figure 3-21 shows the location of these measurements. The water pressure was measured using the test stand’s existing pressure gauge located 1 m upstream of the deflector. The air inlet pressure was measured within the air

supply system 0.2 m upstream of the air inlet, using a DRUCK PDCR 4010 gauge. The air flowrate through the air supply system was measured using the same apparatus and sensor as in the McGill experimental setup, an ALICAT-250SLPMS flowmeter, a DRUCK PDCR 4010 gauge, and a series of ball valves, flexible hosing, and brass fittings.

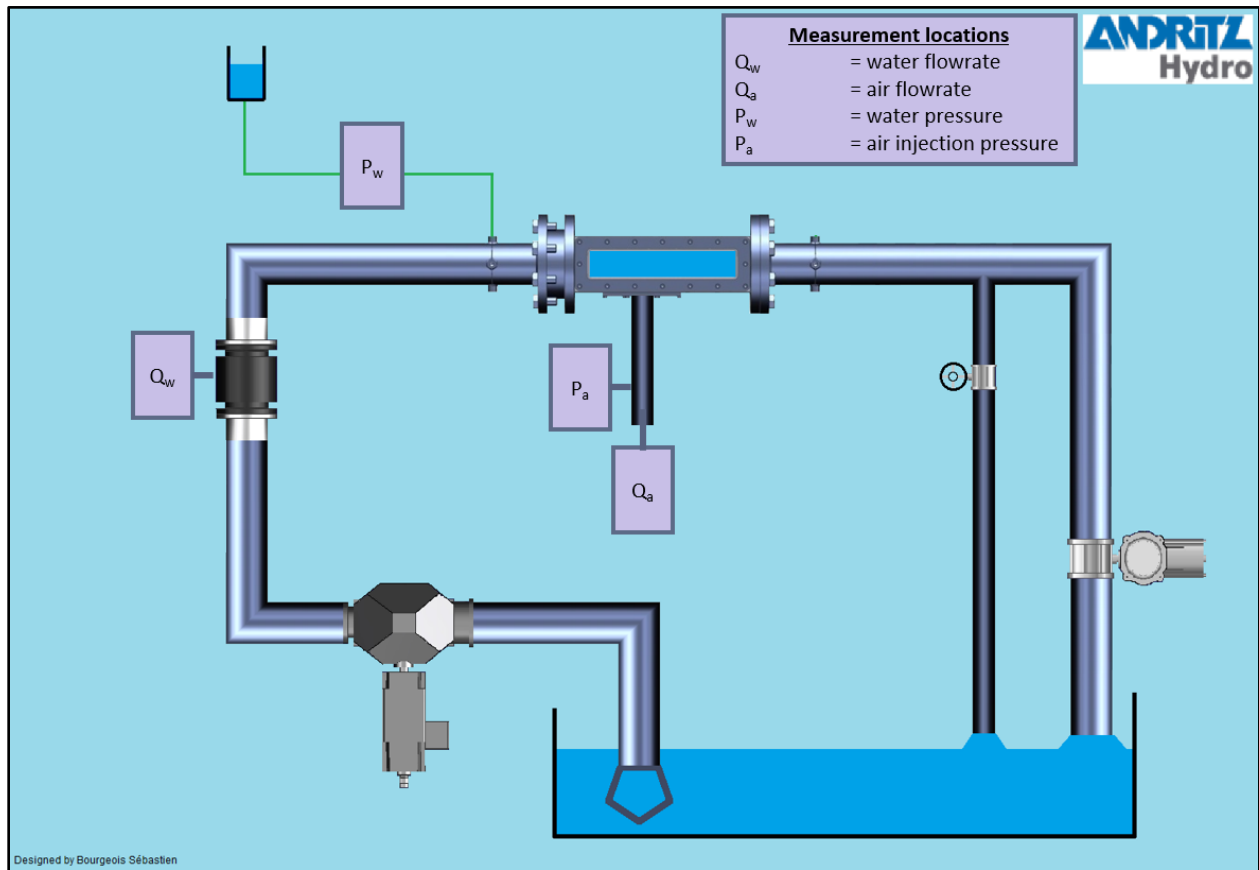


**Figure 3-21: Vevey experimental measurement locations**

To understand the characteristics of the injected bubble swarm at high velocity, a high-speed video (1/9900 Hz exposure time) was taken through the test chamber window, using an iPhone 6.

The following describes the steps of the experimental procedure. Table 3-2 lists the sensors used for this experimental apparatus.

1. The test rig is filled with water and the flowmeter cleared of air bubbles

2. The experimental condition is established (water flow rate and water pressure upstream)
3. The air supply pressure regulator and the air supply valves control the air flow rate into the test rig
4. The high-speed video is taken of the bubble swarm
5. The air flow rate and inlet pressure are measured for 15s

**Table 3-2: Instruments list for Vevey Experimental Apparatus**

Measurement Name	Measurement Label	Instrument	Output Range	Accuracy
Water flow rate	$Q_w$	ABB NW 80	[20, 56] L/s	N/A
Air flow rate	$Q_a$	Alicat 250-SLPMS	[0, 5.0] SL/s	0.001 L/s
Upstream water pressure	$P_1$	ROSEMOUNT 3051S1	[0, 800] kPa	0.8 kPa
Air inlet pressure	$P_2$	DRUCK PDCR 4010	[0, 344.7] kPa	0.14 kPa

### 3.3 Test Parameters

A parametric study of a simplified model elbow deflector was undertaken at the McGill Hydraulic Laboratory and at the Andritz Hydro Vevey Hydraulics Laboratory. The deflector size and air inlet geometry were varied over a range of water and airflow rates and pressures. The following observations were made: the bubble swarm characteristics, the injection air pressure, the upstream water pressure, and the evolution of the dissolved oxygen concentration downstream of the injected bubbles in the McGill rig.

The parameters varied were: the water flow rate -  $Q_w$ , water pressure -  $P_w$ , air flow rate -  $Q_a$  (air/water flow ratio -  $Q_a/Q_w$ , consequently), the size of the deflector -  $H$ , the relative position -  $L/H$ , and size -  $D$  of the air inlet ( $D/H$  was kept constant), as well as the presence of a mesh at the air inlet. Figure 3-22 shows the parameters. The mesh consisted of a circular pattern of 19

drilled holes of constant diameter (3.78 mm) with a total hole area equal to a reference deflector sample with the largest hole size [ $D/H = 1$ ] (Figure 3-23). Table 3-3 provides the test parameters studied at the McGill test rig and Table 3-4 provides the test parameters studied at the Andritz Vevey test rig, where DO concentrations were not studied. The water pressure in the McGill test rig could not independently be changed with respect to the water flow rate and was thus measured.

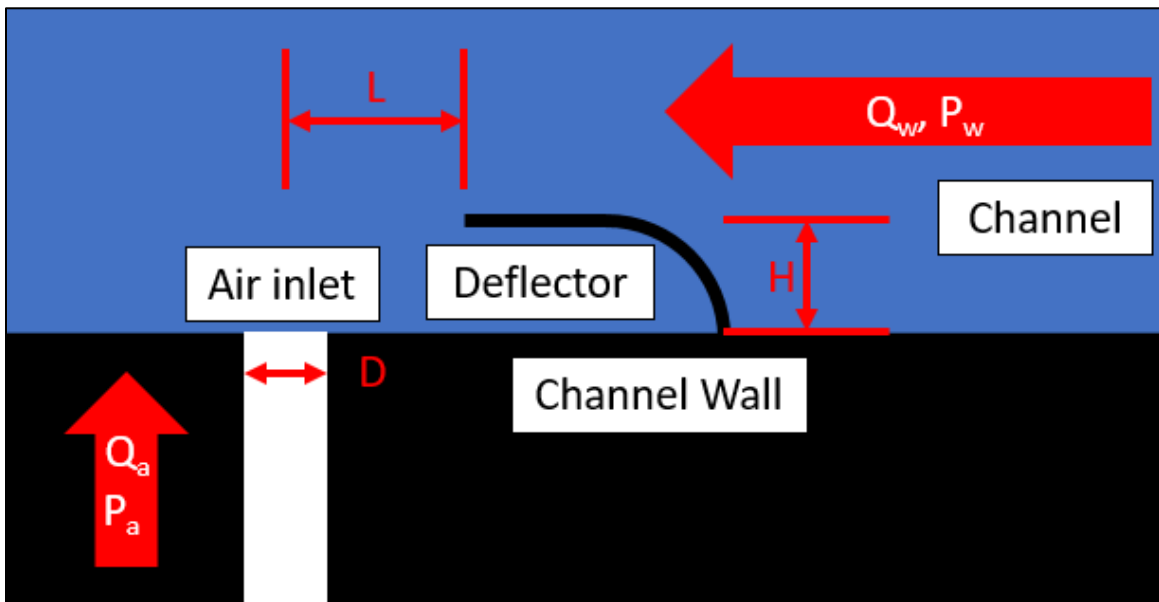


Figure 3-22: Deflector and Experimental parameters

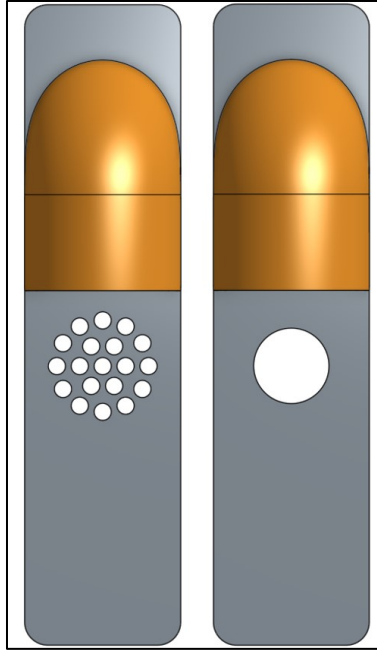


Figure 3-23: Mesh Deflector Configuration with reference sample ( $H = 16.5$ ,  $L/H = 1$ ,  $D/H = 1$ )

Table 3-3: McGill Test Parameter Ranges

Parameter	Symbol	Units	Range
Channel Cross Section	-	mm <sup>2</sup>	[50.15 x 80.2]
Water Flow Rate	$Q_w$	l/s	[1.51, 3.53, 5.55, 8.04]
Air/Water Flow Ratio	$Q_a/Q_w$	%	[0, 3, 5, 7, 10]
Deflector Size	H	mm	[10, 13.5, 16.5]
Air Inlet Position	L/H	-	[0, 1, 2]
Air Inlet Size	D/H	-	[1]

Table 3-4: Vevey Test Parameter Ranges

Parameter	Symbol	Units	Range
Channel Cross Section	-	mm <sup>2</sup>	[54 x 74]
Water Flow Rate	$Q_w$	l/s	[28, 40, 59.9]
Water Pressure	$P_w$	kPa	[347.2, 747.2, 121.2]
Air/Water Flow Ratio	$Q_a/Q_w$	%	[0, 2, 3, 5]
Deflector Size	H	mm	[10, 13.5, 16.5]
Air Inlet Position	L/H	-	[0, 1, 2]
Air Inlet Size	D/H	-	[1]

To organize the collected data, a numeric value was assigned to each deflector configuration, detailed below in Table 3-5:

**Table 3-5: Geometric configurations of deflector samples**

Name	H [mm]	L/H [-]
1	10	0
2	10	1
3	16.5	0
4	16.5	1
5	16.5	1-MESHED
6	10	2
7	16.5	2
8	13.5	0
9	13.5	1
10	13.5	2
11	None	N/A

### 3.4 Signal Acquisition and Data Analysis

The calculation of the oxygenation coefficients and aspiration capacity of each deflector requires the measurement of the oxygen concentration, the water flow rate, the air flowrate, the upstream water pressure and the air inlet pressure. The water flow rate (at both the McGill and Vevey test rig) and the Vevey water pressure were read from the gauge due to the lack of a compatible output signal. The remaining measurements: the air flow rate, the McGill upstream water pressure, the air inlet pressure, and the McGill DOx4 concentration measurements, were electrical signals sampled using a data acquisition (DAQ) system (USB-2408 Measurement Computing). The DAQ is capable of a 1 kHz sample rate (in total for all channels) and 16 single-ended or 8 double-ended voltage measurements.

The DAQ system was configured to measure voltage signals. The DO sensors at McGill output a current based signal and thus a control box was built that placed a 500  $\Omega$  shunt resistor between the DO sensor leads and changed the [4, 20] mA signal to [2, 10] V. The air flowmeter

and pressure transducers required a stable 10V DC power supply, which was also attached within the control box to alleviate the congestion of wires being fed to the DAQ. Figure 3-24 shows a schematic of the circuit within the control box.

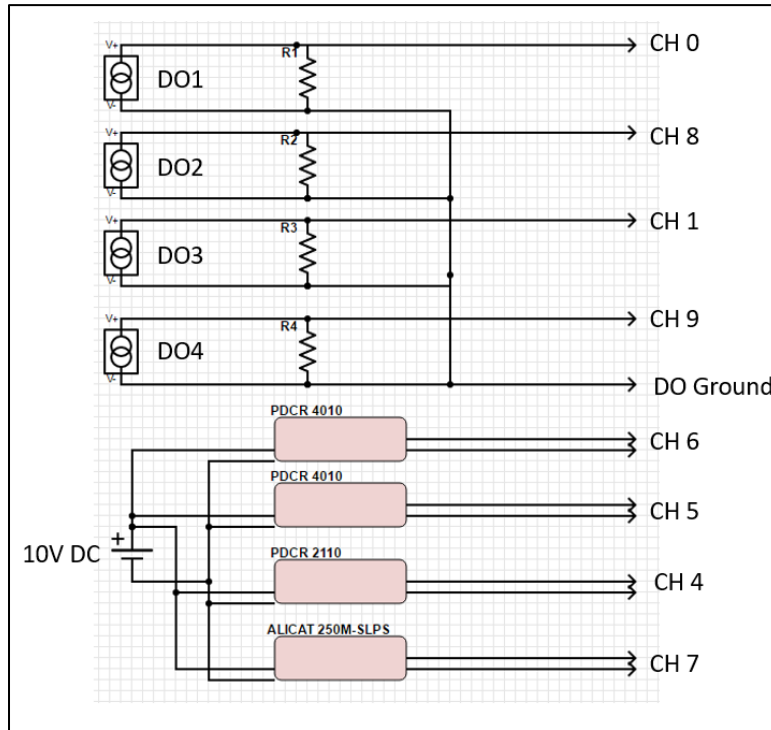


**Figure 3-24: Electronic Control Box Schematic**

To analyze the signals read by the DAQ, LabVIEW was used to collect the experimental data. The LabVIEW VI outputted a text file containing the time series data of the different signals read by the DAQ. To efficiently handle the data generated by this study, several Python scripts were written to generate excel sheets of the experimental data points. MATPLOTLIB, a Python library, was used to generate the figures of the results presented in Chapter 4. The regressions and curve-fitting presented in Chapter 4 was accomplished by the MATLAB curve-fitting app.

While the pressure transducers and air flowmeter output continuous signals, the 4 DO sensors took readings every 100s with the output signal staying constant between readings. The inflow DO sensors were read for 200s (in a situation of constantly increasing DO level), the sample

pot DO sensors for 300s, and the air flow and pressure transducers for 15s (the response time for both was 10ms). The DO sensor readings for each experiment were extracted by looking for a change in the voltage past a threshold of 10 mV. This triggered the storage of the individual DO readings in Python and gave a time series of readings every 100s. The characteristic data point for the differential DO concentration measurements was extracted by choosing a time (50s for the inflow and 250s for the sample pots) and performing a linear regression between the most recent and next DO reading within the time series of stored readings, taking into account the time of the desired measurement and not just an average. This allowed the DO concentrations to be calculated at the same time for the upstream and downstream sensors, even though the sensor readings were not necessarily synchronized throughout the experiment. The characteristic data point for the air flow and pressure transducer measurements was taken by averaging the full time-series of data from the LabVIEW measurement file using a trimmed mean (removal of +/- 1 standard deviation) to eliminate an intermittent sensor error. This assumed a constant value for the pressures and airflows over the course of the experiment.

The equation for oxygen mass transfer does not characterize the oxygenation of an aerating flow by using the raw DO concentration difference between two measurement points. Rather, a non-dimensional oxygen transfer efficiency and a total aeration coefficient are used to quantify the oxygenation. To calculate the oxygen transfer efficiency, the oxygen saturation is calculated using Equations [3, 4], and applied to Equation [6]. Equations [5] and [7] were used to calculate the total aeration coefficient.

To understand the aspiration capacity of the deflector configurations, the pressure difference between a point upstream of the deflector and the air inlet is needed with and without aeration occurring. A non-dimensional form of this pressure difference, known as the Euler

number, is used to quantify this aspiration capacity. Since the air pressure was measured within the air supply conduit, the air inlet pressure was calculated from Equation [1] and the contribution of the hydrostatic pressure removed.

## **Chapter 4: Results and Discussion**

This chapter will present the results and discussion of this research wherein a recirculating flow into which a test chamber housing a deflector, was subjected to a range of water flow rates and air/water flow ratios. Various metrics of oxygenation and aeration were calculated to elucidate the oxygenation physics of the flow in a qualitative and quantitative manner. First, the flow was validated to ensure that the measured oxygen uptake occurred due to the injected air and not to air leaks through the free surface in the reservoir or elsewhere in the flow. Second, an analysis was made to ascertain the most accurate measurement method for the oxygen concentration difference between two points in the recirculating flow. Third, a qualitative description of the injected bubble swarm is given, based on the videos taken during each experiment, to describe the physics of the flow and the aeration mechanisms. Fourth, the quantitative aeration and oxygenation results are presented with a discussion of the governing parameters and the physics of the flow to provide a preliminary description of the oxygenation and aeration physical model. Finally, the sources of error are presented with suggestions to improve the rig and thus the quality of the measurements.

### **4.1 Pre-Tests**

The recirculating flow in the McGill experimental setup was open to the atmosphere, so oxygen exchange at the free surface could contribute to the observed oxygen transfer rate. As described in Section 3.1, a manifold system with a perforated tube connected to a Venturi vacuum pump placed along the rim of the recirculating tank with a plastic bag stretched over the opening was used to isolate the water from the atmosphere and to withdraw the aeration bubbles as quickly as possible from the reservoir and thus reduce this source of error. Preliminary validation tests were used to check that DO levels were not increasing due to oxygen entrained from the free surface but only due to the injected bubbles. These tests ascertained that there was no change in DO levels between the two measurement points for tests with no air injection in which two water

levels and two water velocities were used. Two water levels and velocities were used to investigate a range in the level of free surface agitation and in the volume of water within the recirculating flow. Data was collected for 500s, the approximate duration of each test. The difference in DO concentration between the measurement points was measured every 100s using the sample pot oxygen sensors. The results, detailed in Table 4-1 indicate that there was no significant DO occurring due to oxygen exchange at the free surface of the reservoir. Hence, for subsequent experimental results, measured changes in DO was assumed to be due to deflector aeration.

**Table 4-1: Validation Tests, Results and Parameters**

<b>Test label</b>	<b>Water level [cm below max tank level]</b>	<b>Water Velocity [m/s]</b>	<b>Mean Measured E [-]</b>	<b>Error of E [+/-]</b>
V-1	10	0.38	0.021	0.012
V-2	40	0.38	0.020	0.012
V-3	10	2.0	0.020	0.016
V-4	40	2.0	0.021	0.016

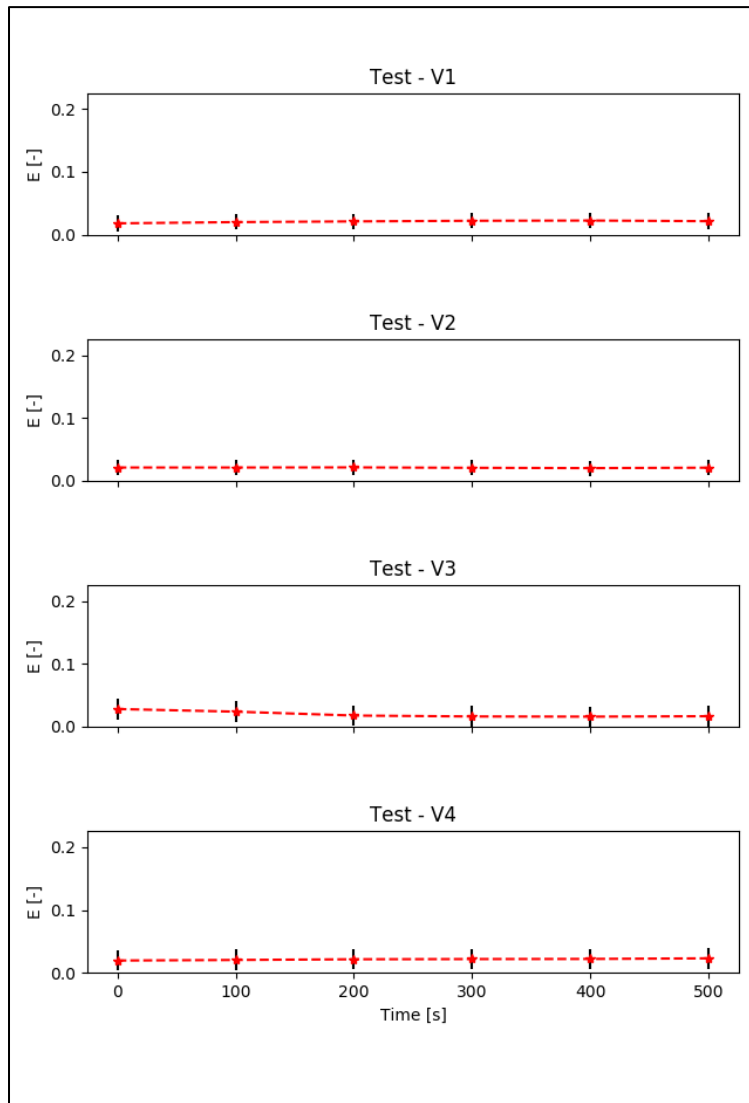


**Figure 4-1: Validation Tests Results**

#### **4.1.1 Comparison between Inflow and Sample Pot DO measurements**

The dissolved oxygen level was measured using the dissolved oxygen sensors both inline and in sample pots. The sensors specification indicated a 100s time for the sensor measurement to stabilize. Sample pots were used to withdraw a sample of the water and measure a constant DO level over a 100s period. The DO sensors were also placed inline (or inflow), and a comparison with the sample pot data was used to determine if the inline sensors were capable of detecting the continuously changing DO levels in the aerated flow. Both the inline and the sample pot DO

concentrations were measured in each experiment. The measured DO concentration data was subsequently used to calculate oxygenation coefficients and is independent of the measurement method. In this report, the sample pot data was used for the determination of the oxygenation coefficients as it was observed to be more reliable for the following reasons:

1. The inline DO measurements were unable to establish measurement stability in the recirculating flow due to the buildup of DO outpacing the stability of the measurements.
2. The Upstream Inflow sensor (DO 1) showed a strong hysteresis effect that resulted in measurement instability. A visual evaluation was made that the sensor read a DO concentration of 0 mg/L well into the time period when the other sensors were reading some level of oxygen within the flow. The sensor values increased as the Eulerian concentration increased but the difference between the two measurements (between DO1 and DO3), which would be due solely to the Lagrangian DO uptake, was not accurately captured. This led to an erroneously high measured DO uptake (DO 1 being artificially too low) when compared to the sample pot DO measurements (see Figure 4-3)
3. The Upstream Inflow sensor (DO 1) broke towards the end of the experimental run, giving significant uncertainty to the validity of its previous data collection

The comparison between the inflow and sample pot raw DO data, shown in Figure 4-2, shows that the inflow sensors did not establish measurement stability within the experimental run time. From the data collected by the sample pot sensors, it was clear that a few readings were required in order for the DO measurement to stabilize even in a sample with an unvarying DO concentration (of the sample pot measurements). The inflow sensors were not able to respond to the rate of change in the sum of the Eulerian and Lagrangian DO increase. The upstream inflow

sensor (DO 1) was not able to capture the fast rate of change in time and the sensor did break towards the end of this study.

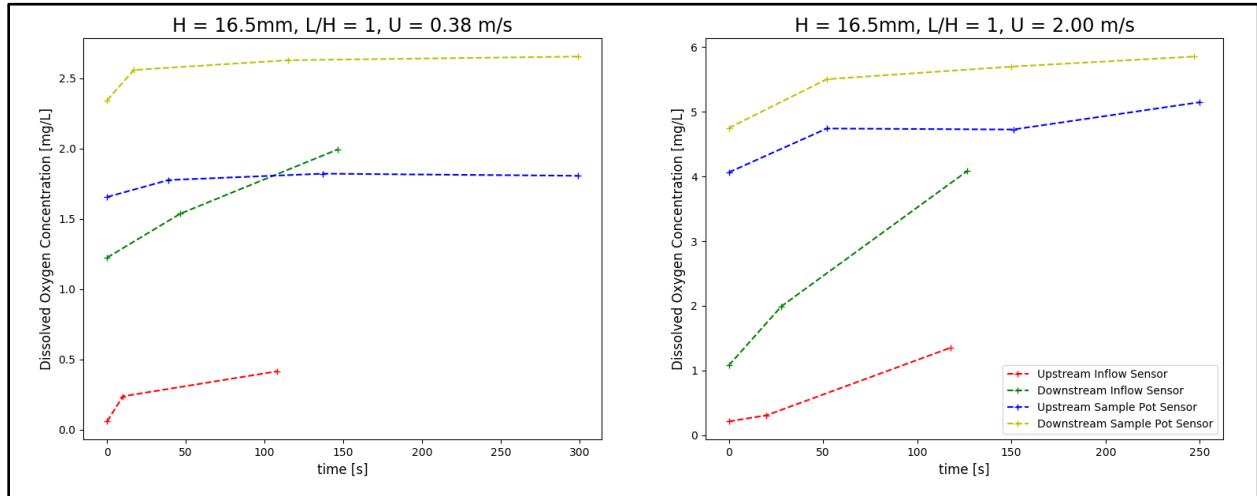


**Figure 4-2: Raw DO data comparison at low and high water velocities,  $Q_a/Q_w = 10\%$  for both**

The comparisons between the inflow and sample pot DO measured oxygenation coefficients, shown in Figure 4-3, exhibited errors stemming from the errors shown in Figure 4-2. Due to Upstream Inflow sensor (DO1) measuring the DO concentration artificially too small (from the earlier point 2) the calculated oxygenation coefficients were much higher and showed little variation when compared to the sample pot DO measurements. The trends in the sample pot data correspond to increasing oxygenation with increasing gas void ratio and discharge as expected. This therefore indicates that the inflow sensors were not able to measure the evolving DO concentration in the flow as the required 100s measurement time was not possible and the effect of the upstream inflow sensor gave erroneous measurements.

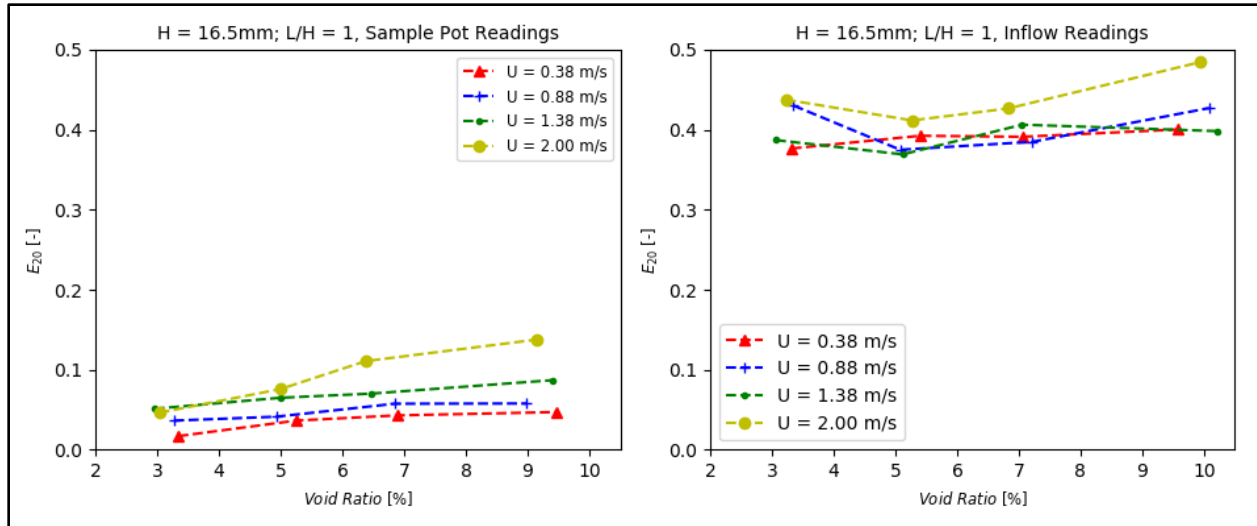


**Figure 4-3: Inflow vs Sample Pot Readings comparison**

It was, therefore, decided to use only the sample pot measurements for the analysis of the oxygenation rates for the different deflector designs at different flow rates and air injection rates. Note that this meant that the oxygenation rate was only measured once per test, as the sample pots could only be filled once during a test. The test duration was 500s and the time required to fill, establish a stable reading, and subsequently flush the sample pot was ~600 seconds (the time spent establishing a stable reading was done while deoxygenating the water for the next experiment).

#### 4.1.2 Repeatability

Repeatability of the experimental data was determined by repeating measurements for one parameter set that was representative of the median configuration:  $H = 13.5$  mm and  $L/H = 1$ . Three experiments were performed for each water discharge and air injection rate. The resulting average oxygen transfer efficiency is plotted in Figure 4-4 with the error bars representing the standard deviation. The standard deviation ranges from 0.003 to 0.01. Using the coefficient of variation as a measure, the percentage error ranged from 4.6% to 47.7%. The highest variability was seen in the lowest air/water flow ratio experiments and experiments with a combination of the highest water velocity and air/water flow ratio experiments.

The variability in the measurements was hypothesized to be due to experimental method errors rather than instrumentation variability. At low water velocities, the injected bubbles immediately rose to the crown of the horizontal pipe and were intermittently retained at the location of the water control valve just upstream of the reservoir. When the level of air just upstream of the valve reached a certain point (the air level reached the opening of the valve), a large slug of air would be released into the reservoir and broken up into a fine mist that oxygenated the water in the reservoir as the bubbles rose to the quasi-free surface covered by the plastic bag system described in Section 3.1. At high water velocities, bubbles would get intermittently recirculated by the pump back into the test chamber, particularly at the higher test air/water flow ratios.

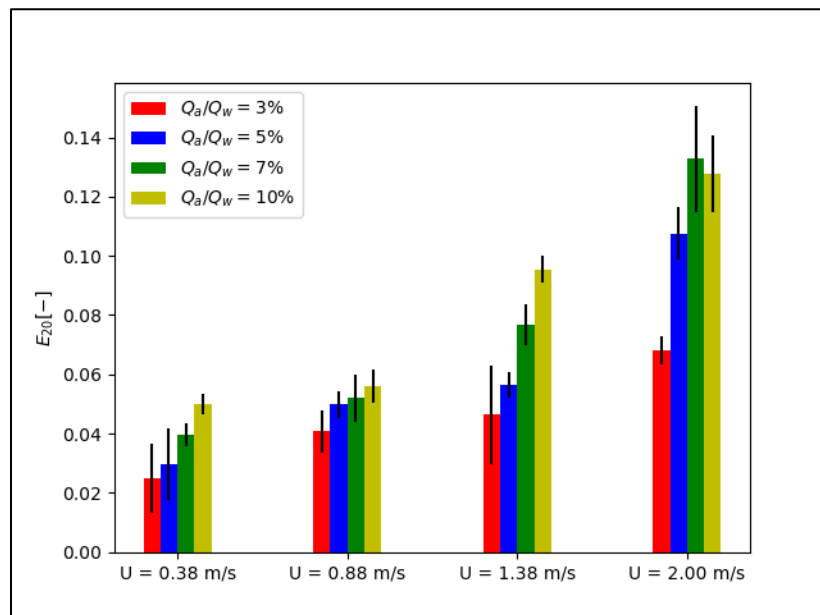


**Figure 4-4: Oxygen transfer efficiency by water velocity and air flow ratio; repeatability experiments;  $H = 13.5$ ;  $L/H = 1$ ;  $U = [0.38, 0.88, 1.38, 2.00]$  m/s;  $Q_a/Q_w = [3, 5, 7, 10]$  %; no mesh**

#### 4.2 Qualitative Observations of the Bubble Swarm created by the deflectors

Characterization of the bubble swarm created by the deflector from the injected air and the subsequent behavior of the injected air and resulting bubbles was undertaken. The qualitative

observation of the injected bubbles was made using a high-speed video of each experiment viewed through the viewing window in the test chamber (dimensions of 60 x 80 mm).

The following general observations were made:

1. At low water velocities, discrete bubbles separate from the air inlet.
2. At high water velocities, the deflector serves as an obstacle behind which the injected bubbles immediately coalesce (i.e. in the lee of the deflector).
3. The presence of a mesh only broke up the injected bubbles into a swarm, to optimize oxygen mass transfer, was only successful at low water velocities.
4. At high water velocities, the bubbles are sheared off the downstream tip of a stable air bubble present in the lee of the deflector.

#### **4.2.1 Defining parameters of the bubble size**

The purpose of the deflector in the flow is to create a low-pressure region behind the deflector that will aspirate air into the draft tube and result in air bubbles from which oxygen is transported to the flow increasing dissolved oxygen levels. In the test rig, the deflector causes a reduced air pressure behind the deflector into which the air is injected (with positive pressure). The flow around the deflector is shown schematically in Figure 4-5. As the flow rate increases, the pressure drop behind the deflector increases and the volume of reduced pressure region also increases in magnitude. When the air is injected in the flow downstream of the deflector, it will either be carried downstream with the flow (at low velocities or for the inlet further downstream) or it will be drawn upstream into the low-pressure region downstream and within the deflector (high velocities or air inlet within the deflector). Bubbles of air are formed directly from the air injection point at low velocities, or due to shearing off the large air bubble that forms within and extends downstream of the deflector at high velocities. Once detached the air bubbles are advected downstream with the flow and simultaneously rise to the top of the conduit.

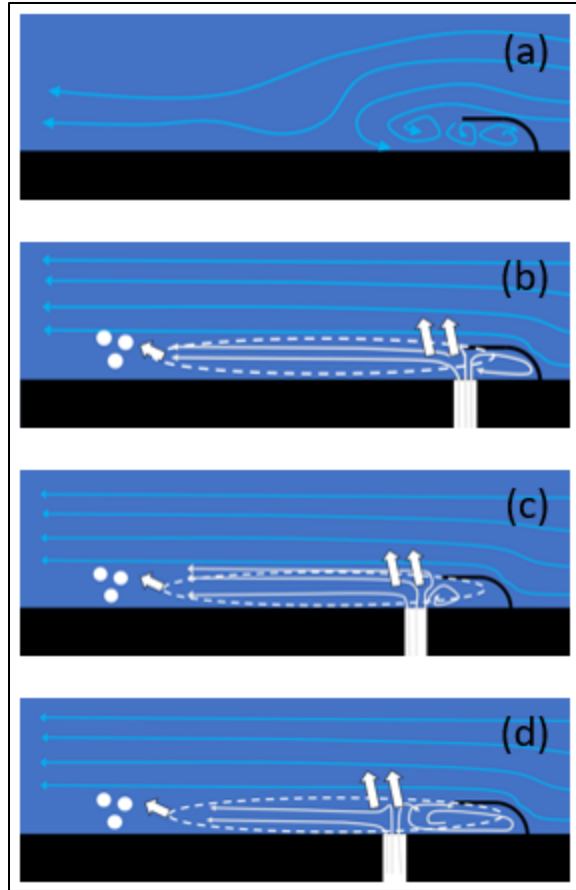


**Figure 4-5: Schematic diagram of flow past a deflector with two locations of bubble formation shown with white arrows. White dashed line indicates approximate extents of stable air bubble at high velocities. (a) No aeration; (b) aeration at  $L/H = 0$ ; (c) aeration at  $L/H = 1$ ; aeration at  $L/H = 2$ .**

The oxygenation rate of the flow is dependent on many parameters, one of which is the mean bubble size. The bubble size depends on the physical processes that occurs as the flow passes by the deflector. The characterization of the bubble swarm could be used to calibrate and validate the oxygenation CFD model being developed for the McGill test rig. An understanding of the parameters setting the initial mean bubble size is necessary to model the initial bubble size and hence, calculate the oxygen transfer efficiency at the prototype scale.

At any given air/water flow ratio, the magnitude of the water velocity determines the size of the air bubbles and the trajectory of the air bubble swarm. For an air/water flow ratio of 3% and

geometry of the deflector of  $H = 10\text{mm}$ ,  $L/H = 0$  (i.e. the air inlet is at the end of the deflector). Figure 4-6 shows the bubble characteristics and trajectory for the low, mid, and high flow velocity (0.38 m/s, 1.38 m/s, and 7 m/s) At the low flow velocity, individual bubbles detach from the deflector and rise (at an angle of  $45^\circ$ ) towards the top of the conduit. At the mid velocity, the air forms a long bubble extending about 3 deflector lengths in the downstream direction, before individual bubbles separate off from the bubble. The bubbles rise at a low angle of  $<10^\circ$ . At the highest velocity, the bubbles do not rise much (top air forming an angle of  $<20^\circ$ ), however, the turbulence of the flow shears lobes off the main air bubble, with each becoming a bubble.

The injected air immediately coalesces in the lee of the deflector at velocity scales close to those found in prototype draft tubes. The bubble size appears to be determined by the deflector size and water velocity rather than the air inlet size and gas void ratio. No appreciable difference in the size of the air bubbles was seen as the gas void ratio increases (holding other parameters constant). The shear intensity at the air-water interface increases with increasing water velocity as visualized by the increase in observed ripples on the surface of the air pocket. (This thesis study collected a vast number of videos from which a more educated measurement of the bubble size can be undertaken at a further time, as well as providing a test rig to which a more sophisticated camera can be attached).

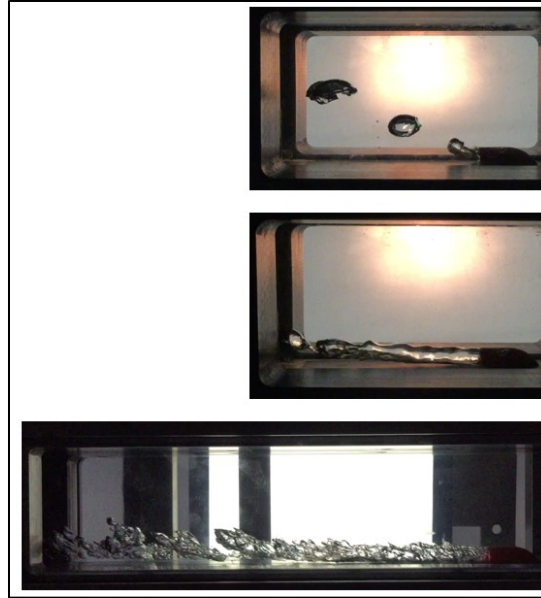


**Figure 4-6: Bubble injection in deflector  $H = 10\text{mm}$ ,  $L/H = 0$ . Top –  $U = 0.38\text{ m/s}$ , Middle –  $U = 1.38\text{ m/s}$ , Bottom –  $U = 7\text{ m/s}$ .  $Q_a/Q_w = 3\%$**

#### 4.2.2 Effect of a mesh at the air inlet

To optimize oxygen mass transfer, the total interstitial contact area between the air and the water must be maximized. It is preferable to have many bubbles with small diameters instead of few bubbles with large diameters thus increasing the total contact surface area. It was hypothesized that a mesh in the air inlet would result in the air flow being broken into a fine mist of smaller diameter bubbles. The effect of the mesh at the air inlet can be seen in Figure 4-7 which compares the with-mesh case to the without-mesh case for flow velocities of 0.38 m/s and 2.0 m/s for the deflector geometry of  $H = 16.5\text{ mm}$ ,  $L/H = 1$ ,  $D/H = 1$  and air/water flow ratio of 5%. At low water velocities, the mesh breaks up the injected air to form many smaller bubbles, which are slowly advected with the flow as they individually rise due to their buoyancy. Without the mesh, larger bubbles separate from the air inlet point. However, at high water velocities (i.e. at magnitudes close to those found in prototype turbines) the mesh did not result in small bubbles forming (see Figure 4-7). At the higher velocities, the low-pressure region downstream of the deflector is larger

and injected air coalesces into the large stable air bubble forming within and downstream of the deflector. In addition, at the higher velocity, the air is advected faster and does not rise significantly within the field of view. Bubbles are sheared off the downstream tip of this air void. The bubble sizes are determined thus by the hydraulic (turbulence) parameters and the deflector geometry. It is therefore not possible to modify the size the injected bubbles by sizing the initial air inlet. In a CFD model studying the oxygenation process in draft tubes, it is thus important to realize that the transport equation for the bubble size, present in many CFD methods, must consider the bubble size as separate from the air inlet size.

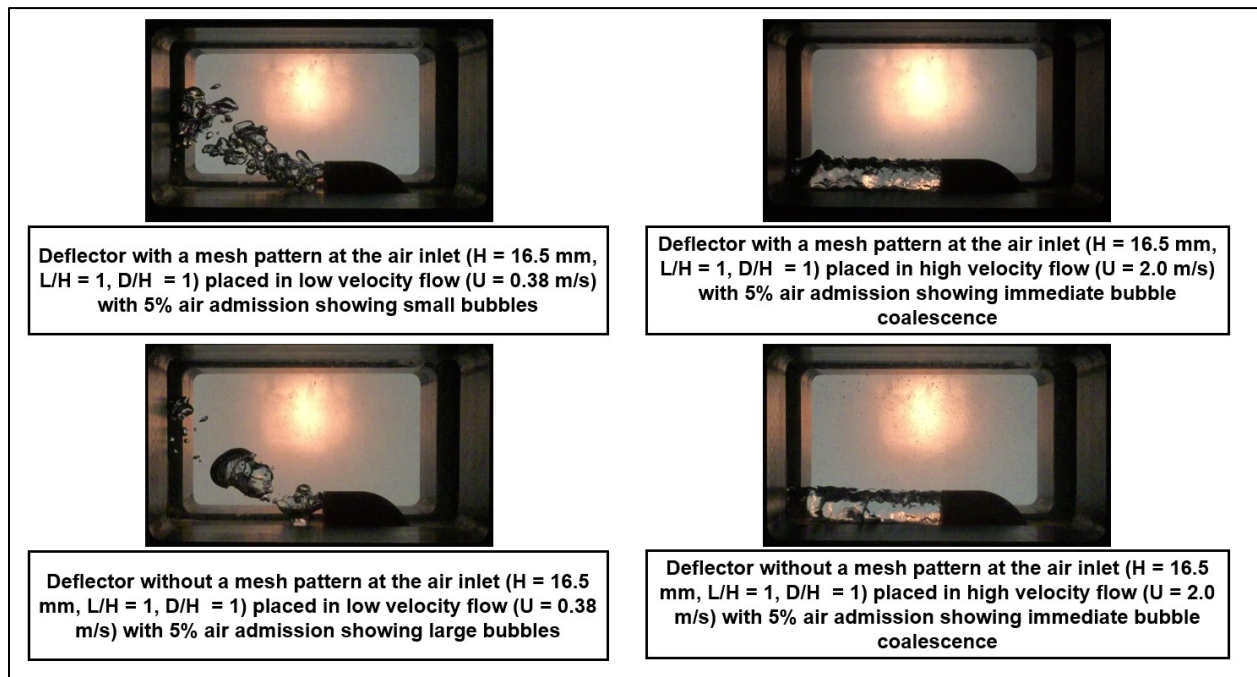


**Figure 4-7: Effect of the mesh presence on the injected bubble swarm**

#### 4.2.3 Air Recirculation in the lee of the deflector

A knowledge of the flow topology around the deflector would serve as an important tool for the validation of the parallel CFD project. A video of the initiation of air injection was taken to understand the transient process of air injection onset and to qualitatively describe the flow field around the deflector. The video of the air injection downstream of the deflector showed evidence

of significant flow recirculation in the lee of the deflector. When the air injection is started, bubbles were observed travelling upstream towards the deflector (see Figure 4-8) and after a short time a large stable bubble of air forms within and downstream of the deflector. As it is the flow around the deflector, that affects the bubble size of the injected air, it is proposed that a subsequent study on this test rig is used to understand parameters affecting the flow around the deflector and their effect on bubble size. One modification to check is to puncture the deflector wall and allow the water to pass through the deflector with the expectation that this will break up the large stable bubble and result in smaller bubbles forming. A deflector design that maximizes the bubble breakup optimizes the oxygenation process within draft tubes and the recirculation of air at the deflector could be an impediment to that process.

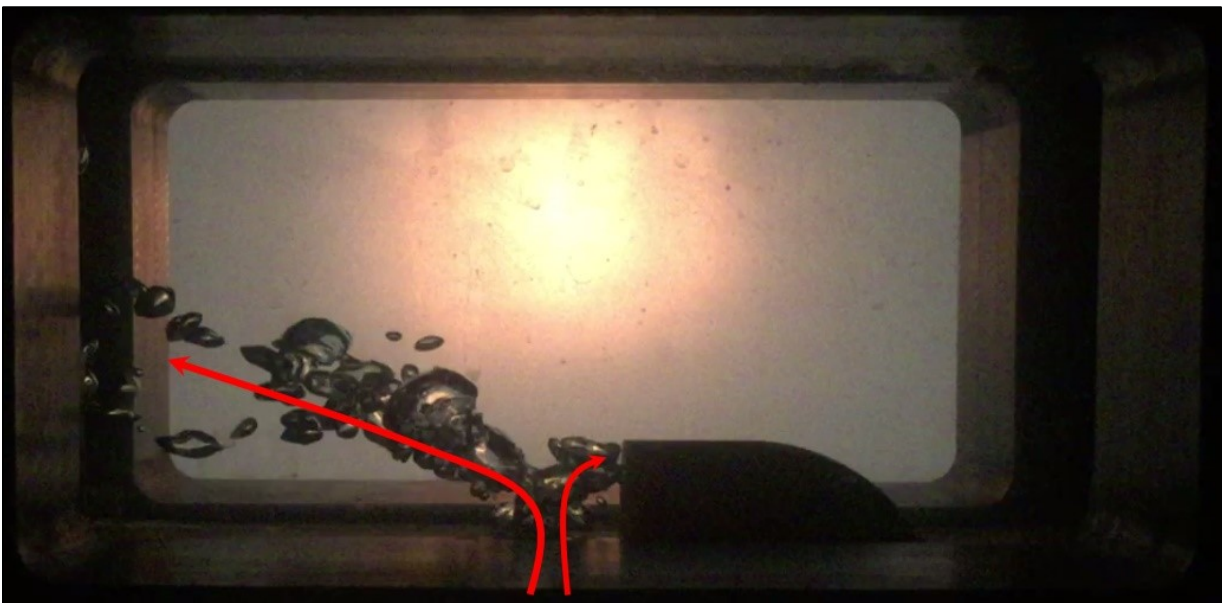


**Figure 4-8: Start-up freeze-frame showing air flow recirculation;  $V_w = 0.38$  m/s,  $Q_a/Q_w = 3\%$**

### 4.3 Air Entrainment Results

The quantification of the induced low-pressure wake, as well as the calibration and validation of the parallel CFD project, requires the measurement of the upstream water and air inlet pressure over a variety of air/water flow ratios at different water velocity scales. A high

velocity test rig at the Andritz Hydro Hydraulics Laboratory in Vevey, CH and a purpose-built low-velocity test rig at the Hydraulics Laboratory at McGill University were used to collect data.

#### **4.3.1 Pressure difference between injection point and upstream flow without aeration, high velocity**

To quantify the aspiration capacity of the deflectors (what volume of air will be entrained into the prototype draft tube) and to elucidate the optimal positioning of the air inlet, the pressure difference between a point just upstream of the deflector (P1) and the air inlet (P2) was measured at high water velocities without aeration (refer to Figure 3-21) in the Vevey test rig. In the prototype, a pressure below atmospheric pressure at the air inlet within the deflector's low-pressure wake induces the air flowrate by aspiration. The pressure difference between P1 and P2 was not large enough in this experimental setup to reach pressures below atmospheric pressure at the air inlet. However, the prototype onset of air injection is induced by this initial no-aeration pressure difference between the air inlet and the ambient atmosphere. Thus, the measurement of this pressure difference without aeration gives an indication of the aspiration capacity of the deflector and reveals the aeration physics of the different deflector configurations, as well as providing an important validation benchmark for the parallel CFD project.

The pressure difference between a point just upstream of the deflector (P1) and the air inlet (P2) was measured at high water velocities (in the Vevey test rig) without aeration to quantify the aspiration potential. In the prototype draft tube, the combination of the deflector's presence, the high water velocity and low pressure in the area just downstream of the turbine runner results in a pressure below atmospheric at the air inlet. This below atmospheric pressure drives the natural aspiration of air into the draft tube. In the Vevey experimental set-up, the lack of a turbine means that the pressure within the test chamber is never low enough to result in a below atmospheric

pressure at the air inlet, even with a significant value for P1-P2. Figure 4-9 shows the experimental data.

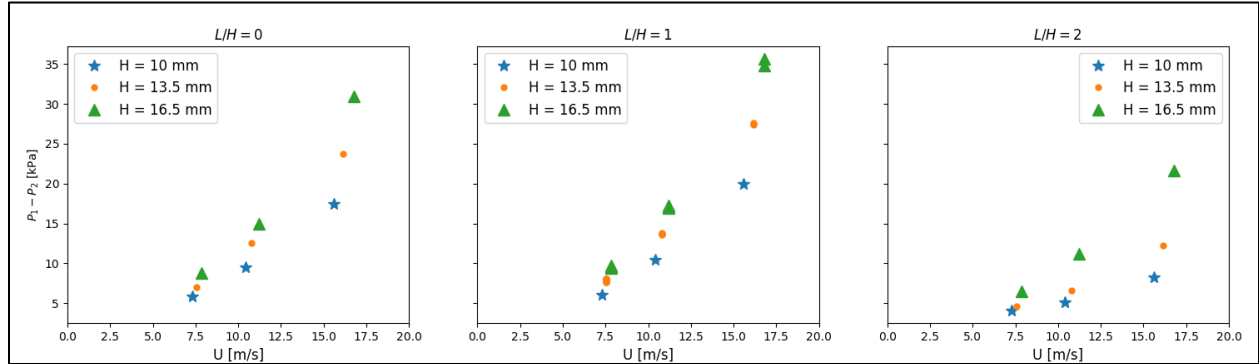


**Figure 4-9: P1-P2 vs water velocity for high water velocities without aeration**

The magnitude of the pressure difference between the upstream flow and the deflector cavity increased with both increasing water velocity and with increasing deflector size. Importantly, across all deflector and water velocity scales, the air inlet position of L/H = [1] showed the greatest pressure difference and is thus the optimal position of the air inlet determined by this study.

To reveal the important design parameters of the deflectors at the prototype scale, a dimensional analysis was undertaken. From the Bernoulli equation, an equation can be written of the form:

$$P_1 - P_2 = \zeta \frac{1}{2} \rho_1 U^2 \quad [21]$$

where  $\zeta = f(H, \frac{L}{H}, \text{deflector shape, etc})$  dimensionless scale effect. The linear dependence of the pressure drop (P<sub>1</sub>-P<sub>2</sub>) on the dynamic pressure ( $\frac{1}{2} \rho_1 U^2$ ) is verified in Figure 4-10.

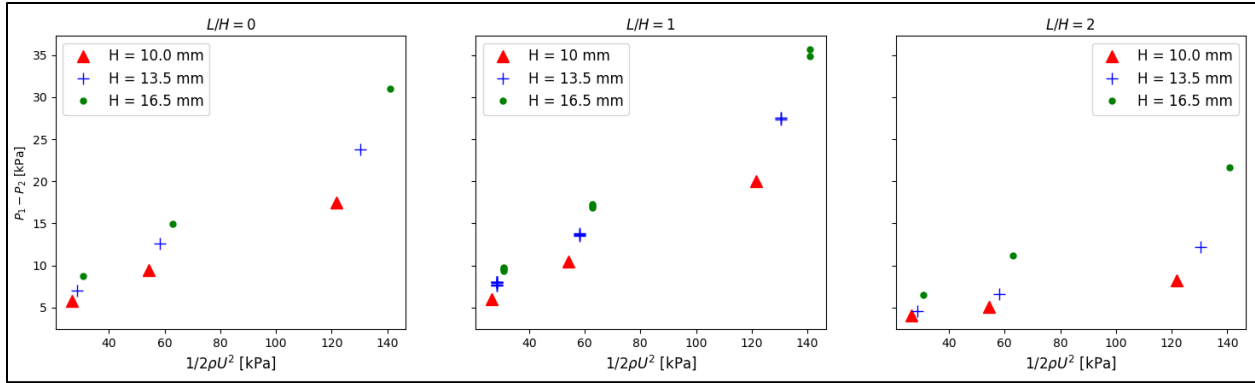


**Figure 4-10: Bernoulli Loss Coefficient, No Aeration;  $U = [7, 10, 15]$  m/s**

The linear dependence of the pressure drop with the dynamic pressure is seen for all three air injection locations. A scale effect can be seen, as the ratio of the pressure drop to the dynamic pressure ( $\zeta$ ) increases as the scale of the deflector increases (i.e. as the effect of viscosity decreases). The highest ratio of the pressure drop to the dynamics pressure ( $\zeta$ ) is for the air injection point at  $L/H = 1$ , which is slightly larger than that at  $L/H = 0$ . There is a very low ratio of pressure drop to dynamic pressure ( $\zeta$ ) when the air injection point is further from the deflector at  $L/H = 2$ .

The ratio of the pressure drop to the dynamic pressure ( $\zeta$ ) decreases exponentially with flow velocity and increases approximately linearly with the scale of the deflector increases, as shown in Figure 4-11.

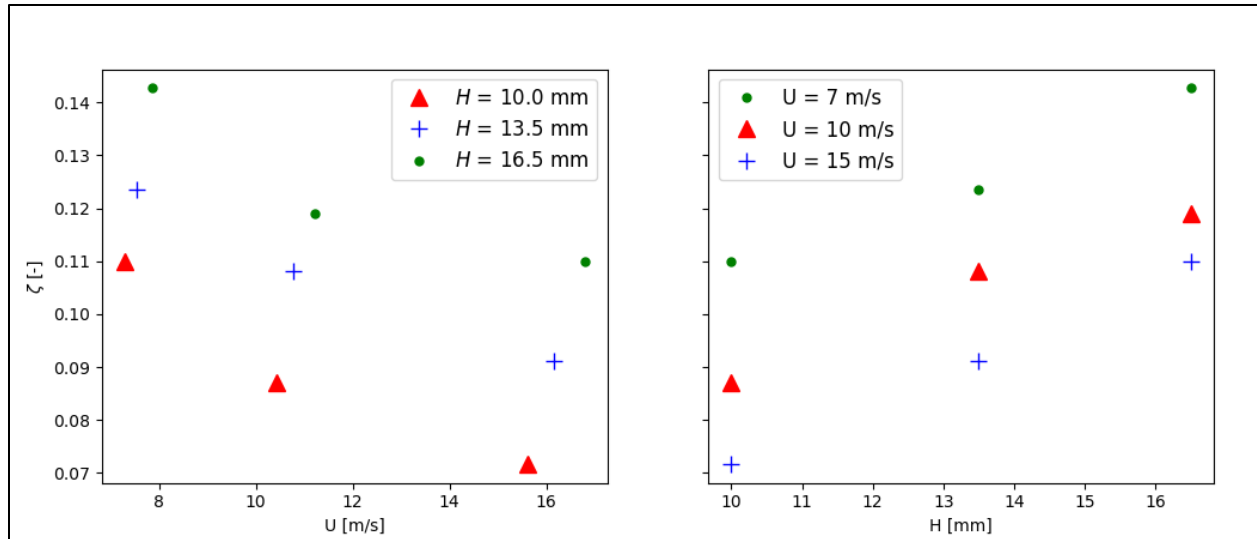


**Figure 4-11: Dimensionless parameter dependence;  $L/H = 1$ , No Aeration**

### 4.3.2 Effect of aeration on pressure difference between injection point and upstream water pressure

A full understanding of the flow topology and the low-pressure wake requires knowledge of the pressure difference ( $P1-P2$ ) when aeration is occurring at high and low water velocities. In the prototype, the flowrate of the air is driven by the sub-atmospheric pressure at the air inlet, and without a compressor or blower attached to the air supply system, the upper limit to the entrained gas void ratio is fixed. The Vevey test rig was used to quantify aeration parameters at high velocities and, also, to study the changing flow topology around the deflector as the aeration reduces the induced flow separation. The McGill test rig was used to quantify the aeration parameters at low velocities, not analogous to the prototype draft tube, to provide calibration and benchmark validation for the parallel CFD project.

The high velocity flow in the draft tube causes a zone of flow separation downstream of the deflector. At high flow velocities, aerating within a prescribed zone in the lee of the deflector reduces the intensity of the flow separation by streamlining the flow. This, in turn, reduces the pressure difference between the draft tube and the air inlet.

Figure 4-12, Figure 4-13, and Figure 4-14 show the pressure difference ( $P_1 - P_2$ ) for a range of high water velocities (7 – 15 m/s) and a range of air/water flow ratios (0 – 5%) for the three different deflector scales ( $H = 10, 13.5,$  and  $16.5$  mm), respectively. The pressure drop increases with flow velocity and with increasing scale of the deflector. The pressure difference is smaller when the flow is aerated, as the flow separation is attenuated, than when not aerated, but the magnitude of the air/water flow discharge (<5%) does not affect the pressure drop. The location of the air inlet affects the pressure difference similarly to the case with no aeration. It is greatest for  $L/H = 1$ , slight lower for  $L/H = 0$  and much reduced for  $L/H = 2$ . It will be important to study in CFD what the pressure difference will be at the air inlet in the prototype upon the onset of aeration where no compressor is forcing air into the draft tube.

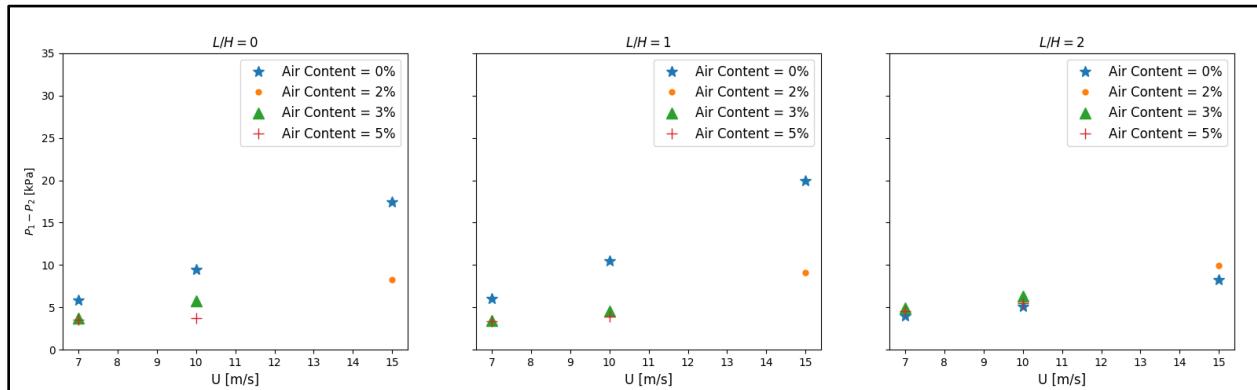


**Figure 4-12:  $P_1 - P_2$  vs  $U$  at high water velocities with aeration;  $H = 10$ mm**

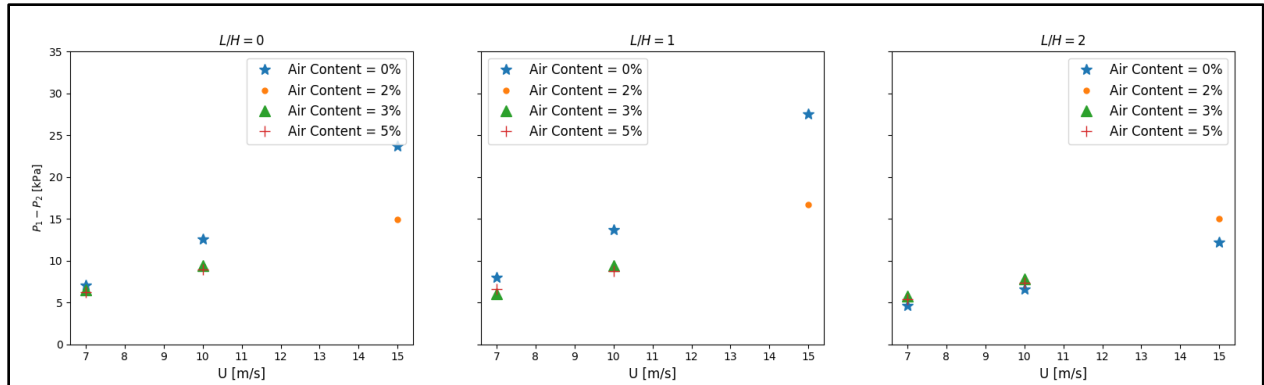


**Figure 4-13: P1-P2 vs U at high water velocities with aeration; H = 13.5mm**

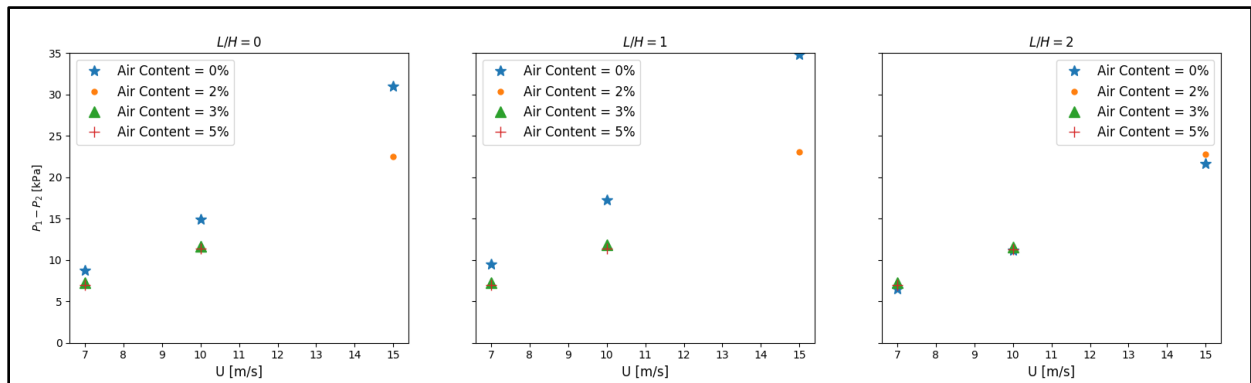


**Figure 4-14: P1-P2 vs U at high water velocities with aeration; H = 16.5mm**

From the above figures, it is evident that the amount of air injected does not have a significant effect on the measured pressure difference. This may be due to the relatively small range of injected air flow rates studied, or because the act of aerating the lee of the deflector stably reduces the degree of flow separation and changes the flow topology. The act of aerating forces the flow to follow a more regular path downstream of the deflector and results in a lower pressure difference between the upstream flow and the deflector cavity. However, at  $L/H = 2$ , aeration does not reduce the pressure drop, which suggests that the injected air does not interact with the low-pressure regions downstream of the deflector.

Compared to the high velocity aeration measurements, the behavior of the low velocity pressure measurements at the McGill test rig were different (see Figure 4-15, Figure 4-16, and Figure 4-17). As the physical processes cannot logically explain the trends in behavior of the pressure drop, it is hypothesized that the pressure transducers were not operating correctly. No similar effect was seen with the Bernoulli loss coefficient or the dynamic pressure shown in Figures 4-10 & 4-11 in the McGill test rig. An attempt to explain the behavior follows.

As the water velocity in the McGill rig was much lower than the operating points at the Vevey rig, the wake induced by the deflector was of lower intensity. At the lowest velocities, the wake had a higher pressure than the ambient flow because of the decrease in velocity within the wake. An increase in  $P_1 - P_2$ , corresponding to a lower air inlet pressure, is observed as the water velocity is increased. The linear dependence on the dynamic pressure appears only after the water velocity is increased to the values studied in the Vevey test rig and in general, the behavior is much less stable when compared to the high velocity case. While prototype draft tube conditions will not be within this low-velocity range, this set of data serves as a validation tool for the CFD parallel project which is better able to study the flow topology around the deflector with aeration occurring.

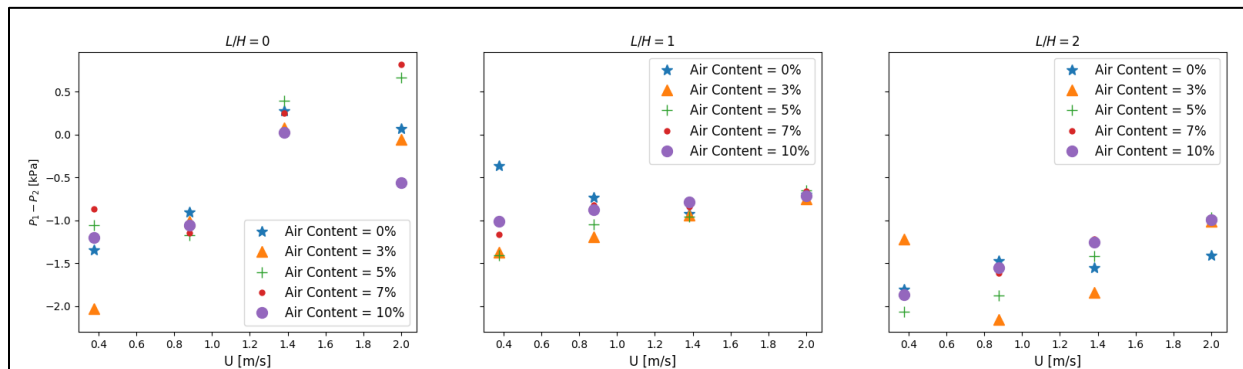


**Figure 4-15:  $P_1 - P_2$  vs  $U$  at low water velocities with aeration;  $H = 10\text{mm}$**

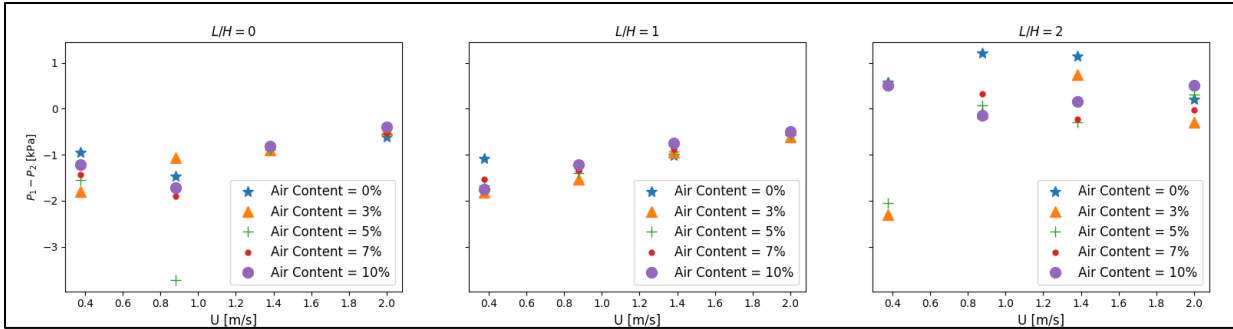


**Figure 4-16: P1-P2 vs U at low water velocities with aeration; H = 13.5mm**

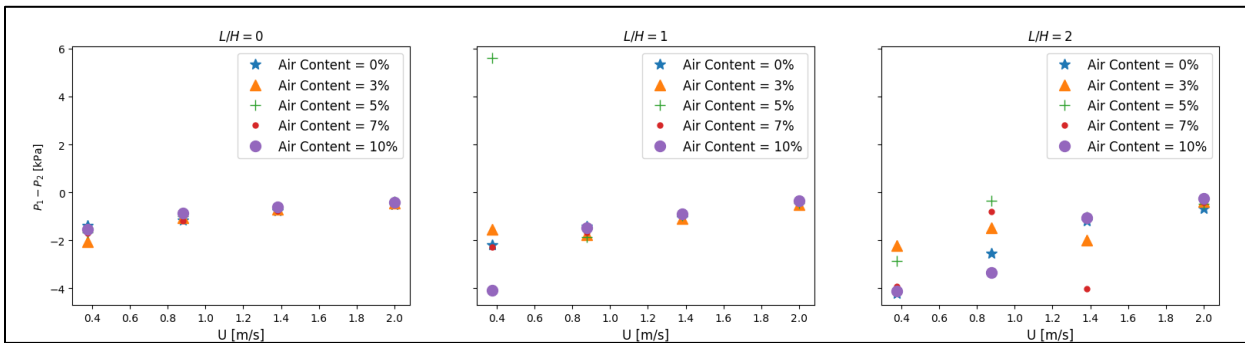


**Figure 4-17: P1-P2 vs U at low water velocities with aeration; H = 16.5mm**

#### 4.4 Oxygenation Results

The oxygen concentration difference was measured within the McGill test rig (at the two DO measurement points within the recirculating flow) to quantify the oxygenation in the recirculating flow caused by the injected bubble swarm. In this section, the oxygenation coefficients calculated from the measured data are presented. As described in a previous section, the sample pot DO measurements were used to calculate all the DO coefficients due to the evidence that the inflow DO sensors did not have a rapid enough response rate for inline measurements. A model, estimating the DO uptake between the headwaters and tailwaters of the hydropower plant using turbine design parameters, is then developed from the calculated oxygen coefficients and a non-linear regression.

#### 4.4.1 Oxygenation coefficients

The raw, measured DO concentration difference was processed in order to quantify the oxygenation physics. Using the methods established in Section 3.4, the oxygenation data is transformed into two parameters,  $E_{20}$  (oxygen transfer efficiency standardized to 20°C) and  $K_{La}$  (total aeration coefficient). Both measures indicate the level of oxygenation within the flow however,  $E_{20}$  considers the contribution of the contact time between the air bubbles and the flow while  $K_{La}$  is solely a measure of the oxygenating parameters of the flow (the turbulence characteristics and the oxygen diffusivity). Both can be used to rank the oxygenating capabilities of different aerating schemes but only  $K_{La}$  can be implemented within a computational model. These two parameters will be used subsequently to validate and calibrate the parallel CFD model and could be used to develop a model used to predict the DO uptake between the headwaters and tailwaters of a hydropower plant based on the injected gas void ratio, average water velocity in the draft tube, and water temperature. This model would be a relatively simple method of checking the design of aerating deflectors but, would over predict the prototype DO uptake due to a potentially reduced site-specific water quality in the prototype inhibiting oxygenation. The presence of algae, other gases and chemicals can inhibit oxygenation.

Nine different baseline deflector configurations (no mesh and with deflectors) were tested for their relative oxygenation potential. Figure 4-18 shows the oxygen transfer efficiency, standardized to 20°C, plotted against the gas void ratio at the different water velocity operating points. All the data shows a general trend, in agreement with the literature (Jun, 1991), of a power relationship with respect to the water velocity and a roughly linear relationship with respect to the gas void ratio.

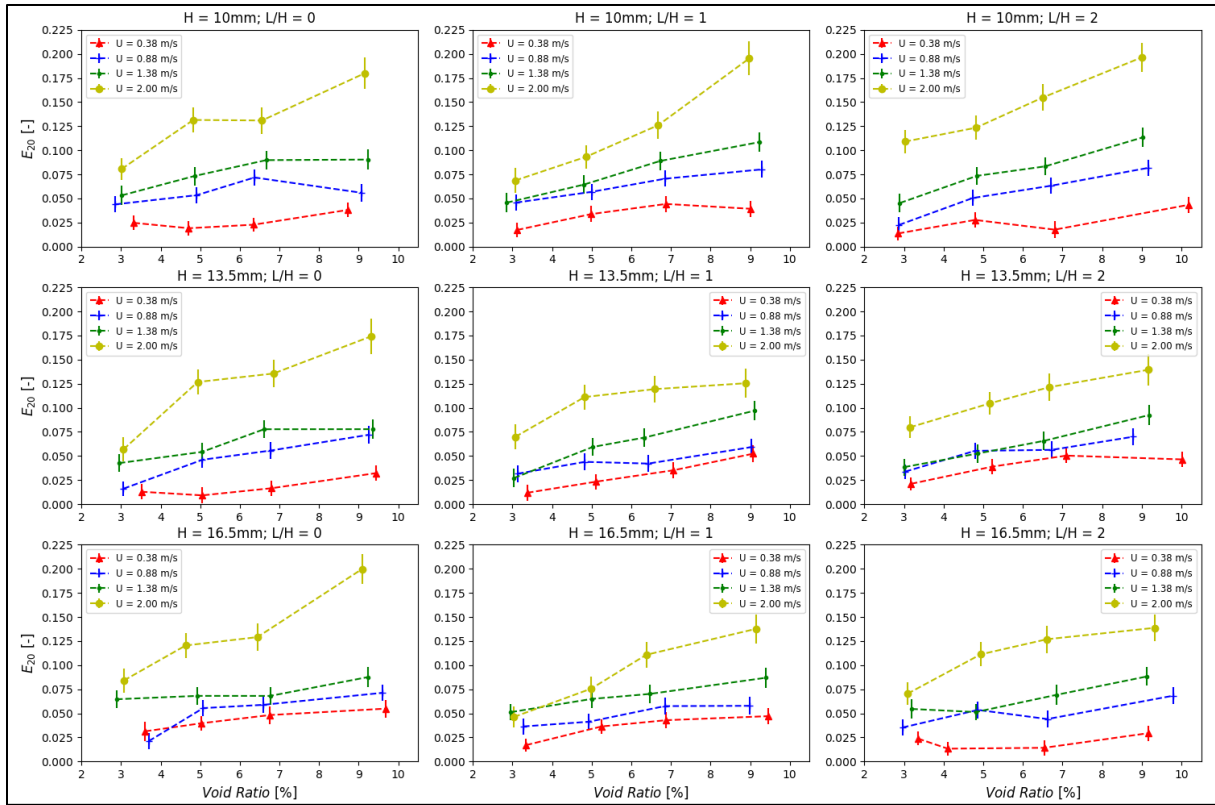


Figure 4-18: Oxygen Transfer Efficiency vs. Air Void Ratio at specific water velocities

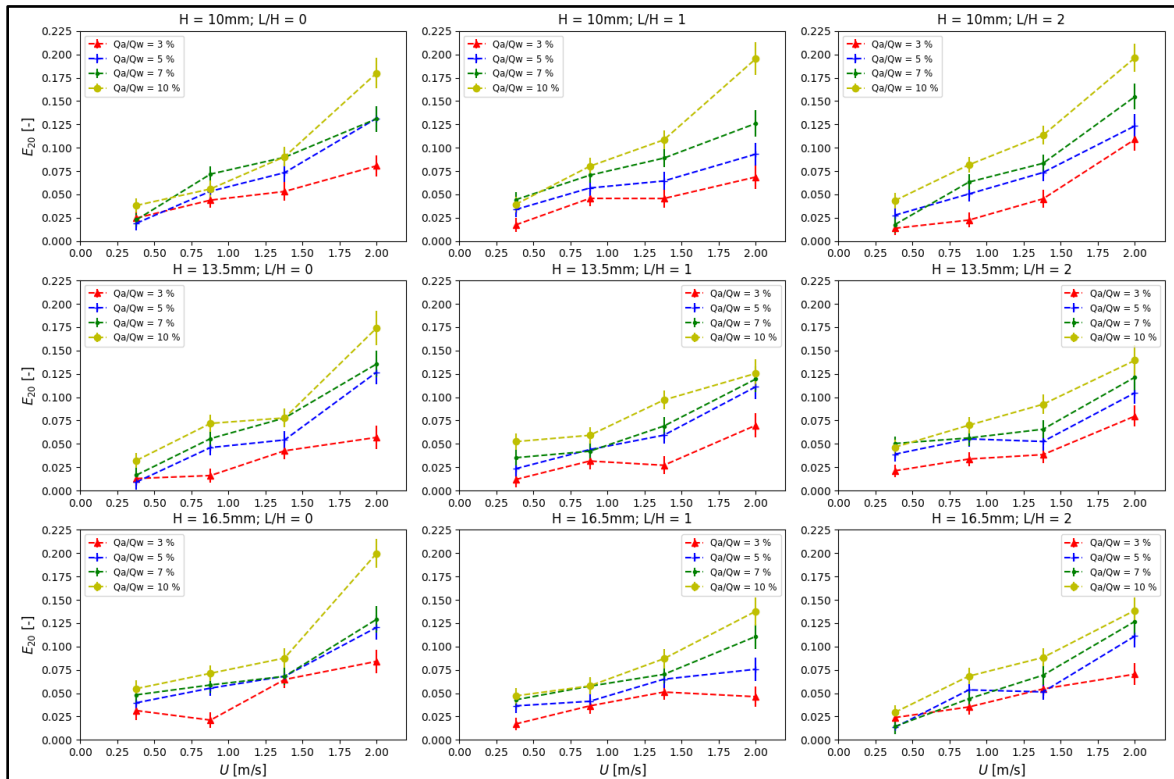
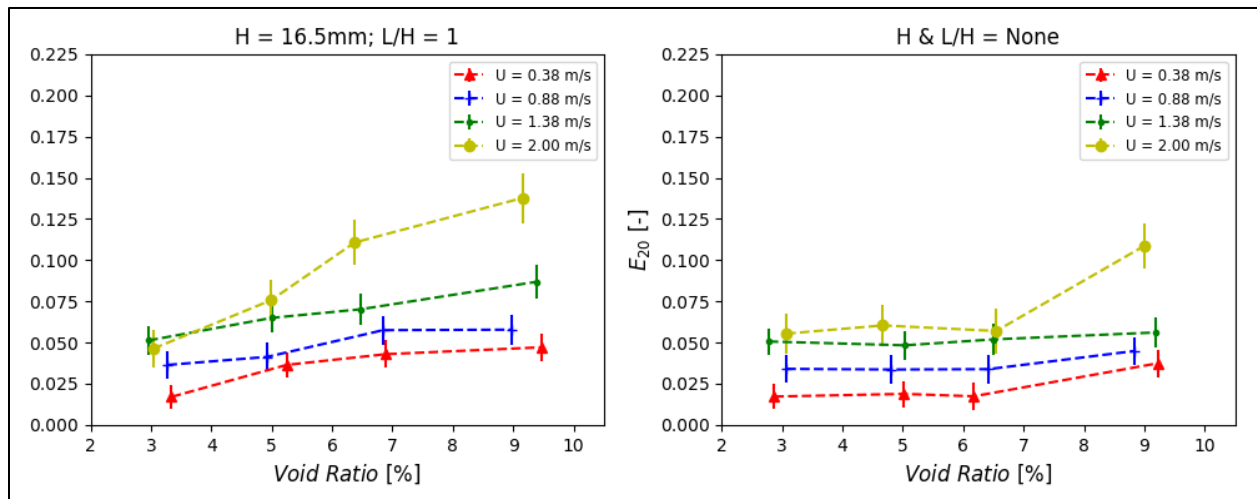


Figure 4-19: Oxygen Transfer Efficiency vs. Water Velocity at specific air/water flow ratios

Interestingly, the effect of an increased bubble residence time (low water velocity) did not increase DO concentrations. Oxygenation was always higher with increased water velocity. This is because our experimental setup only had one set distance between the two measurement points, meaning that the residence time and turbulence of the flow varied together. The influence of the reduced residence time (increased water velocity) was outweighed by the influence of the increased turbulent shear forces within the flow breaking up the bubbles and increasing the surface area over which oxygenation could occur. The influence of the residence time could be isolated using DO concentration measurements located further downstream. However, this was not possible with the current set-up.

The reference sample without a deflector showed similar oxygenation for all air/water flow ratios. When compared to the case with a deflector, the oxygen transfer efficiency was similar at low air/water flow ratios (Figure 4-20). Note that the presence of the deflector is needed in the prototype draft tube as the flow separation caused by the presence of the deflector provides the required sub-atmospheric pressure to aspire air into the draft tube.



**Figure 4-20: Effect of deflector presence. Oxygen Transfer Efficiency vs. Air Void Ratio at specific water velocities**

The meshed air inlet sample (Deflector 5) showed no increase in oxygenation when compared to the reference sample with  $H = 16.5$  and  $L/H = 1$  (Deflector 4) (see Figure 4-21). This was due to the lack of the initially hypothesized increased bubble breakup at the air inlet, further discussed in Section 4.2. At the lowest water velocities, where the mesh at the air inlet produced a large number of small bubbles, no measured difference in the oxygen transfer efficiency was observed when compared to the reference sample. This is hypothesized to be due to the bubbles rising to the crown of the pipe and immediately coalescing as they were slowed by the effect of friction. The interstitial contact area between the injected bubbles and the water flow was thus no different between the meshed and reference samples at all velocity scales.

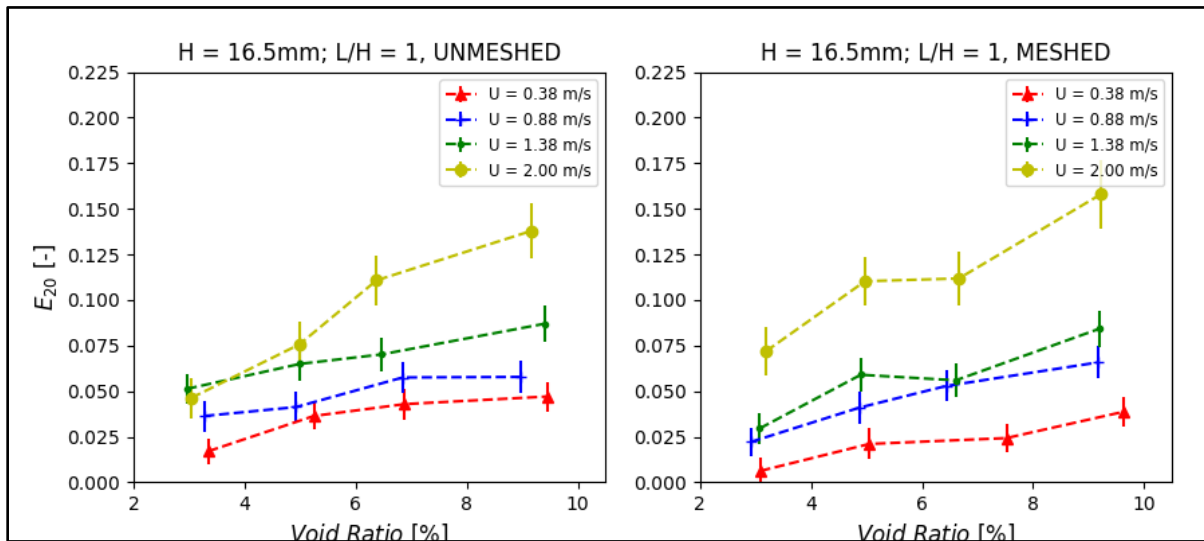


**Figure 4-21: Effect of mesh presence. Oxygen Transfer Efficiency vs. Air Void Ratio at specific water velocities**

Following the methods of Section 3.4, the total aeration constant,  $K_{La}$ , can be calculated from the oxygen transfer efficiency. Figure 4-22 is a plot of the total aeration constant vs the gas void ratio at the water velocity operating points. The total aeration coefficient is a measure of the average aeration occurring between the two measurement points.

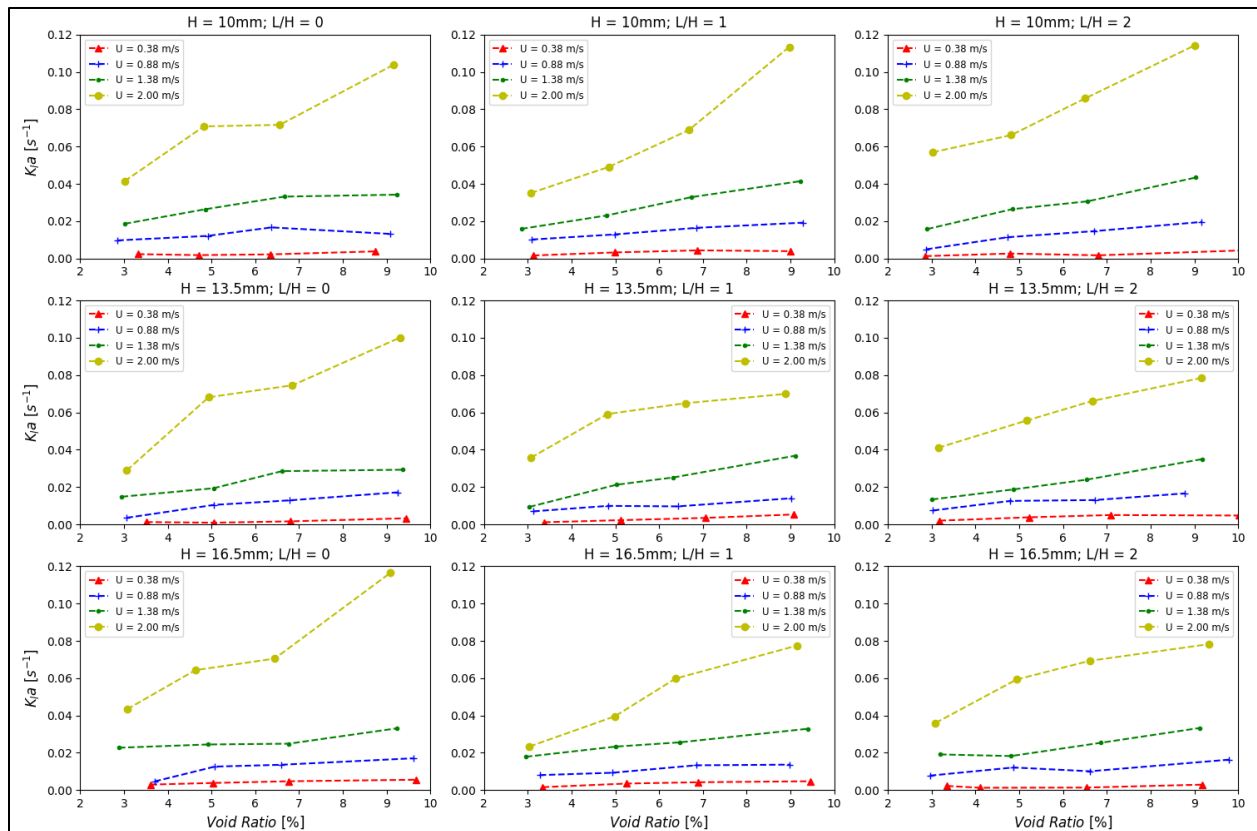


**Figure 4-22: Total Aeration Constant vs Air Void Ratio at specific water velocities**

In agreement with Figure 4-18, the total aeration coefficient shows a power relationship with respect to the water velocity (Figure 4-23) and a roughly linear relationship with respect to the gas void ratio, both are expected findings based on theoretical considerations and evidence in the literature. As an indexing tool, the total aeration coefficient is used to compare the aeration occurring from different aerating schemes or at different test rigs, but, in reality, does not accurately describe the local aeration physics. To properly describe the local physics, knowledge of both the local liquid film coefficient and the local interstitial contact area is needed, which is not possible without an accurate measure of the bubble size distribution along the length of pipe downstream from the test chamber.

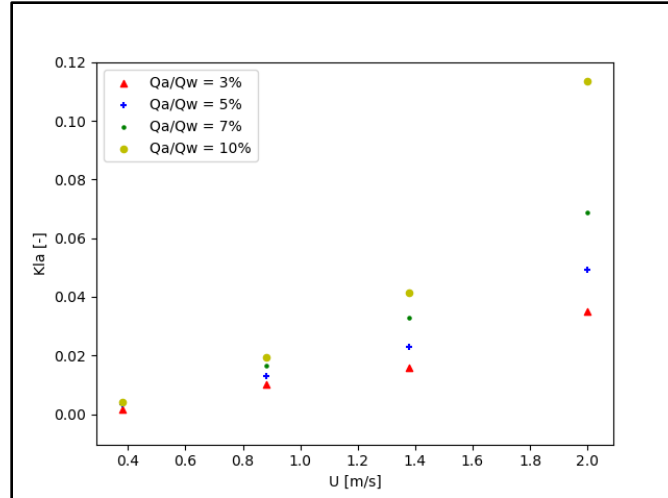


**Figure 4-23: KLa vs Water Velocity; H = 13.5 mm, L/H = 2**

To develop a model that could predict the DO uptake between the headwaters and tailwaters of a hydropower plant, a regression using the collected data can be calculated using the MATLAB curve-fitting app or other similar tools. From simplified theoretical considerations, an equation can be developed of the form (based on the work of Thompson and Gulliver (1997)):

$$K_L a = k * \phi * \frac{U^{\frac{6}{5}}}{L^{\frac{2}{5}}} * \left( \frac{D U^{\beta}}{v^{\beta-1} L^{2-\beta}} \right)^{\frac{1}{2}} \quad [22]$$

No observable trend with respect to the deflector size or air inlet position was seen and thus the equation above was used as it was developed based on studies within auto-venting turbines (AVT) at low gas void ratios and is based solely on the upstream water velocity, the hydraulic diameter of the pipe, the injected gas void ratio, and the hydraulic parameters (captured in k). However, the independence of the deflector size and air inlet position is most likely due to the uncertainty in the DO concentration measurements. In reality, the deflector size affects the initial bubble size (see Section 4.2) and thus, the interstitial contact area of the bubbles.

Using the MATLAB curve-fitting app, the regression constants were found to be  $\beta = 2.54 \pm 0.28$  and  $k = 0.1042 \pm 0.17$  (with 95% confidence intervals), with an  $R^2 = 0.92$  for this study. The exponential coefficient agrees with that found in Jun (1991) ( $\beta = 2.72$  and  $k =$  not reported). The first use of such a model in studying mass transfer processes was by Azbel (1981) who studied the oxygenation process induced by bubbles rising a quiescent flow. The mixing process was driven by the turbulence created by the rising bubbles. However, Thompson *et al.* (1997) studied the oxygenation process in an auto-venting turbine AVT and introduced a free variable,  $\beta$ , which allowed for the Azbel model to be applied to many different aerating schemes. They found  $\beta = 11/10$  in the process of developing a similarity relationship between aerating turbines of different geometries and rotational speeds. Their results agreed well with the Azbel model regardless of the significant difference in turbulent intensities. They commented on the significant difference in  $\beta$  when compared to the Jun (1991) study and speculated that it was a result of a lack in applicability in studying a recirculating flow to model an AVT. Jun *et al.* (1993) measured  $K_{La}$  and extrapolated a relationship for just  $K_L$  based on pictures of the bubble size distribution. It is possible that their sampling technique was biased, leading to an incorrect regression for  $K_L$ , however the results of this thesis does show a significantly stronger dependence on the water velocity in predicting the total aeration coefficient. The comparison between the measured and theoretical (from the above model)  $K_{La}$  can reveal biases in the experimental method. The theoretical  $K_{La}$  is calculated for each experimental point using the above described model and the measured  $K_{La}$  is calculated from the measurement of the oxygen transfer efficiency and Equation [5]. Figure 4-24 shows the measured vs theoretical  $K_{La}$ .

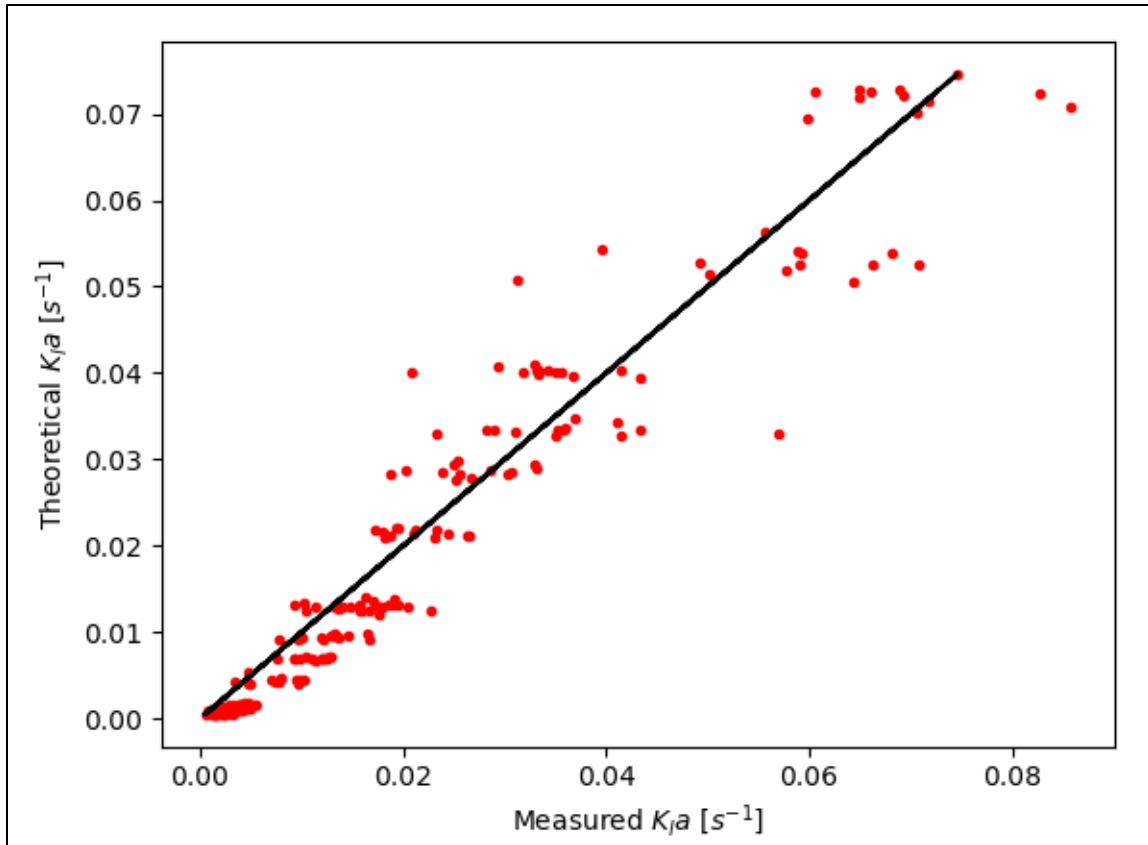


**Figure 4-24: Measured vs Modelled Total Aeration Coefficient**

The points of  $U = 2\text{m/s}$  with void ratios = 10% were not included in the regression due to the pump recirculating a significant amount of bubbles intermittently during these operating points, which increased the measured oxygen concentration difference. One additional data point was not considered, as it was a significant outlier most likely because of experimental bias. The model is less successful at predicting the value for the aeration constant at the lowest water velocities. This is because, at this velocity, the injected bubbles rise to the surface of the pipe immediately after injection and coalesce. The expression for the interstitial contact area used is invalid under these conditions.

A regression of this sort could allow hydraulic engineers to use the operating point of an aerating turbine (water flow rate and gas void ratio) and predict the oxygen transfer efficiency between the headwaters and tailrace.

#### **4.5 Sources of Error**

The accurate measurement of the difference in DO concentration between the two longitudinal positions within the recirculating flow presented certain challenges, which should be considered with further study of turbine aeration in a laboratory setting. The oxygen mass transfer process is relatively slow. Considering that the upstream DO concentration was generally on the order of 1.5 +/- 1.0 mg/L, the DO uptake was a small proportion of the full possible range of oxygen gas solubility in water. The measurement of differential oxygen concentrations was thus extremely sensitive to sensor and experimental variability. The oxygen sensors suffered from numerous issues such as hysteresis, and a large time to achieve measurement instability. Further studies should measure differential oxygen concentrations using a more accurate methodology such as an automated Winkler method, where the amount of oxidizer required to fully react the dissolved oxygen is measured and accurately calculates the dissolved oxygen concentration within a sample pot of water subjected to an air/water flow ratio and a water velocity. Importantly, while the rates of chemical reactions change with respect to temperature, the amount of chemical required to react with a given amount of dissolved oxygen is independent of temperature. The oxygen sensors used in this thesis modified the measured induced dissolved oxygen fluorescence with the temperature of the water. This method is accurate when dissolved oxygen concentrations change slowly within a flow, such as in a waste-water treatment plant, but results in errors when a recirculating flow undergoes rapid cycles of deoxygenation and aeration as in this thesis. These problems together caused the general variability described in Section 4.1.2 . This is most likely the reason that no dependence was visible on the total aeration coefficient by the deflector size. In theory, the deflector size affects both the level of turbulence within the flow and the mean bubble size downstream of injection and thus this dataset is not deemed wholly reliable. This dependence

would be visible with more accurate sensors, and a rig which better prevents the recirculation of the injected bubbles while still adequately mixing the recirculating reservoir.

## **Chapter 5: Summary and Conclusions**

When planning to implement hydropower systems, it is of chief concern to mitigate any environmental effects. A sustainable and resilient hydropower scheme should seek to prevent the development of anoxic conditions in the dam tailwaters. Anoxic conditions, which develop from thermal stratification within the reservoir can be resolved through several methods. For the scope of this study, a draft tube aeration scheme was examined in a simplified physical model to gain an understanding of the oxygenation and aeration parameters. A parallel project at Andritz Hydro seeks to develop a CFD model to design draft tube elbow deflectors, and the data from this study provides an important benchmark validation and calibration tool.

To qualitatively describe the injected bubble swarm, a high-speed video was taken through the test rigs' test chamber viewing window for a range of water velocity and air/water flow ratios. It was found that the presence of the deflector allows the bubbles to immediately coalesce downstream of the injection point, reducing the interstitial contact area between the bubbles and the flow, which can inhibit the mass transfer process in the draft tube. The presence of a mesh at the air inlet was not successful in setting the initial bubble size diameter at high water velocities. The bubble size distribution is therefore based on the size of the deflector and the turbulence characteristics within the flow. However, a more technical analysis of the bubble size distribution will need to be done in a subsequent study for this test rig.

The mechanism by which air is entrained into the draft tube at the prototype scale is aspiration due to the sub-atmospheric pressure which is produced in the lee of the deflector due to the flow separation induced by the flow obstruction (the deflector) in the high velocity draft tube

flow. The air flow rate within the draft tube is dictated by the pressure gradient between the ambient atmosphere and the location of the air inlet in the draft tube. It was found that this pressure gradient varies based on whether aeration is or is not occurring, but that it is not strongly dependent on the air flow rate itself. Rather, a non-linear relationship exists between the deflector size, water velocity and air inlet position. The data from this study will be used in the parallel CFD project to investigate the scale effect and attempt to develop an equation to predict the air flow rate within the draft tube for a range of hydraulic operating points.

To understand the oxygenation process in draft tubes with elbow deflector aeration schemes, the DO uptake between two points in a recirculating aerated flow was measured for a range of hydraulic and deflector geometric conditions. The measured DO concentration difference was non-dimensionalized using experimental parameters. A non-linear regression of the total aeration coefficient found a positive power relationship with respect to the water velocity and a linear relationship with respect to the injected gas void ratio in agreement with the literature. The model can be used as a first estimate of the DO uptake between the head and tailwaters of a hydropower plant using parameters related to the turbine operating point. This would provide an educated estimation for the design and operation of draft tube elbow deflectors at the prototype scale to meet specified environmental limits for DO concentrations in hydropower plant tailwaters.

It is important to note that a key difference between this study and the prototype draft tube is that for the scope of this study's test rig, a compressor was attached to the air inlet, providing a range of air flow rates. In the prototype draft tube, the driving pressure gradient is due to the high velocity flow within the draft tube being deflected away from the wall by the presence of a deflector; depending on the submergence of the turbine, the ensuing low-pressure wake leads to a negative pressure at the air inlet and sets the upper limit of the air flow in the prototype draft tube.

If a blower or compressor is used, the pressure gradient between the air inlet and the “ambient” atmosphere is not locked to the hydraulic and air flow parameters and the air flowrate can be more carefully controlled, however incurring operational costs. Further study is needed to determine whether the behavior of a prototype draft tube compressor/blower aeration system behaves similarly to this laboratory setup, with a stable pressure difference between the air inlet and the upstream water over a range of air flowrates, or if the flow topology around the deflector changes enough to cause a change in this pressure difference (P1-P2).

### **5.1 Recommendations for future work**

This study has set-up a framework for the development of a future, more detailed and precise, experimental investigation. Where this study reduced the degrees of freedom to the key parameters, further studies should reintroduce the applicable variables to model draft tube aeration within an industrial context and also reduce the sources of error identified within this study. At present, several aspects of the gas exchange mechanism in closed conduits are not fully understood particularly related to bubble coalescence and bubble shearing processes, which define the surface area for gas exchange to take place. Direct improvements to the current experimental set up would require reducing the sources of error and quantifying the bubble size distribution downstream of the injection point in the lee of the deflector.

Reducing the sources of error identified in this study is crucial to developing a model that hydraulic engineers could use for preliminary design to size the deflectors and orifices that will be used to aerate draft tube flows. Achieving accurate and precise measurements of the differential oxygen concentration is important due to the relatively slow of the gas exchange process. However, the larger the distance between the oxygen concentration measurement points the more difficult developing the experimental test rig becomes. Working with smaller distances between

the measurement points reduces the complexity of the test rig but also reduces the time during which gas exchange is occurring thus reducing the uptake of dissolved oxygen. If two dissolved oxygen sensors are used to quantify the differential oxygen concentration, each sensors' inaccuracy is compounded, and the final measurement has a larger uncertainty. Ensuring a high degree of confidence in any developed model will depend greatly on this measurement.

As camera technology improves, the tools available should be used to study the bubble size distribution within aerated draft tubes. Quantifying the bubble size distribution downstream of the injection point will achieve several things, including: improved optimization in design, and accurate computational modelling. Understanding how to create a fine swarm of bubbles with a high interstitial contact area between the injected air and water by varying the geometric design parameters of the deflectors will allow hydraulic engineers to better balance the achieved gas exchange with any potential efficiency losses caused by the presence of deflectors within the draft tube. Also, once the bubble size distribution can be quantified based on the hydraulic and geometry parameters of the deflector aerating scheme, the necessary transport equation for the bubble size can be accurately incorporated within the computational models that are generally developed before final design on turbine projects.

## References

- Almquist, C. W., Hopping, P., & March, P. (1991). *Energy Losses Due To Air Admission In Turbines*. Paper presented at the Hydraulic Engineering, Nashville, Tennessee.
- Atkins, P., & De Paula, J. (2006). *Physical Chemistry*: W. H. Freeman and Company.
- Azbel, D. S. (1981). *Two-phase flows in chemical engineering*. Cambridge; New York: Cambridge University Press.
- Best Practice Catalog - Francis Turbine Aeration*. (2012). Retrieved from
- Black, J. L., Taft, E. P., Davis, D. A., & Dixon, D. A. (2002). *Methods for Meeting and Monitoring Dissolved Oxygen Standards for Hydroelectric Projects*. Paper presented at the Proceedings of Hydrovision.
- Bunea, F., Houde, S., Ciocan, G. D., Oprina, G., Baran, G., & Pincovschi, I. (2010). Aspects concerning the quality of aeration for environmental friendly turbines. *IOP Conference Series: Earth and Environmental Science*, 12(1), 012035.
- Canadian Water Quality Guidelines for the Protection of Aquatic Life - DISSOLVED OXYGEN (freshwater)*. (1999). Retrieved from Winnipeg:
- Cantwell, B. (2005). *Fundamentals of Compressible Flow*: Stanford Bookstore Custom Publishing.
- Chanson, H. (1996). *Air bubble entrainment in free-surface turbulent shear flows*: San Diego : Academic Press.
- Chanson, H. (2002). Air-water flow measurements with intrusive, phase-detection probes: Can we improve their interpretation? *Journal of Hydraulic Engineering*, 128(3), 252-255.
- Desy, N., Demers, É., Grenier, R., & Hulse, D. O. (2004). *The Dissolved Oxygen Experience at Canyon Ferry*. Paper presented at the Proceedings of Hydrovision.
- EPRI. (1990). *Assessment and Guide for Meeting Dissolved Oxygen Water Quality Standards for Hydroelectric Plant Discharges*. Retrieved from
- EPRI. (1997). *Aerating weirs design*. Retrieved from
- EPRI. (2002). *Maintaining and Monitoring Dissolved Oxygen at Hydroelectric Projects*. Retrieved from
- EPRI. (2009). *Technology Update on Aerating Turbines*. Retrieved from
- EPRI. (2013). *Assessment of aerating hydroelectric turbine developments and related research needs*. Retrieved from
- Foust, J., & Coulson, S. (2011). *Using Dissolved Oxygen Prediction Methodologies in the Selection of Turbine Aeration Equipment*. Retrieved from
- Foust, J. M., Fisher, R. K., Thompson, P. M., Ratliff, M. M., & March, P. A. (2009). Integrating Turbine Rehabilitation and Environmental Technologies: Aerating Runners for Water Quality Enhancement at Osage Plant. *Proceedings of Waterpower*, 27-30.
- Fraser, R., Désy, N., Demers, É., Energy, G., Deschênes, C., Fau, J., & Hamel, S. (2005). Improvements to Self-Venting Francis Turbines. *Proceedings of Waterpower*.
- Ghaly, A. E., & Kok, R. (1988). The effect of sodium sulfite and cobalt chloride on the oxygen transfer coefficient. *Appl Biochem Biotechnol Applied Biochemistry and Biotechnology : Part A: Enzyme Engineering and Biotechnology*, 19(3), 259-270.
- Grenier, R., Rose, J., & Demers, É. (2010). *Dissolve Oxygen experience at John H. Kerr Power Plant*. Paper presented at the Proceedings of Hydrovision.
- Gulliver, J. S., Rindels, A. J., & Thene, J. R. (1990). Indexing Gas Transfer in Self-Aerated Flows. *Journal of Environmental Engineering*, 116(3), 503-523.

- Hinze, J. O. (1955). Fundamentals of the hydrodynamic mechanism of splitting in dispersion processes. *AIC AIChE Journal*, 1(3), 289-295.
- Hopping, P., March, P., & Wolff, P. (2009). *Justifying, specifying, and verifying performance of aerating turbines*. Paper presented at the Proceedings of Waterpower.
- Jacobs, N. (Producer). (2014). Nutrient Pollution and eutrophication. [Powerpoint Presentation]
- Jun, K. S. (1991). *Oxygen Transfer in Closed-conduit Turbulent Shear Flows*: University of Iowa.
- Jun, K. S., & Jain, S. (1993). Oxygen Transfer in Bubbly Turbulent Shear Flow. *Journal of Hydraulic Engineering*, 119(1), 21-36. doi:10.1061/(ASCE)0733-9429(1993)119:1(21)
- Kuhlert, K. H., & Ware, A. D. (2004). *A CFD System to Predict Dissolved Oxygen Uptake in Hydraulic Turbines*. Paper presented at the Proceedings of Hydrovision.
- Levich, V. G. (1962). *Physiochemical hydrodynamics*. Englewood Cliffs, N.J: Prentice-Hall.
- March, P. (2011). *Hydraulic and Environmental Performance of Aerating Turbine Technologies*. Paper presented at the EPRI, Palo Alto, California, Proceedings of EPRI/DOE Conference on Environmentally-Enhanced Hydropower Turbines: Technical Papers Report.
- Papillon, B., Sabourin, M., Couston, M., & Deschenes, C. (2002). *Methods for Air Admission in Hydro Turbines*.
- Pastorok, R. A., Lorenzen, M. W., & Ginn, T. C. (1982). *Environmental Aspects of Artificial Aeration and Oxygenation of Reservoirs: A Review of Theory, Techniques, and Experiences*. Retrieved from
- Peterson, M. J., Cada, G. F., Sale, M. J., & Eddlemon, G. K. (2003). *Regulatory approaches for addressing dissolved oxygen concerns at hydropower facilities*. Retrieved from
- Politano, M., Arenas Amado, A., Bickford, S., Murauskas, J., & Hay, D. (2010). Investigation into the Total Dissolved Gas Dynamics of Wells Dam Using a Two-Phase Flow Model. *Journal of Hydraulic Engineering*, 137(10), 1257-1268. doi:10.1061/(ASCE)HY.1943-7900.0000383
- Ruane, R. J., & McGinnis, D. F. (2007). *Applications of the Discrete-Bubble Model for Turbine Aeration Systems*. Paper presented at the Proceedings of Waterpower.
- Smith, C. D., & Saskatchewan, U. o. (1995). *Hydraulic Structures*: University of Saskatchewan Printing Service.
- Thompson, E. J., & Gulliver, J. S. (1997). Oxygen transfer similitude for vented hydroturbine. *Journal of Hydraulic Engineering*, 123(6), 529.
- Unsal, M., Baylar, A., Tugal, M., & Ozkan, F. (2008). Increased aeration efficiency of high-head conduit flow systems. *Journal of Hydraulic Research*, 46(5), 711-714. doi:10.3826/jhr.2008.3360
- USEPA. (1988). *Water Quality Standards Criteria Summaries: A Compilation of State/Federal Criteria*. Retrieved from Washington, DC:
- Wahl, T. L., Miller, J., & Young, D. (1994). *Testing turbine aeration for dissolved oxygen enhancement*. Paper presented at the Fundamentals and Advancements in Hydraulic Measurements and Experimentation:.
- Ware, A. D., & Sullivan, A. (2006). *Additional Dissolved Oxygen Enhancement at Bagnell Dam: Field Test Results from a Retrofit Aeration System for an Existing Osage Hydroturbine*. Paper presented at the Proceedings of Hydrovision.
- Wilhelms, S. C., Schneider, M. L., & Howington, S. E. (1987). Improvement of hydropower release dissolved oxygen with turbine venting. Available from the National Technical Information Service, Springfield Virginia. 22161. Technical Report E-87-3, March 1987. Final Report. 106 p, 19 fig, 4 tab, 39 ref, 4 append.

- Wilkinson, P. M., Haringa, H., & Van Dierendonck, L. L. (1994). Mass transfer and bubble size in a bubble column under pressure. *Chemical Engineering Science*, 49(9), 1417-1427. doi:[http://dx.doi.org/10.1016/0009-2509\(93\)E0022-5](http://dx.doi.org/10.1016/0009-2509(93)E0022-5)
- Xu, S. L., & Xu, S. M. (2002). Bubble formation characteristics from a sieve tray with liquid cross-flow. *Chinese Journal of Chemical Engineering*, 10(4), 416-419.
- Yin, Z., Zhu, D. Z., Cheng, D., & Liang, B. (2012). Oxygen transfer by air injection in horizontal pipe flow. *Journal of Environmental Engineering*.

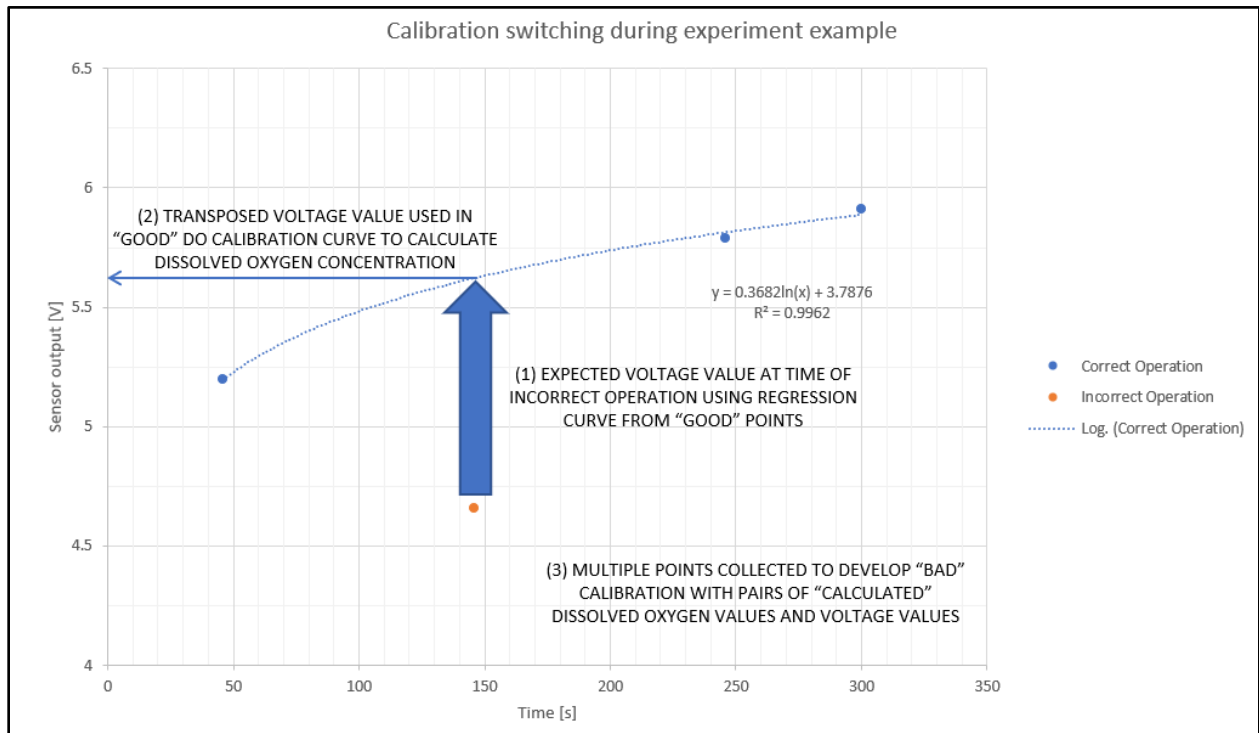
## Appendix A: Discussion of measurement errors

Several instruments used in the study suffered from measurement inconsistencies. A more detailed discussion about these issues follows.

The Vevey test rig was an existing test rig (for cavitation studies) modified for use in this study. Typical water pressures and velocities within the Vevey test rig used in cavitation studies are in the range of 800 kPa and 50 m/s. Therefore, the sensors used in the Vevey test rig were purchased and calibrated for much higher values than were used in this study. In the case of the water flowrate, the error was considered negligible due to a non-linear correction factor which was developed by the Vevey laboratory operators and automatically implemented within the testing scheme. The pressure gauges in the Vevey rig also had an accuracy of  $\pm 1\%$ , which is  $\pm 0.8$  kPa. The magnitude of the differential pressures that were to be measured on the rig were of the order of 1.0 kPa. The accuracy of the pressure gauges would therefore have introduced to great an error. It was assumed that the pressure gauge readings were repeatable but had an offset. To calibrate the gauges, this offset was determined by repeating a set of test conditions that were run in the McGill rig. The correction determined was an offset of 7.3 kPa.

The dissolved oxygen sensors used in the study are a discontinued model and relatively old ( $> 10$  yrs). The upstream sample pot DO sensor was noticed to intermittently incorrectly measure the temperature of the water when DO readings were being taken. The temperature reading would be erroneously high exclusively during the short time that the DO reading was being taken and lead to a much lower calculated DO concentration value (calculation within the sensor). This arose due to the reduced solubility of oxygen in water at higher temperatures. To correct for this a second calibration was developed. The second, “bad” calibration was developed

by searching for DO sample pot reading files which showed one or more of the DO readings to exhibit a sudden drop or increase. The point would then be fitted to the curve formed by the remaining points and the calibration curve developed through this process. The figure below illustrates this procedure.



**Appendix Figure 1: Procedure for developing "bad" calibration for upstream dissolved oxygen sensor**

If a sensor was judged to have not functioned during an experimental run (reading far out of range), it was repeated.